THE UNIVERSITY OF MICHIGAN
COLLEGE OF ENGINEERING
Department of Chemical and Metallurgical Engineering

Technical Report

MASS AND ENERGY TRANSFER BETWEEN A CONFINED PLASMA JET AND A GASEOUS COOLANT

Dean L. Smith

S. W. Churchill
Project Director

ORA Project 05607

under contract with:

NATIONAL SCIENCE FOUNDATION
GRANT NO. GP-331
WASHINGTON, D.C.

administered through:

OFFICE OF RESEARCH ADMINISTRATION ANN ARBOR

February 1965

This report was also a dissertation submitted by the first author in partial fulfillment of the requirements for the degree of Doctor of Philosophy in The University of Michigan, 1965.

ACKNOWLEDGMENTS

The author wishes to express his appreciation to all those persons who have aided in this investigation.

In particular, he wishes to acknowledge the interest, guidance, and criticism offered by Professor Robert H. Kadlec, chairman of the doctoral committee. The interest and suggestions of the other members of the doctoral committee, Professors R. E. Balzhiser, S. W. Churchill, W. N. Lawrence, and J. J. Martin, were also appreciated.

The author wishes to express his gratitude to Dr. George R. Chludzinski for his friendship, interest, and aid during the first part of this study.

The shop personnel of the Department of Chemical and Metallurgical Engineering and the purchasing staff of the Office of Research Administration were most cooperative and helpful.

The author is also indebted to his wife and parents for their encouragement and aid and to the Institute of Science and Technology and the National Science Foundation for their financial assistance.

ABSTRACT

The mass and energy transfer between confined plasma and coolant gas streams was studied experimentally. An 11 millimeter diameter axially symmetrical plasma jet was introduced into a surrounding concentric, cocurrent flow of coolant gas. The resulting flow system was confined in a 27 millimeter diameter quartz tube. The plasma generator was of the direct current arc type and was operated with axial flow through the arc region. Argon was used as the plasma gas at flow rates of 40 to 80 grams per minute with a net power input to the gas of approximately 3 kilowatts. Nitrogen was used as the coolant gas at flow rates of 2 to 20 grams per minute. The plasma and coolant mixing took place at atmospheric pressure.

The temperature profiles present in the mixing region were determined by optical spectrographic methods. Both the electronic excitation temperature of the argon atoms and the rotational temperatures of the nitrogen molecules were determined. The compositions and axial velocities present in the plasma-coolant mixing region were determined by sampling probe methods. Sampling probe measurements of enthalpy were found to be unreliable. The water-cooled sampling probe was 3.5 millimeters in diameter.

The measured nitrogen temperatures were found to be much lower than the argon temperatures present at the same point in the flow. The difference could be explained on the basis of the inability of argon atoms

to give their translational energy directly to the rotational modes of nitrogen molecules. The composition profiles indicated that direct induction of coolant into the high velocity plasma jet and the formation of a recirculation eddy greatly increased the mixing of plasma and coolant. Mass and energy balances computed at various axial cross-sections in the mixing region indicated that from 1/2 to 3/4 of the nitrogen coolant was present in the high temperature region of the flow but that this coolant fraction contained less than 10% of the total energy present. The solution of the differential equation describing argon-nitrogen diffusion indicated that flow and turbulent diffusion controlled the mixing of the plasma and coolant.

From a plasma jet chemical reaction standpoint, the results of this study indicate that the mixing with the plasma of a reactant injected into a plasma jet reaction chamber would be very rapid but that the internal energy modes of the reactant molecule would not be fully excited during the short residence time in the high velocity flow.

TABLE OF CONTENTS

TABLE OF CONTENTS (Continued)

TABLE OF CONTENTS (Concluded)

LIST OF ILLUSTRATIONS

LIST OF ILLUSTRATIONS (Continued)

LIST OF ILLUSTRATIONS (Concluded)

1. INTRODUCTION

1.1 SCOPE AND DESCRIPTION OF WORK

This thesis is primarily concerned with the mass and energy transfer between a confined plasma jet and a gaseous coolant. However, as a necessary part of the work, techniques for the measurement of plasma properties had to be considered and developed. Included among the techniques were spectrographic and sampling probe methods. Such methods could hopefully be used to independently measure the same properties.

The plasma was studied in detail only after it emerged from the nozzle of the arc-type plasma generator and began mixing with the gaseous coolant. Hence the phenomena occurring in the arc region itself were not of immediate interest. Early in the work, however, some consideration had to be given to these phenomena in order to obtain satisfactory generator design and performance. Satisfactory performance was found possible while employing axial flow (no tangential components) through the arc region. In comparison, most commercially built plasma generators employ vortex flow through the arc region. Such vortex flow complicates data analysis.

In studying the mixing of the plasma and coolant, primary emphasis was on where and how the plasma and coolant interchanged energy. Such information is important from a chemical kinetics' standpoint. Diffusion and flow both had to be considered. Each had a significant effect upon the confined mixing process. Description of the phenomena occurring was

derived from measured temperature, composition, and velocity profiles. In the course of the work, it was found that spectrographic methods were most feasible for temperature, and sampling probe methods for composition and velocity.

Certain considerations dictated the choice of gas for the plasma and coolant. Argon was the logical choice for the plasma gas since it is inert, has a reasonable ionization potential, and causes stable plasma operation. The thermodynamic and spectral properties of argon are well known. Ease of supply was also important. Determination of the coolant gas was based upon structure (mono- or di-atomic), toxicity, explosiveness, and availability. The toxicity and explosiveness considerations ruled out gases like carbon monoxide and hydrogen. Oxygen was considered too corrosive for use in this work.

Preliminary study indicated that either helium or nitrogen met the requirements for the coolant gas. Examination of the spectra produced upon mixing with the argon plasma showed that the monoatomic helium was not sufficiently excited for its spectra to be visible. Good spectra, however, was obtained with the diatomic nitrogen. Generally, this behavior is to be expected because of differences in spacing of energy levels. Years of effort have gone into the study of the spectral and thermodynamic properties of nitrogen, so all of these considerations made nitrogen the obvious choice for coolant gas.

1.2 REASONS FOR INTEREST

The confined jet mixing type of geometry was selected for study since it is typical of what might be encountered in plasma jet chemical reactors. Information about the transfer of mass and energy between the jet and coolant could be of value in studying the selective heating of reactants for a chemical reaction or for studying the quenching of a reaction which has already occurred in the plasma jet.

Although any coolant gas would provide useful information, the use of a diatomic gas like nitrogen is especially interesting since chemical reactions normally involve molecular gases.

2. SURVEY OF RELATED PLASMA WORK

2.1 NATURE OF PLASMA WORK

A plasma is defined as (43) "an ionized gas (as in the atmosphere of stars) containing about equal numbers of positive ions and electrons and differing from an ordinary gas in being a good conductor of electricity and in being affected by a magnetic field." Plasmas are present in such common things as fluorescent and neon lamps as well as in the huge machines for the study of controlled nuclear fusion. Plasma jets, as distinct from plasmas in general, are characterized by the fact that they are steady-state flow devices. The plasma flow is available for use or study in field-free regions as well as in the region where strong electric or magnetic fields are used to form the plasma. Plasma jets are usually produced by passing a gas capable of ionization through an electric arc or through an induction coil. The primary uses of plasma jets are in re-entry simulation (56), the cutting and forming of metals (75), growth of refractory crystals (73), and chemical synthesis.

The work in this thesis was motivated by the need of a better understanding of the mass and energy transfer mechanisms which are involved in any chemical synthesis. Some pertinent plasma jet chemical synthesis work is discussed in the following section and supporting work in plasma fluid flow and property measurement is discussed in Sections 2.3 and 2.4.

2.2 CHEMICAL SYNTHESIS

The interest in chemical synthesis work here is to look at the type of reactor geometry used and at the type of information needed for a more detailed analysis of results. A typical reactor arrangement is to use one of the reactants, if it is noncorrosive, as the plasma gas and then mix the other reactant with it downstream in a mixing chamber. If all of the reactants are corrosive, an inert gas like argon can be used for the plasma. Downstream mixing may also be indicated if the desired molecular product would be thermodynamically unstable in the extremely high-temperature arc region.

Freeman and Skrivan (39) studied the decomposition of ammonia and methane in a plasma jet by mixing these gases with an argon plasma in a mixing chamber. The plasma was fed along the axis of the chamber while the ammonia or methane was added radially. Only mean reactor temperatures were obtained from energy balances. The reseachers explain the low observed rate of decomposition by proposing the slow diffusion of reagent into the plasma as the rate-limiting step. Biggerstaff et al. (9) studied the production of elemental boron by mixing BF_3 or BCl_3 with argon or argon-hydrogen plasma jets. They used a mixing chamber which permitted radial, axial, or tangential introduction of the boron compounds into the plasma jet. The various introduction methods all produced approximately the same boron yields. These researches also used an energy balance for temperature determination. Anderson and Case (5) studied the reactions of methane when mixed with a hydrogen plasma jet. In their

reactor, the methane was introduced radially into the plasma jet. Only heat-balance determined temperatures were used. Their discussions indicate the importance of and need for knowledge about how the plasma and reactant mix and interchange energy. Marynowski et al. (66) have studied the thermodynamics of systems for use in a mixing chamber type of plasma jet reactor.

Some workers like Selover (79) passed their reactant through the arc region along with the inert plasma gas. Still other workers, like Leutner (64), used consumable electrodes as reactants. Grosse et al. (50) report work which employed a wide variety of reactor configurations including both arc and induction power supplies. Such reactor systems are not directly related to the research reported in this thesis but may be of interest if a gaseous mixing type of reaction quench is employed.

2.3 FLUID FLOW AND HEAT TRANSFER

The majority of studies of plasma flow and heat transfer have been done in connection with missile re-entry simulation or controlled nuclear fusion. Thus they are not directly related to the work of this thesis.

Grey, Jacobs, Williams, and Sherman (46-48, 53, 54, 83) have made detailed studies of the unconfined mixing of plasma jet (argon) and coolant (helium) streams. Both laminar and turbulent plasmas were used. All of their results were obtained from sampling probe measurements.

Tourin et al. (81) measured the temperatures in the unconfined flow

produced when argon, nitrogen, or helium plasma jets were mixed with carbon monoxide or carbon dioxide streams. They used infrared emission and absorption methods to determine the average temperatures of the added gases.

Freeman et al. (38) measured the velocity of a plasma jet by following the luminous fluctuations. Kamura (59) measured the velocity in an arc jet by measuring the thrust on small plates passed through the plasma.

2.4 TEMPERATURE AND PROPERTY MEASUREMENT

Numerous reports of work concerning plasma temperature and property measurement are found in the technical literature. Specific reference to some of these reports will be made in other chapters of this thesis as their results are needed. Probably the best summary of all of this literature is given by Edels (34). The book edited by Dickerman (29) is a good introduction to optical spectrographic temperature measurement methods.

3. PERTINENT JET MIXING THEORY

3.1 GENERAL DESCRIPTION OF PHENOMENA

The typical confined jet mixing pattern is shown in Figure 1. In terms of the nomenclature of jet literature, the plasma jet would be termed the primary flow and the coolant stream called the secondary flow. As shown in the figure, part or all of the secondary flow is entrained or inducted into the primary flow shortly after they enter the mixing tube. Further downstream a recirculation eddy may form as a stable part of the flow. The phenomena shown are especially evident when the primary flow has a much greater velocity than does the secondary flow.

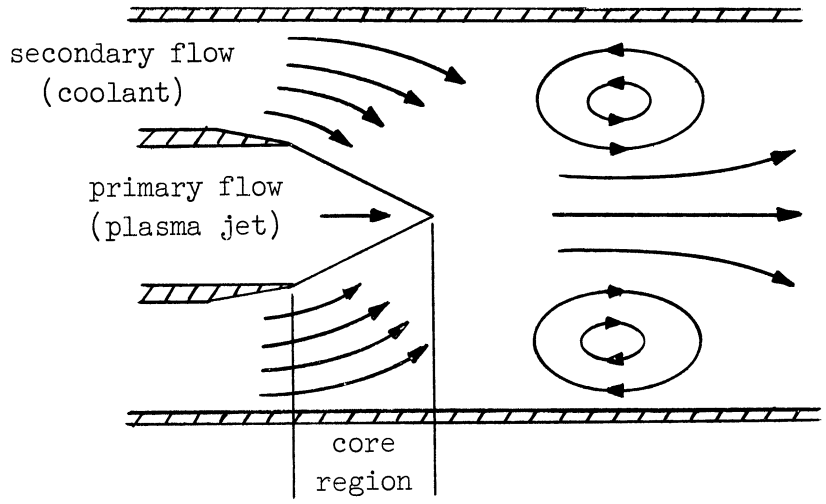

Figure 1. Jet mixing pattern.

The inductive capability is a characteristic of any high velocity jet and is due to both turbulent momentum transport and radial pressure

gradients (27). The recirculation phenomena can be explained in several ways. Curtet (24) describes recirculations simply as the mechanism which supplies fluid to be inducted into the thirsty mixing region after all the secondary flow has been swallowed up. Abramovich (1) has a more formal description of recirculation. He observes that mixing in a confined field results in a pressure rise, and that if this pressure rise is sufficiently high, it will retard the ambient flow to zero, resulting in recirculation.

3.2 SUMMARY OF JET RESEARCH

3.2.1 Confined Jets

As mentioned in the general description, an eddy of recirculation may exist in the mixing tube as a stable part of the flow. It is of interest to establish a criterion for the occurrence of such an eddy and a method of correlating the total rate of recirculation. For this purpose, several single-parameter similarity criteria have been suggested. All such parameters are functions of the jet source radius, R_1, the mixing tube radius, R_2, the initial average velocity of jet source, V_1, the initial average velocity of the secondary flow, V_2, or the volumetric flow rates, Q, and fluid densities, ρ.

Thring and Newby (80) assumed that an enclosed jet grows at the same constant rate as does a free jet until it reaches the wall. They were interested in the mixing of air and fuel and they concluded that the proper similarity parameter for a cold flame model would be

$$\left(\frac{\rho_1 Q_1}{\rho_1 Q_1 + \rho_2 Q_2}\right)\left(\frac{R_2}{R_1}\right) \quad . \tag{3.1}$$

Curtet (25), during theoretical studies of plane confined jets of constant density, found that after integrating the equations of motion across the flow, the parameters appearing in the equation were (R_2/R_1) and a "momentum parameter," m. As generalized for a cylindrical jet, this parameter is

$$m = \frac{\pi R_2^2}{Q_t^2} \int_0^{R_2} \left(v^2 - \frac{V_2^2}{2}\right) 2\pi r dr - \frac{1}{2} \quad . \tag{3.2}$$

Curtet's measurements indicated that this parameter is practically a constant of the flow and does not vary from one section to another. For a constant density system having uniform jet and secondary flow velocities, the initial value of the Curtet similitude parameter is

$$m_o = \frac{R_1^2(V_1^2 - V_2^2) + \frac{V_2^2 R_2^2}{2}}{Q_t^2/\pi^2 R_2^2} - \frac{1}{2} \quad . \tag{3.3}$$

Becker (7) made a more general analysis of jet-type flows and demonstrated the fundamental significance of the parameter, m_o, for the particular kind of jet model considered by Curtet. Based on his unified analysis of jet flows, Becker suggests a more useful modification of the parameter, m_o. He calls the new parameter the Craya-Curtet number and gives it the symbol Ct:

$$Ct = \frac{1}{\sqrt{m_o}} \quad . \tag{3.4}$$

Becker's general treatment also shows that the Thring and Newby parameter is the proper similarity parameter only for an ideal or point source jet. For a circular gas jet Becker experimentally found that recirculation occurred for values of Ct less than 0.75.

Dealy (26, 27) additionally demonstrated the relationship between recirculation and the parameters m_o and Ct. His work includes a momentum factor which is calculated from the structure of the jet. For a harmonic velocity profile he calculates the critical value of Ct to be 0.83. Experimental work with axially symmetric water jets gave results in agreement with Becker's value of 0.75 for the critical value of Ct.

3.2.2 Jet Entrainment

In addition to work concerned with confined jets, some studies of entrainment in free jets are also of immediate interest.

Donald and Singer (30) employed a dye and chemical indicator technique to study, visually, the flow in the ambient fluid as well as in the mixing region of a submerged water jet. They found that the entrained fluid appears to enter the jet at right angles.

Ricou and Spalding (74) experimentally studied entrainment in axially symmetric gas jets of various densities. At axial distances, z, much larger than the diameter of the orifice, R_1, they found the mass of fluid entrained to be

$$M_1 \left[0.32 \frac{z}{R_1} \left(\frac{\rho_2}{\rho_1} \right)^{1/2} - 1 \right] \qquad (3.5)$$

where M_1 is the mass flow rate of the jet.

3.2.3 Other Jet Work

A very large jet literature exists. Extensive bibliographies on jets have been compiled by Forstall and Shapiro (36) and by Krzywoblocki (62). The treatise by Abramovich (1) contains many interesting discussions of jet flows. For this thesis, only those concerned with mass and energy transfer are of some interest.

The work by Grey et al. (47, 54, 83) in plasma jet-coolant mixing has already been mentioned in Chapter 2. Both experimentally and from an analytical model they found that concentration spread more rapidly than temperature and that temperature spread more rapidly than velocity.

Corrsin (21) and Uberoi (22) studied a round turbulent jet of heated air and used a hot wire system to determine velocity and temperature profiles. They found that the transport of heat occurred more rapidly than that of momentum. Hinze and van der Hegge Zijnen (52) also found that heat and matter spread faster than velocity. Other jet work of general interest has been done by Baron and Alexander (6), Alpinieri (3), and Cleaves and Boelter (19). Cleaves and Boelter studied both isothermal and heated jets. The 1280°F jet which they used had the highest temperature employed by nonplasma jet workers.

4. SPECTROGRAPHIC PLASMA TEMPERATURE MEASUREMENT

4.1 MEANING OF TEMPERATURE

Studies of the physical and chemical processes occurring in a plasma require a knowledge of the temperature of the plasma. To fully appreciate this property of the plasma, the physical interpretation and definition of the temperature of a gas needs to be understood.

Temperature is conveniently defined by considering an isolated gas assembly containing a large number of identical particles which possess kinetic energy. By means of statistical mechanics, it can be shown that an equilibrium distribution of particle energies will be established. Temperature is intrinsically connected with this equilibrium distribution of energy or velocity known as the Maxwell-Boltzmann distribution (called the M.B. distribution in the remainder of this discussion). In the analytical derivation of the equilibrium distribution it is found that a quantity defined as the temperature of the particle may be related to the most probable particle velocity. The product of this quantity (temperature) and the Boltzmann constant is equal to the most probable kinetic energy of a particle in the assembly. The definition of temperature in this manner at once ascribes an M.B. distribution of energies to any assembly to which a temperature value is given. Conversely, if an M.B. distribution of energy exists, a temperature value can be assigned.

An ionized gas or a mixture of gases may be considered as composed of a finite number of different particle assemblies. Each of these as-

semblies may initially possess a different energy distribution (and thus temperature). In an isolated set of such assemblies different final conditions can result dependent upon the conditions of collision and energy exchange. On the one hand, if energy exchange takes place only between similar particles, different temperatures would be obtained for the different particle assemblies when "equilibrium" was reached. Each particle assembly would have its own temperature dependent upon the number of particles and the initial total energy. This temperature would be unaffected by the existence within the same boundary of other types of particle. On the other hand, if all particles exchange energy, a single final distribution would be obtained and a single temperature could be assigned to the system. Under this final condition the different types of particle may be described as being in thermal equilibrium.

The isolated system discussed above can actually never exist. Thus it is necessary to consider conditions under which an M.B. distribution exists when energy exchange takes place with the surroundings. Normally, in an assembly which is accepting or giving energy to its surroundings, all parts of the assembly will be subjected to a directional flow of energy. If a section of the assembly containing enough particles for equilibrium conditions to exist is considered, and if at any instant the average energy being transferred is small compared with the total energy of the section, an M.B. distribution may be obtained. This results from the consideration that due to the small amount of energy being transferred, the collisions between particles not directly connected with energy trans-

fer are predominant and will maintain the distribution. Under these conditions, the assembly may be considered as being made up of sections each having an M.B. distribution corresponding to a specific temperature. Such an assembly is said to be in local thermal equilibrium (LTE). For practical purposes, the change in temperature may be considered as continuous with the temperature at any point defining the distribution at that point. The concept of LTE has been discussed in detail by Griem (49).

The system of interest in the thesis is a free-field argon plasma jet mixing with a nitrogen coolant. This system consists of the following particles: argon atoms, argon ions, electrons, nitrogen molecules, nitrogen molecule ions, and perhaps nitrogen atoms. In addition to the translational energy possessed by all of the particles, all particles except the electrons can possess electronic excitation energy, the molecules have rotational and vibrational energy, and the ions have ionization energy.

Thermal equilibrium in the argon-argon ion-electron system has been the subject of many studies. Representative of theoretical studies is the one made by Williams and co-workers (83). From an experimental standpoint, Olsen (69) independently measured the excitation temperatures of argon atoms and of argon ions and found them to agree in his atmospheric pressure plasma. The conclusion, which always seems to be reached for plasmas at atmospheric pressure and above, is that the system is very close to equilibrium and that approximately the same temperature can be assigned to translation, electronic excitation, and ionization. Since

the photons which result from transitions between the excited electronic states normally escape without interaction, and since no compensating radiation field is present, true radiative equilibrium does not exist. However, since collisional energy exchange is completely dominant at atmospheric pressure, this has no significant effect upon the distribution of energy among the electronic states. In this thesis, as described in Section 4.2, argon temperatures were determined from the spectra of these emitted photons.

The literature appears to contain no discussions of equilibria in connection with nitrogen mixed with an argon plasma. This equilibria will be discussed in the Results (Section 7.2.3) of this thesis. For pure nitrogen a number of studies are summarized by Herzberg (51) and Edels (34). In most, but not all, cases, the temperature determined from the distribution of energy among the rotational states agreed with the translational temperature of the system. Vibrational temperatures were frequently found to differ from the temperature of the other energy modes. In this thesis, as described in Section 4.3, the rotational energy distribution was used as a measure of the nitrogen temperature.

4.2 TEMPERATURE MEASUREMENTS BASED UPON ATOMIC LINES

4.2.1 Relationship Between Line Intensity and Temperature

As mentioned in the discussion of temperature, an atom can acquire energy in the form of electronic excitation. This gain in potential energy occurs when energy gained by collision causes an orbital electron

of the atom to make a transition to an orbit of higher energy value. The electron in this higher energy state may subsequently make a spontaneous transition to a lower level with the emission of a photon of light having an energy equal to the difference in the energies of the upper and lower level. The number of such downward transitions per second depends upon the concentration of the atoms in the higher excited level and upon a constant known as Einstein's probability of spontaneous transition. The frequency of the emitted photons is given by

$$\nu_{nm} = (E_n - E_m)/h \tag{4.1}$$

and the intensity of the radiation is expressed by

$$I_{nm} = \frac{1}{4\pi} Lch\nu_{nm}A_{nm}N_n \tag{4.2}$$

where

A_{nm} = Einstein's spontaneous transition probability for transition from level n to level m

c = Velocity of light

E_n, E_m = Energy of upper level n and lower level m respectively, with respect to the ground level

h = Planck's constant

ν_{nm} = Frequency of emitted photon

I_{nm} = Radiant intensity (energy emitted per unit time per unit area per steradian)

L = Path length through source

N_n = Number density of atoms with an electron in the excited state n.

For an equilibrium system (i.e., one having an M.B. distribution), the concentration N_n of the atoms in the excited state n is given by statistical mechanics as

$$N_n = N_o \frac{g_n}{g_o} \frac{1}{Q} \exp(-E_n/kT) \qquad (4.3)$$

where

N_o = Concentration of atoms in ground state

g_n, g_o = Statistical weight of atoms in state n and ground state, respectively

Q = Electronic partition function

k = Boltzmann constant

T = Absolute temperature.

From Equations (4.2) and (4.3), intensity and temperature are related by

$$I_{nm} = \frac{1}{4\pi} LchN_o \nu_{nm} A_{nm} \frac{g_n}{g_o} \frac{1}{Q} \exp(-E_n/kT) \quad . \qquad (4.4)$$

For argon atoms, the ground electronic state has a statistical weight of 1 and the electronic partition function is essentially 1 for temperatures below 10,000°K. Thus the intensity expression simplifies to

$$I_{nm} = \frac{1}{4\pi} LchN_o \nu_{nm} A_{nm} g_n \exp(-E_n/kT) \quad . \qquad (4.5)$$

The transition probabilities, A_{nm}, are different for each spectral line. In theory they are calculable from quantum mechanics (51), but in practice for heavy atoms like argon, they must be determined experimentally. Two experimental approaches are possible. One is seeding hydro-

gen into the argon plasma. Since the transition proabilities for hydrogen lines are known from quantum mechanics, these lines can be used to determine the plasma temperature. The argon transition probabilities are then calculated from the observed argon line intensities. The other method, known as the Fowler-Milne method, uses only the observed argon spectra. The Fowler-Milne method is described in Section 4.2.2. The various determinations of argon transition probabilities are summarized by Adock and Plumtree (2). For many lines, the values found by different investigators differ by as much as a factor of 2. In this thesis the values of Gericke (41), which are generally considered reliable, were used.

4.2.2 "Single-Line" Temperature Determination

If the transition probability of a spectral line is known and the absolute intensity of the line is measured, the temperature can be determined from Equation (4.5). To do so, however, is a trial and error procedure since the number density of atoms in the ground state, N_o, is a function of temperature. Argon at the temperatures encountered in this work (below 10,000°K) is less than 1% ionized. Thus N_o can be determined from the ideal gas law as being

$$N_o = \frac{P}{kT} \tag{4.6}$$

where P is the system pressure. This temperature determination method was used in this thesis. The trial and error calculations were performed

with a digital computer.

Under certain special circumstances, a single line can be used for temperature determination even if the transition probability is not known. This method, known as the Fowler-Milne method, makes use of the fact that the intensity of a line goes through a maximum as temperature is increased. As can be seen from Equations (4.5) and (4.6), the exponential term increases with temperature while the N_o term decreases. The N_o term also decreases due to ionization. The net result is that an intensity maximum exists at about 15,000°K. Now if the plasma source contains temperature gradients, and if the temperature is known to be above 15,000°K at some point, the position of maximum intensity corresponds to 15,000°K. Since corresponding temperature and intensity values are then known, the transition probability can be calculated.

4.2.3 "Multi-Line" Temperature Determination

By comparing the intensities of 2 or more spectral lines, temperature can be determined from relative, rather than absolute, values of intensity and transition probability. If two lines produced by transitions from levels m to r and from n to s are considered, their intensity ratio is given by Equation (4.5) as

$$\frac{I_{ns}}{I_{mr}} = \frac{\nu_{ns} g_n A_{ns}}{\nu_{mr} g_m A_{mr}} \exp\left[-E_n - E_m)/kT\right] . \qquad (4.7)$$

When solved for temperature, Equation (4.7) yields

$$T = \frac{(E_n - E_m)/k}{\ln\left(\frac{\nu_{ns} g_n A_{ns}}{\nu_{mr} g_m A_{mr}}\right) - \ln\left(\frac{I_{ns}}{I_{mr}}\right)} \quad . \tag{4.8}$$

Although the temperature values obtained from 2-line pairs could be averaged to increase accuracy, the averaging can be done another way. Equation (4.5) can be written for a nonspecified line as

$$I = K\nu gA \exp(-E/kT) \tag{4.9}$$

where

$$K = LhcN_o/4\pi \quad . \tag{4.10}$$

When Equation (4.9) is rearranged as

$$\ln(I/K\nu gA) = -E/kT \tag{4.11}$$

it can be seen that a plot of $\ln(I/K\nu gA)$ versus E for a number of lines would yield a straight line having a slope of $-1/kT$. Since K does not depend on E, it does not enter the calculation, and $I/K\nu gA$ can be expressed in arbitrary units. This method was used for some of the preliminary work in this thesis.

4.2.4 Accuracy of Temperature Determination

It is interesting to calculate how much variation is introduced into the temperature determination by precision or accuracy errors in the intensity determinations. For the single-line method the intensity of a line is given from Equations (4.5) and (4.6) as

$$I = C \frac{1}{T} \exp(-E/kT) \tag{4.12}$$

where C contains all of the various constants. When this expression is differentiated and then divided by itself, the following result is obtained if $E/k \gg T$ (i.e., $T < 15{,}000°K$):

$$\frac{dT}{T} = \frac{k}{E} T \frac{dI}{I} \quad . \tag{4.13}$$

For the 4198 Å argon line at 9000°K, this indicates that a 20% change in measured intensity causes only a 1% change in temperature.

In the case of the 2-line method, like manipulation of Equation (4.8) gives

$$\frac{dT}{T} = \frac{1}{\ln\left(\frac{\nu_{ns} g_n A_{ns}}{\nu_{mr} g_m A_{mr}}\right) - \ln\left(\frac{I_{ns}}{I_{mr}}\right)} \frac{d\left(\frac{I_{ns}}{I_{mr}}\right)}{\left(\frac{I_{ns}}{I_{mr}}\right)} \quad . \tag{4.14}$$

For the argon 4198-5606 Å pair of lines at 9000°K, this indicates that a 20% change in the intensity ratio causes a 29%, or 2600°K, change in temperature. This great sensitivity is caused by the closeness in spacing of the upper energy levels associated with the 4198 and 5606 Å lines. In argon it is difficult to find usable lines having a greater energy spacing. Errors in the values of the transition probabilities produce a result exactly equivalent to that of intensity. The quantities like ν and E are known with great precision.

In making intensity measurements, self-absorption of a spectral

line by cooler portions of the plasma may introduce errors. Ryan et al. (78) have studied this absorption in an atmospheric pressure argon plasma. They found that the plasma had no absorption, i.e., was optically thin, in the 2700 to 7000 Å region. The argon lines measured in this thesis were in the 4000 to 6000 Å region.

4.3 TEMPERATURE MEASUREMENTS BASED UPON MOLECULAR BANDS

4.3.1 Origin of Band Spectra

The previously discussed line spectra occurs only for atoms, the spectra of molecules always consists of bands.

A diatomic molecule consists of two atoms, the nuclei of which are affected by internuclear forces in such a way that the nuclei vibrate about equilibrium positions along the internuclear axis. At the same time the nuclei rotate about their common center of mass while the electrons describe orbits about the individual atoms. The total energy of the molecule can be assumed to be of the form

$$E = E_e + E_v + E_r \tag{4.15}$$

where E_e is the electronic energy and is the energy the molecule would have if the atoms were fixed in their equilibrium positions. E_v is the vibrational energy and is the extra energy which must be added to the electronic energy if the atoms are vibrating. This energy term is expressed as a function of the vibrational quantum number v. E_r is the rotational energy and is the extra energy of the molecule due to the ro-

tation of the nuclei about their common center of mass. Since vibration alters the size and thus the moment of inertia of the molecule, the rotational energy is a function of the vibrational quantum number v as well as the rotational quantum number J.

The electronic energy levels of a diatomic molecule are separated by the same order of energy as that found in free atoms. But, as a consequence of the vibration and rotation, each electronic energy level has associated with it a number of levels of vibrational energy. For each such vibrational energy level there are a number of rotational energy levels. This is represented schematically in Figure 2. For heteronuclear molecules certain transitions are permitted between any of the energy levels. For homonuclear molecules, like N_2, quantum mechanical selection rules permit transitions only between different electronic energy levels and even then only for certain changes in the values of the rotational quantum number J. The allowed transitions between any pair of the vibrational levels are for $\Delta J = \pm 1$ and in some cases $\Delta J = 0$. The series of lines formed from the different pairs of J values is called a band. Each band is made up of lines all corresponding to the same vibrational transition. The collection of these bands for the vibrational levels corresponding to the same electronic energy transition is called a band system. Within a band a line is identified by the rotational quantum number of the upper level. Since different lower levels can be associated with the same upper level, what are called band branches, are formed. Transitions corresponding to $\Delta J = +1$ form the

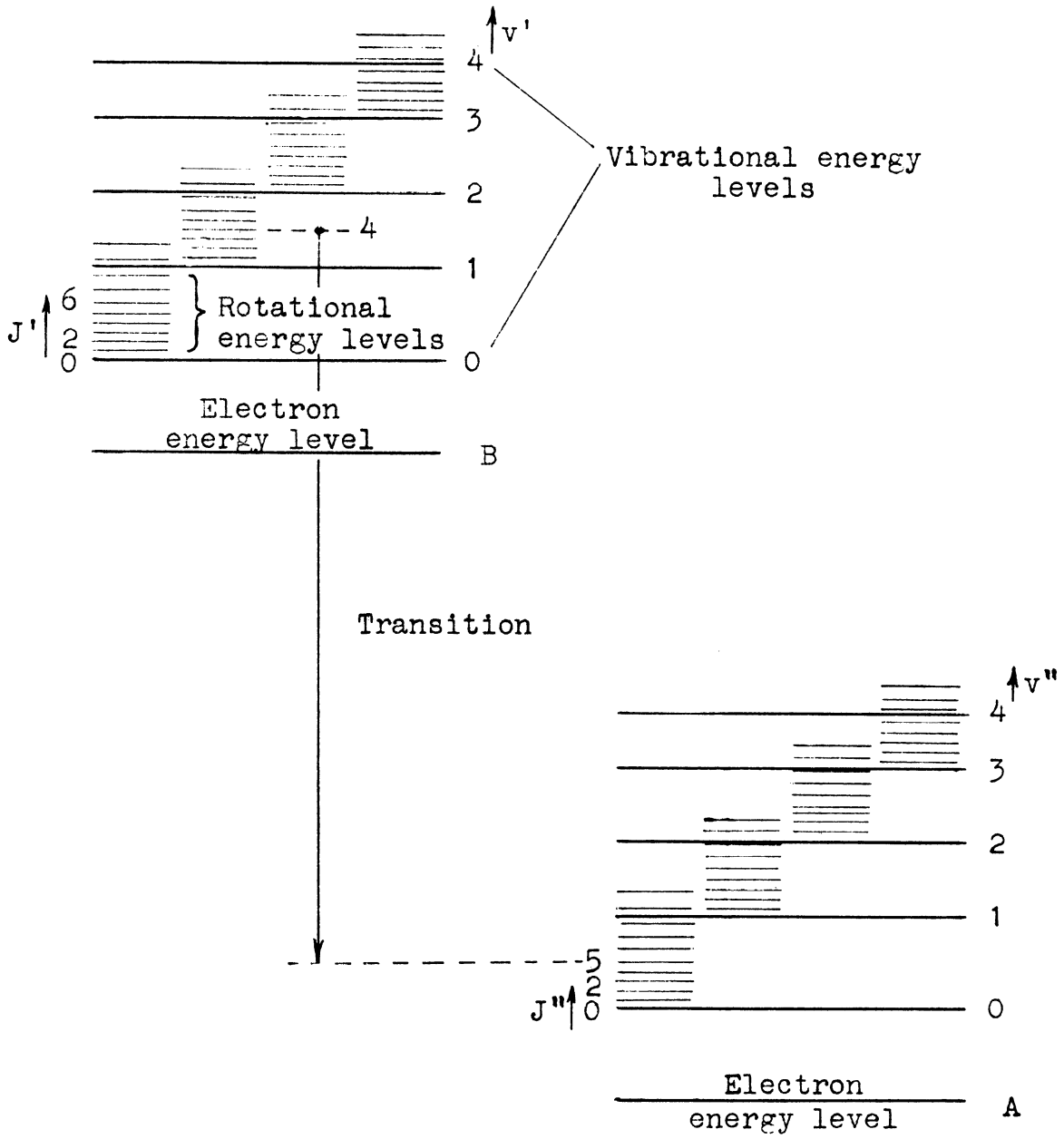

Figure 2. Schematic representation of the energy levels of a molecule.

P-branch, $\Delta J = -1$ form the R-branch, and $\Delta J = 0$ the Q-branch. The line formed by the transition shown in Figure 2 would be the $J = 4$ member of the P-branch of the 1, 0 band of the $B \rightarrow A$ band system. Bands formed as described above are called electronic vibrational rotational bands.

4.3.2 Temperature Determination from Bands

Both vibrational and rotational temperatures can be determined from the molecular bands. The vibrational temperature can be determined from the distribution of total intensities of bands in a band system while the rotational temperature can be determined from the distribution of line intensities within a single band. Only the rotational temperature determination will be discussed here. In emission, the intensity I of a line of quantum number J' is given by

$$I = \frac{C\nu^4}{Q_r} S_J \exp\left[-B_{V'}J'(J'+1)hc/kT\right] \qquad (4.16)$$

where C is a constant dependent upon the total number of molecules in the initial vibrational level and upon the quantum mechanical transition moment. Q_r is the rotational partition function and is a constant at a given temperature. The rotational constant $B_{V'}$ is a function of the initial electronic and vibrational states. It is inversely proportional to the moment of inertia of the molecule. An extensive tabulation of B's is given in Herzberg. The line strength S_J is a function of J which depends upon the type of transition taking place. If both electronic levels have zero electronic angular momentum, S_J is equal to $J' + J'' + 1$.

Equation (4.16) is based upon the rigid rotator approximation which neglects some high-order terms in J in the exponent. The effects of the approximation are negligible (51). A variety of methods can be used in connection with (4.16) for the determination of temperature. The classical method is to rearrange Equation (4.16) as

$$\ln \frac{I}{S_J} = \frac{C\nu^4}{Q_r} - \frac{B_{v'}J'(J'+1)hc}{kT} \quad . \tag{4.17}$$

This indicates that a plot of $\ln(I/S_J)$ for a number of lines in a band versus their $J'(J'+1)$ values will give a straight line having a slope of $-B_{v'}hc/kT$. Lines from any of the branches can be used as long as their proper upper quantum number J' is used. A plot of this type is called a molecular Boltzmann plot and the existence of a straight line is dependent upon thermal equilibrium. The disadvantage of the method, especially in plasmas where temperature gradients are present, is the large number of lines whose intensities must be measured.

The branches which compose an electronic vibrational rotational band normally overlap. In some cases members of the R- and P-branches having greatly different upper quantum numbers lie side by side in the recorded spectra. The relative intensity of such a pair of lines can be used to determine the temperature as is shown by writing Equation (4.16) for the line in each branch as

$$\frac{I_R}{I_P} = \frac{S_J^R}{S_J^P} \exp \frac{B_{v'}hc}{kT} \left\langle \left[J'(J'+1)\right]_P - \left[J'(J'+1)\right]_R \right\rangle \tag{4.18}$$

where the sub- or superscripts R and P refer to the respective branch. The frequencies ν have been cancelled since they are about equal. This method requires accurate measurement of the intensity ratio I_R/I_P. For most transitions the line strengths S_J are very nearly equal to 2J' for the P-branch and 2(J'+1) for the R-branch.

Another method which makes use of the branch overlap but which does not require intensity measurements has been developed by Greenshields (45) and by Knauss and McCay (61). Examination of the behavior of Equation (4.18) shows that at a given temperature there are a set of J' values for which the intensities of the R and P branches are equal. Now if the spectra is sufficiently resolved so that the position of equal branch intensity can be identified, the temperature can be calculated from Equation (4.18) by using the observed overlap quantum numbers. Unfortunately, many band spectra are not resolved adequately enough for use of this method.

4.3.3 Rotational Temperatures from Nitrogen Bands

In this thesis rotational temperatures were determined from the electronic vibrational rotational bands of N_2^+ molecules as well as from those of N_2 molecules. For the N_2^+ molecules, the band used was the 0, 0 band of the first negative band system. For the N_2 molecule, the band used was the 0, 0 band of the second positive band system. Both of these bands were free of overlap from other bands and contained only a few argon lines. None of the other observed bands were free from over-

lap. The various members of the N_2^+ band have been identified by Fassbender (35) while those of the N_2 band have been identified by Coster (23).

The first negative system of N_2^+ results from what is known as $^2\Sigma - {}^2\Sigma$ transition in the nomenclature of molecular structure (51). Because of a net electron spin, each of the $^2\Sigma$ energy levels is double, but in N_2^+ the spacing is extremely small. The two energy levels are assigned different values of the quantum number J (which is a measure of the total angular momentum including electron spin) but are assigned one value of the quantum number K (which excludes spin). Since the lines from the two levels are unresolved in most recorded spectra, the single observed line is described by the quantum number K. For all practical purposes, the quantum number J used in Section 4.2.3 can be replaced by K.

In the spectral data recorded for the 0, 0 N_2^+ band, the first 11 lines of the R-branch were exactly overlapped by lines 26 to 36 of the P-branch. The lower quantum number lines of the P-branch formed the unresolved band head. The R-branch lines 12 to 16 were covered by argon lines. This left for analysis only the numbers of the R-branch having quantum numbers greater than 16 since the P-branch intensity was too low to record in this high quantum number region. For data of this type, the molecular Boltzmann plot discussed in Section 4.3.2 is suitable for use. For the N_2^+ first negative band system the line strength S_J is given by $K' + K'' + 1$.

The second positive band system of N_2 results from a $^3\Pi - {}^3\Pi$ transition (51). Each of the $^3\Pi$ energy levels is triple because of electron spin. The bands formed actually consist of 3 P-branches, 3 R-branches, and 3 very weak Q-branches. The 3 P-branches are close together and the 3 R-branches are close together. The corresponding members of the triplet branches are specified by a single quantum number K. Since the triplet spacing is small, the single K value can be used to represent the energy levels involved. For all except small K values, the line strengths S_J of the N_2 second positive system are calculated on the basis of what is known as Hunds' coupling case (b). Expressions for the line strengths are given by Budó (14).

A tracing of the 0, 0 N_2 second positive band is shown in Figure 3. Not only are the triplet branches unresolved, but also the members of the P- and R-branches overlap each other. The identification numbers on the tracing are the quantum number of the R-branches. The P-branch quantum number corresponding to each peak is equal to the R-branch quantum number plus 19. The P-branch members of low quantum number form the bandhead at the left. The small peaks at K_R equal to 36 and 40 are due to argon lines. A change in the relative intensities of the overlapping lines can be seen in going from K_R equal to 19 to K_R equal to 26.

Unfortunately, none of the methods discussed in Section 4.3.2 is suitable for determining rotational temperatures from this spectra. A method which permitted the use of the unresolved peaks was developed. Since the 6 lines which made up each peak could be identified from

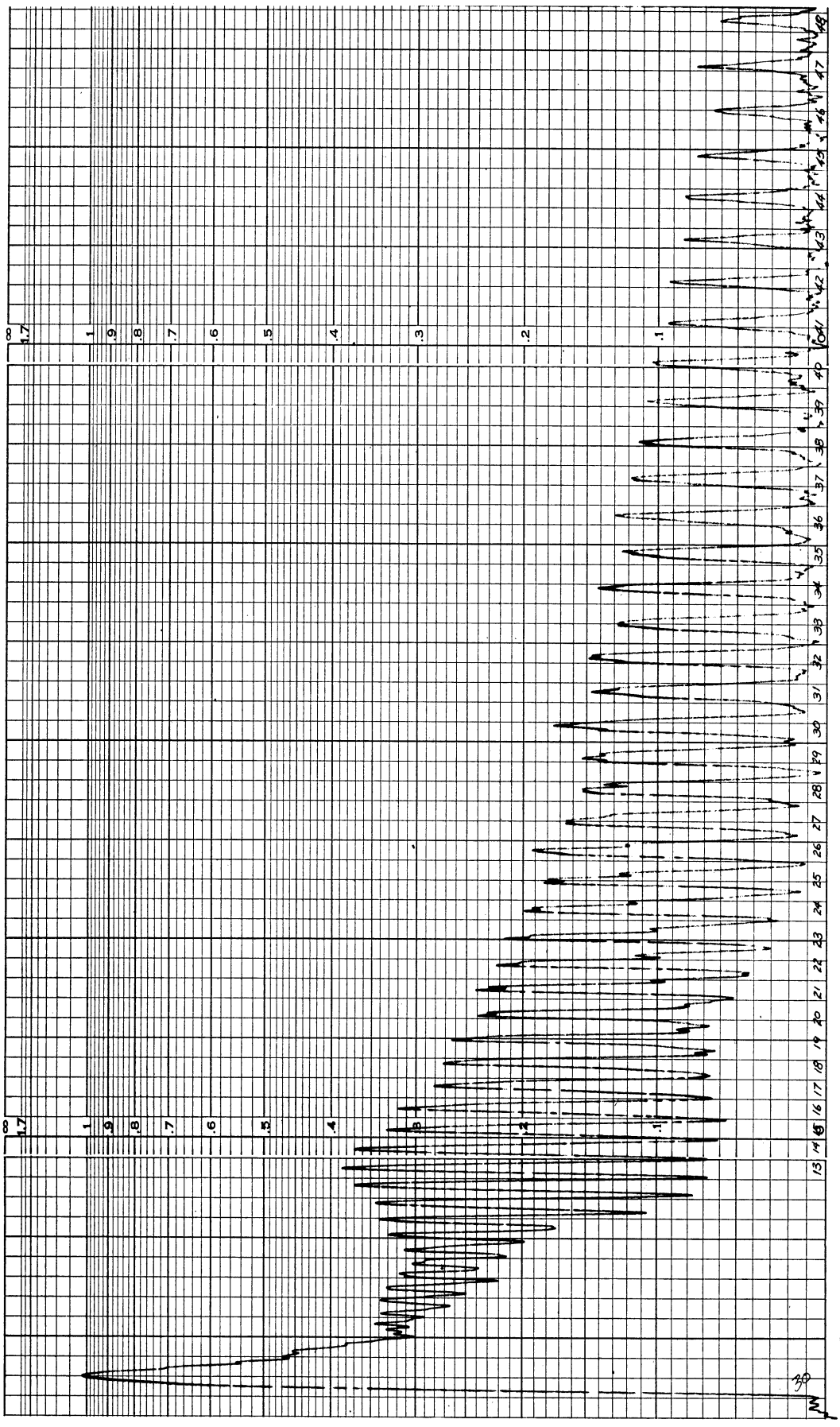

Figure 3. Typical tracing of the 0, 0 band of the nitrogen second positive systems.

Coster's data, the total intensity of each peak could be calculated from Equation (4.16) for a variety of temperature. Figure 4 is a plot based upon such calculations. All peak intensities were normalized to the one represented by $K_R = 13$. From the figure, it is seen that the variation in total intensity from peak to peak is a sensitive function of temperature. To determine a temperature, a similar plot was made from the measured peak intensities. Comparison with Figure 4 then indicated what temperature corresponded to the experimental values. (The plot shown incorporates a slight correction for the wavelength sensitivity of the spectrograph plates used in this work.)

4.4 TEMPERATURE DETERMINATION BY OTHER SPECTROGRAPHIC METHODS

Spectrographic methods can also be used to determine the electron temperature as well as the translational temperature of the atoms.

A continuum radiation is generated in a plasma by electron and positive ion recombination (radiative recombination) and by free-free electronic transitions (bremsstrahlung radiation). The intensity of this radiation can be used to determine the electron temperature. In argon plasmas such determinations have been made by Petschek (71) and by Rutowski (77). In an atmospheric pressure plasma the electron continuum radiation is about an order of magnitude lower in intensity than are the strong atomic lines. For this reason, and also since the determination involves the use of several arbitrarily determined constants, this method has no advantages over atomic lines for temperature determination.

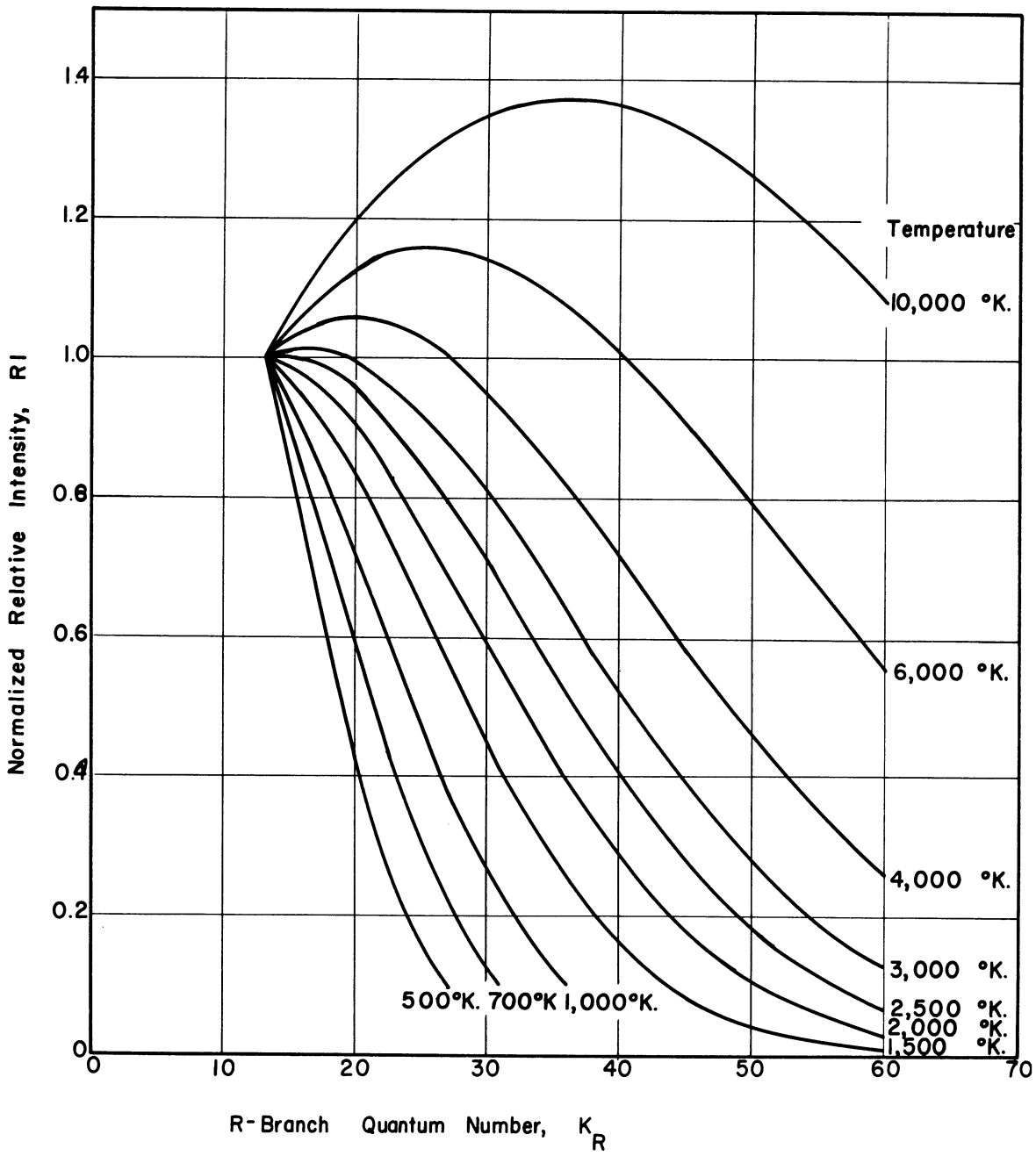

Figure 4. Combined R- and P-branch intensities of the 0, 0 band of the nitrogen second positive system.

The motion of atoms causes a broadening of spectral lines because of the Doppler effect. The motion is primarily due to random thermal motion and thus can be related to the translational temperature of the atoms. By means of very accurate spectrographic or by interferometric methods, the line broadening can be measured. Unfortunately in atmospheric pressure plasmas, collision (pressure) and Stark effect broadening are much greater than Doppler broadening (40). Thus it is very difficult to calculate reliable values for the translational temperature.

4.5 INVERSION OF LATERAL INTENSITY MEASUREMENTS TO RADIAL DISTRIBUTION

A spectrograph records all of the radiation coming along a chord passed through the plasma source. The lateral intensity which it records is equivalent to the integral of the various intensities along the chord. In an axial symmetric source which contains temperature gradients, the intensity actually has a radial distribution. It is thus necessary to convert the observed lateral intensities into true radial intensities.

The observed lateral intensity I(x) is given by Abel's integral equation as

$$I(x) = 2\int_{x}^{R} \frac{i(r)\ r\ dr}{(r^2-x^2)^{1/2}} \qquad (4.19)$$

where i(r) is the radial intensity considered as a point source. The radial distance r and the lateral distance x are measured from the cen-

terline of the source. R is the limit of the source beyond which there is no radiation. Abel's equation can be inverted analytically to give

$$i(r) = -\frac{1}{\pi}\int_r^R \frac{\frac{dI(x)}{dx}\,dx}{(x^2-r^2)^{1/2}} \quad . \tag{4.20}$$

Since it is not convenient to express the measured I(x) as an analytic function, Equation (4.20) must be solved by numerical methods.

The method used in this thesis was the one developed by Nestor and Olsen (68). Their method divides the x-axis into zones of equal width and solves Equation (4.20) by dividing the integral into sub-integrals over each zone. I(x) is assumed to be a linear function of $\sqrt{x}$ in each zone. Their final result is the radial intensity I(r) averaged over the zone thickness. A digital computer was used to perform the calculations for this thesis. The x-axis was divided into from 11 to 34 zones for this work.

Although the method of Nestor and Olsen avoids directly forming the derivative dI(x)/dx in Equation (4.20), the net effect of the conversion from laterial to radial intensities is the differentiation of the input data. Thus small errors in I(x) cause large changes in I(r). This is especially true near the centerline. Slightly better results are obtained when the I(x) data are graphically smoothed before inversion.

The method of Nestor and Olsen puts no requirement upon the behavior of I(r) other than that it be continuous. Sometimes better re-

sults can be obtained by specifying slopes or discontinuities in I(r) (12). Freeman (37) also suggests several modifications in the inversion method.

4.6 SPECTROGRAPHIC COMPOSITION MEASUREMENT

The intensity of a spectral line is always a function of the number of atoms present as well as the temperature. Thus if the temperature is known by some independent measurement, the number of atoms in a mixture, or the composition, can be determined from the measured line intensity. The temperature must be known with great accuracy since it affects line intensity exponentially while composition only causes a linear change.

When atomic multi-line temperature determinations or molecular band determinations are used, the same data can give both temperature and composition. The temperature is determined from the relative line intensities while the composition is determined from the absolute intensity of one of the atomic lines or of the band. The calculation of course involves the use of absolute transition probabilities. These have already been mentioned in connection with argon lines. For the N_2 second positive band system and the N_2^+ first negative system the appropriate transition data are given by Keck (60).

In this thesis the temperature determinations were not considered to be of sufficient accuracy for meaningful spectrographic composition determinations.

5. SAMPLING PROBE MEASUREMENT OF PLASMA PROPERTIES

5.1 INTRODUCTION

A water cooled sampling probe can be used for the determination of plasma jet properties. With proper instrumentation such a probe can measure composition, flow velocity, and perhaps enthalpy. The advantage of a probe is that it is capable of making a measurement at a specific point within the plasma. As discussed in Section 4.5, spectrographic results require mathematical inversion before they apply at a given point. A sampling probe consists of little more than a pitot tube equipped with water jacket. The probe used in this work is shown in Figure 10 in the apparatus section. Grey (46) and Chludzinski (18) have used similar probes.

5.2 DETERMINATION OF COMPOSITION

By aspirating through the probe, a gas sample can be withdrawn from the plasma. The use of a sampling rate less than or equal to the rate of arrival of material at the probe tip should cause no perturbation of the upstream flow conditions. The gas sample, which is cooled to ordinary temperatures in passing through the probe, can be analyzed in a variety of ways. For the simple argon-nitrogen system used in this work, a thermal conductivity cell was adequate. Gas chromatography could be used for more complicated systems.

5.3 DETERMINATION OF VELOCITY

The sampling probe when used for velocity measurements is exactly equivalent to a pitot tube. The free stream velocity is calculated by application of the Bernoulli energy equation

$$v_2^2 - v_1^2 = -2\int_1^2 \frac{1}{\rho}\, dP \quad . \tag{5.1}$$

In the equation, ρ is the fluid density, P the hydrodynamic pressure, and v the velocity. When applied to a pitot tube, v_1 is the free stream velocity, v_2 is zero, and dP corresponds to the change between free stream (1) and probe tip stagnation (2) pressure. The integral is path dependent. For an isothermal constant density change its value is $(P_2 - P_1)/\rho$. However, for a water cooled probe placed in a high temperature plasma jet, the pressure increase does not occur under constant density conditions. If it is assumed that the decrease in temperature between the free stream and probe tip occurs in inverse proportion to the pressure increase, the integral can be easily evaluated. For densities determined from the idea gas law the result is

$$v_1^2 = \frac{2(P_2 - P_1)}{\rho_1} \frac{T_1 + T_2}{2T_1} \tag{5.2}$$

where T_1 is the free stream temperature and T_2 the temperature of the probe tip.

The assumption of proportionality between the temperature and pres-

sure changes is equivalent to assuming equal momentum and thermal boundary layer thickness. For flow across a heated plate (10), the ratio of the thermal to momentum boundary layer thickness if approximately equal to the one-third power of the Prandtl number ($\mu c_p/k$). At 5000°K, a temperature between that of the plasma and that of the probe, the Prandtl number for argon is about 0.75. The ratio of boundary layer thickness is thus 0.91. This result indicates that the assumed proportionality between temperature and pressure is reasonable.

Grey made no correction for the density change in his work.

5.4 DETERMINATION OF ENTHALPY

The cooling water jacket of the sampling probe can be equipped with thermocouples so that the energy absorbed by the cooling water can be determined. The temperature of the gas sample at the exit from the probe can also be determined.

The probe method of enthalpy determination makes use of a "tare" measurement which eliminates the need to know the heat transfer rate to the outside of the probe. A valve in the gas sample line is closed, thus preventing gas from entering the probe, and the rate of energy addition to the cooling water is measured. Then the value is opened, allowing a gas sample to flow through the probe, and the same measurements are repeated together with those of the gas temperature at the probe exit and the gas sample flow rate. The energy content of the gas sample is given by the difference between the rates of energy addition to

the cooling water. Since the exit enthalpy of the gas can be determined from the measured gas temperature, the unknown gas enthalpy at the probe entrance can be calculated. The effectiveness of the "tare" measurement is critically dependent upon the duplication of flow conditions near the probe tip in the "flow" and "no-flow" cases. This problem will be discussed in the results section.

Once the enthalpy and composition of the plasma is determined, the temperature can be found by reference to tables of the thermodynamic properties of the plasma gas. For argon and nitrogen plasmas, Drellishak et al. (31,32) have used statistical mechanics to calculate extensive tables of partition functions and thermodynamic properties.

6. EXPERIMENTAL APPARATUS AND PROCEDURES

6.1 PLASMA GENERATOR

6.1.1 General Description

The plasma generator used was of the direct-current arc type. The design of the generator, as shown in Figure 5, is typical of many generators in use. The plasma gas, usually argon, was passed through an arc struck between the cylindrical tungsten cathode and the annular copper anode.

The generator was fabricated in the machine and welding shops of the Department of Chemical and Metallurgical Engineering. The generator was designed to permit flexibility in its operation and maintenance. The copper anode, tungsten cathode, and gas distribution ring are all removable. The separate cooling water passages for the anode, cathode, and main body are all completely sealed in metal, so there is no possibility of water leaks into the plasma stream through "o"-ring seals, etc. The anode was held in place either by a brass retaining ring or the mixing chamber which is described in Section 6.2.

The gas for the plasma was supplied through a calibrated Fischer-Porter rotameter. The cooling water used was from the room tap supply at approximately 60 psig and was supplied to the generator through calibrated rotameters. Calibrated copper-constantan thermocouples were used in all gas and water streams. The outputs from the various thermocouples

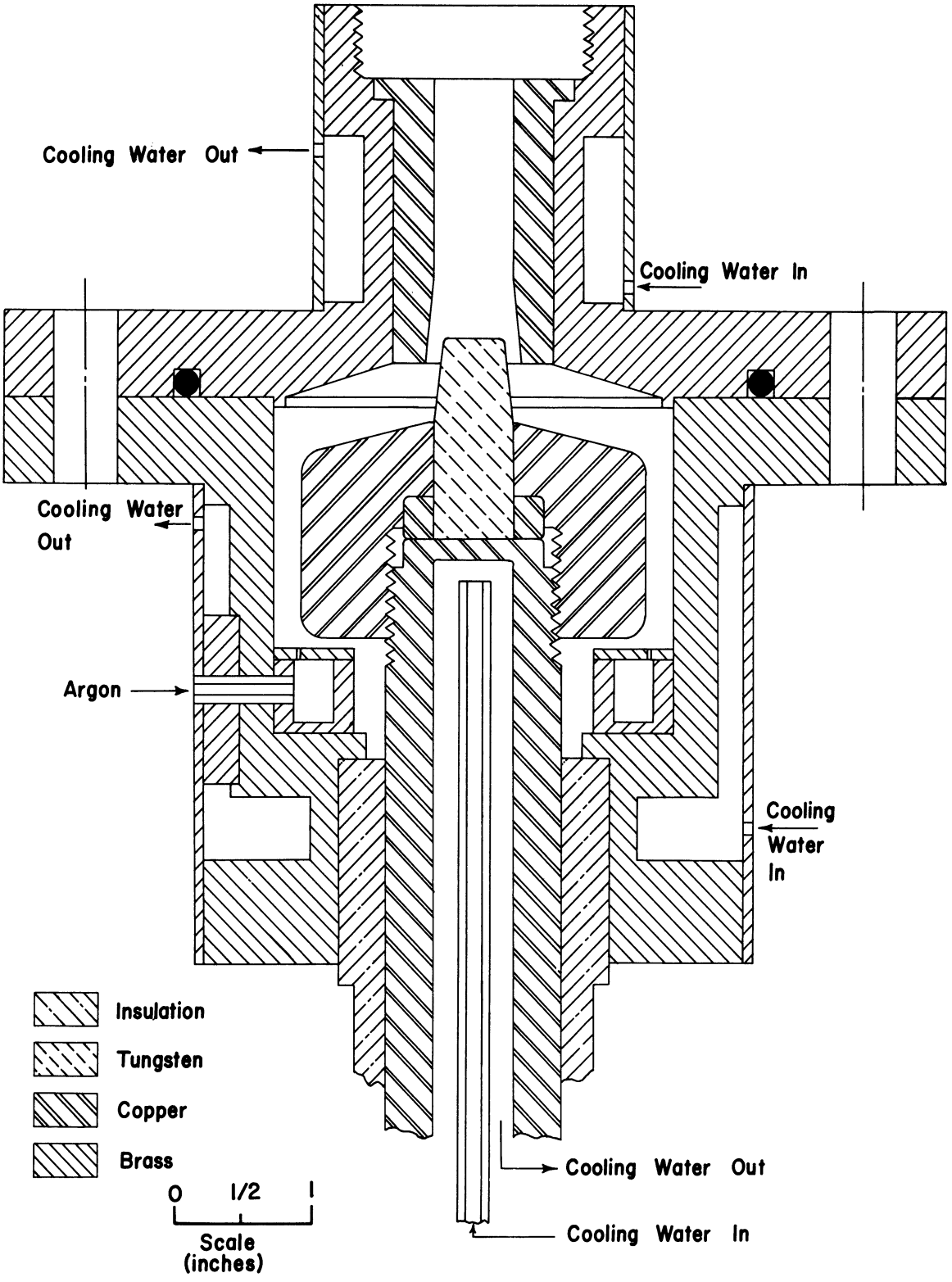

Figure 5. Arc plasma generator.

could be switch-selected and recorded on a Leeds & Northrup Speedomax HARZ recording potentiometer. The direct current power for the plasma generator was obtained from two General Electric Model 6WD33B1 welding generators. Each welding generator was capable of 40 volts at 300 amperes. The generators were connected to a control panel which permitted their outputs to be connected in either series or parallel and which provided for their simultaneous starting. The control system also monitored the voltage and current and provided for automatic stopping of the generators in case of low cooling water or plasma gas pressure. The plasma generator system is shown schematically in Figure 6 and a photograph of the system is presented in Figure 7. In the photograph, the scanning and condensing system (Section 6.3.3) is at the extreme left, the plasma generator is in the left center, the flowmeters and recording potentiometer are in the right center, and the generator control panel is at the extreme right.

6.1.2 Start-up Procedures

The generation of the plasma was initiated by using a Miller Model HF-20-2 high frequency arc starter. In starting the plasma generator, the argon flow was first started and then the arc starter turned on. With the starter on, the concentricity of the anode and cathode could be determined by looking into the nozzle of the generator. If everything appeared satisfactory, the argon flow was increasdd to its maximum operating rate, and the welding generators were started. After the plasma

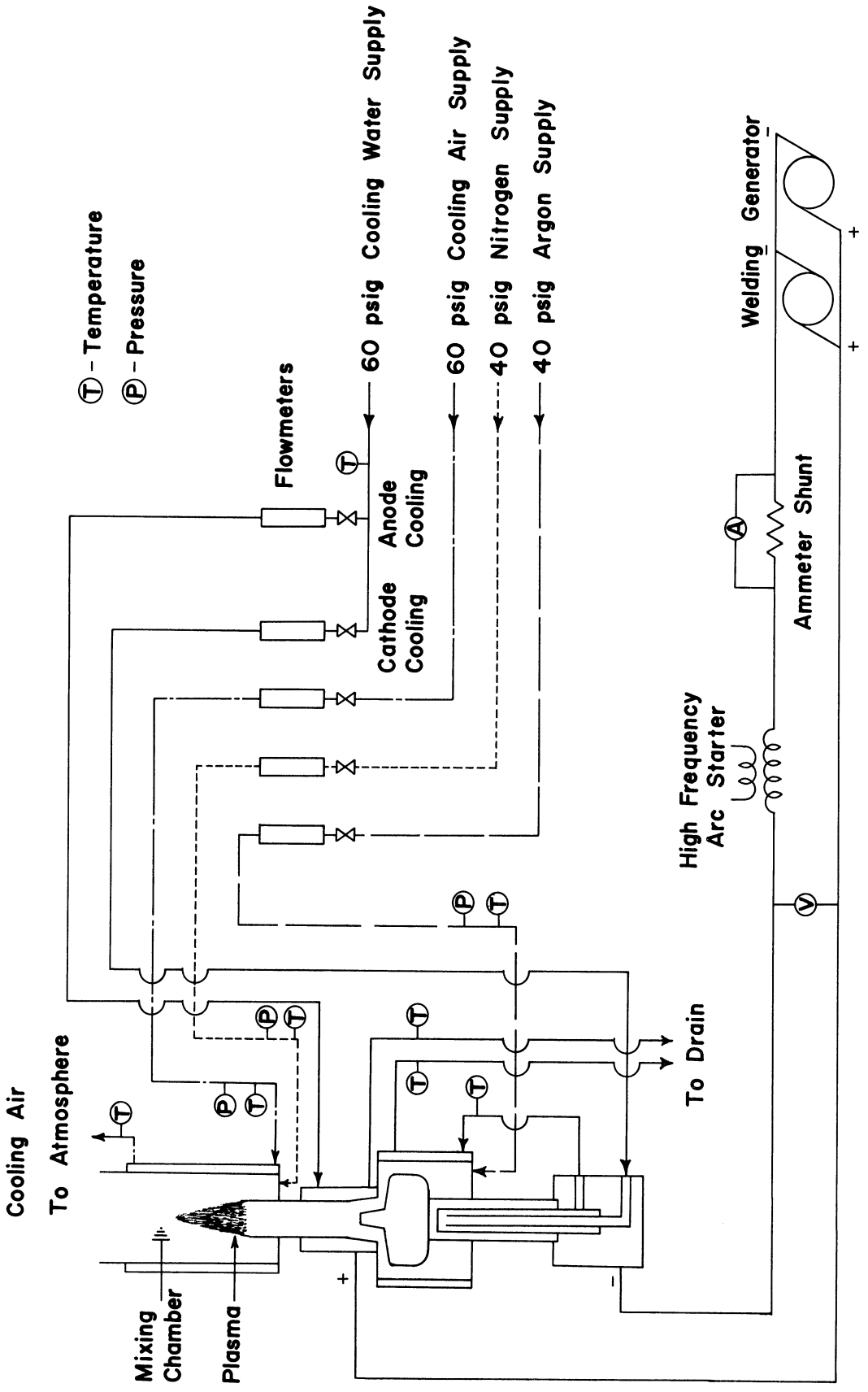

Figure 6. Schematic diagram of experimental set-up.

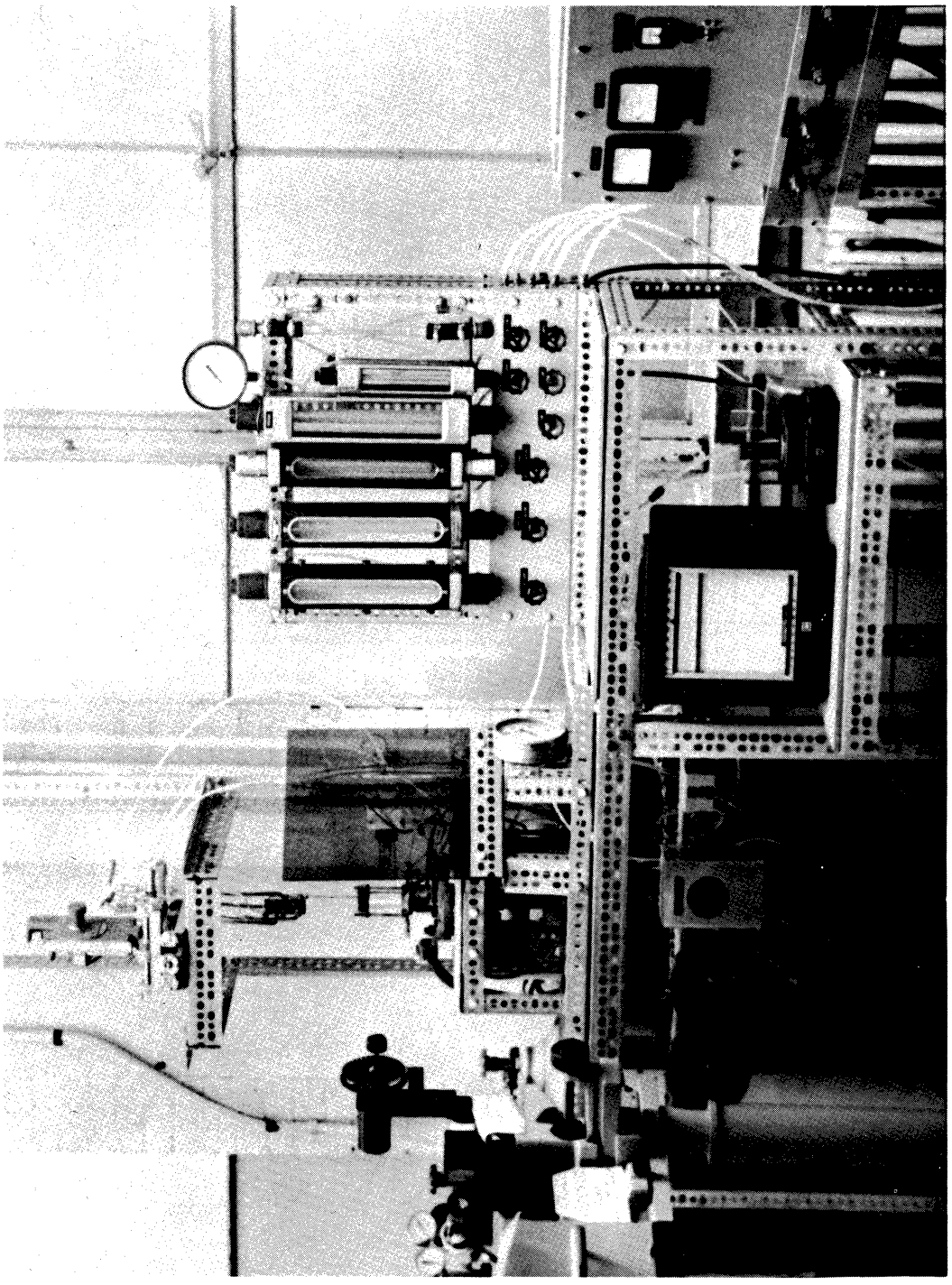

Figure 7. Photographic view of experimental equipment.

appeared, the arc starter was turned off.

6.1.3 Operating Characteristics

By use of an appropriate gas distribution ring, the plasma generator could be operated with either vortex or axial gas flow through the arc region. Most commercially built plasma generators employ vortex stabilization (42, 56). This permits operation at higher voltage, and thus higher efficiency, and also allows a slightly larger range of usable flow rates. Many laboratory units also use vortex stabilization or rotate the arc by using a transverse magnetic field. If used only as a source of high temperature, a vortex stabilized plasma is probably optimum. But if the flow and mixing properties of the plasma stream itself are to be studied, the more easily analyzed axial flow situation is desirable.

The plasma generator fabricated for this thesis was operated initially with vortex flow and later with pure axial flow. All of the reported measurements were made while using axial flow. With vortex flow, the plasma jet had an unsteady "cork-screw" appearance. With axial flow, the jet had a steady symmetrical appearance. Rittenhouse (76) reported corresponding results for a plasma generator similar to the one used here. Other workers, such as Wheaton (82), have also employed axial flow.

The plasma generator was operated at various times using helium and nitrogen in addition to argon. For operating with argon, the welding generators were connected in parallel, and the plasma generator operated

with approximately 20 volts between the cathode and anode. For operation with either helium or nitrogen, the welding generators were connected in series. The plasma generator was always started with argon, and then increasing amounts of helium or nitrogen were added until the argon was completely replaced. With helium the plasma generator operated stably and maintained approximately 50 volts between the electrodes. With nitrogen the operation was unstable and caused noticeable erosion of the nozzle.

The plasma generator was operated with argon flow rates from 20 to 90 grams per minute. In the low flow rate region (20 to 40 grams per minute), operation was quiet, and the plasma jet had a steady, highly luminous, cone-shaped appearance. In the high flow rate region (50 to 90 grams per minute), operation was noisy, and the plasma had a more cylindrical shaped appearance. Wheaton observed similar phenomena with his plasma generator. In plasma jet discussions, the low flow rate jets are considered laminar, and the high flow rate jets are considered turbulent. However, in neither case, is the luminosity of the jet constant. In this work the frequency of the fluctuations was measured with the undispersed radiation monitor (described in Section 6.3.2) and an oscilloscope. The frequency of the predominant waveform was found to be 2000 cycles per second but the magnitude was not measured due to the complicated waveform present. The welding generator dc power supply itself had a rms ripple of 0.9% at 2000 cycles. Jahn (55) took high speed photographs (5000 frames per second) of his plasma jet and found that the apparently

steady cone-shaped luminous region was in fact a region of rapidly changing irregular shape.

For all of the work reported in this thesis, the plasma generator was oriented with its axis vertical and with flow upward. Most of the data were obtained with a power input to the generator of about 8 kilowatts. Under these conditions the generator operated at an efficiency of about 40%. The efficiency was highest at high flow rates.

6.1.4 Contamination

Under normal operating conditions the plasma generator operated with no erosion or change in the visual appearance of the electrodes. The plasma spectra under these conditions contained no copper lines but did contain a few weak tungsten lines. The presence of tungsten in the plasma flow is discussed again in the section describing the mixing chamber (Section 6.2).

On some occasions when high power input rates and low argon flow rates were being employed, the plasma generator would malfunction. Then the voltage between the electrodes would decrease, the current input increase, and the plasma become green due to the presence of strong copper lines. This malfunction was probably due to the formation of a hot spot on the copper anode. Noticeable erosion of the anode occurred unless the generator was immediately turned off.

6.1.5 Run Time

The plasma generator was capable of indefinitely long operation. During the course of the work the generator was operated for a total of about 70 hours. The duration of a typical data taking run was approximately 1.5 hours.

During a run the voltage between the electrodes remained constant but the current decreased slightly due to the heating up of the windings of the welding generators. This drop could be removed by advancing the field control rheostats on the welding generators. By making this adjustment, the power level during a run could be held within about 1% of being constant. The voltage was monitored with a Weston laboratory voltmeter which gave a measurement accuracy of 1.5% (0.3 volt). The current was measured using a General Electric 1000 ampere shunt having 1% accuracy and a calibrated Simpson millivolt meter.

6.1.6 Gas Supplies

The gases used during this study were welding grade argon and helium and oil pumped nitrogen all supplied by General Dynamics in size 1A cylinders. The output from the cylinders was reduced to approximately 40 psig with Matheson regulators for supply to the plasma generator system.

Runs were made using argon for both the plasma and coolant gas in order to determine the purity of the argon supply. Under these conditions only a very faint molecular nitrogen spectra was present and its intensity was below the threshold of measurement.

6.2 MIXING CHAMBER

6.2.1 General Description

The mixing chamber is shown in Figure 8. The mixing chamber screwed directly into the top of the plasma generator. It was found necessary to line the plasma jet nozzle with a copper liner in order to obtain adequate cooling. The inside diameter of the resulting nozzle was 11 millimeters. Not shown in the drawing is a circumferential copper tube which was soldered around the lower brass section of the mixing chamber to provide additional cooling. The nitrogen gas entered the mixing chamber through an annular porous stainless steel ring around the plasma nozzle. To obtain adequate flow, the ring also contained 8 equally spaced 1/32 inch holes. The ring was force-fitted into place. The plasma jet and nitrogen flow was confined inside the 27 millimeter inside diameter (30 mm OD) quartz tube. The length of the tube was approximately 5 inches. This length was selected to prevent organ-pipe resonance with the 2000 cycle ripple component present in the power supply and plasma.

6.2.2 Mixing Chamber Cooling

As shown in Figure 8, the quartz mixing chamber was surrounded by a 38 millimeter outside diameter Pyrex tube. The annular space was designed to provide for cooling with either water or air. During operation with water it was found that a violet-black mirror like deposit rapidly formed on the inside of the quartz tube. This deposit is believed to be tungsten from the plasma jet which condensed on the cold wall. The de-

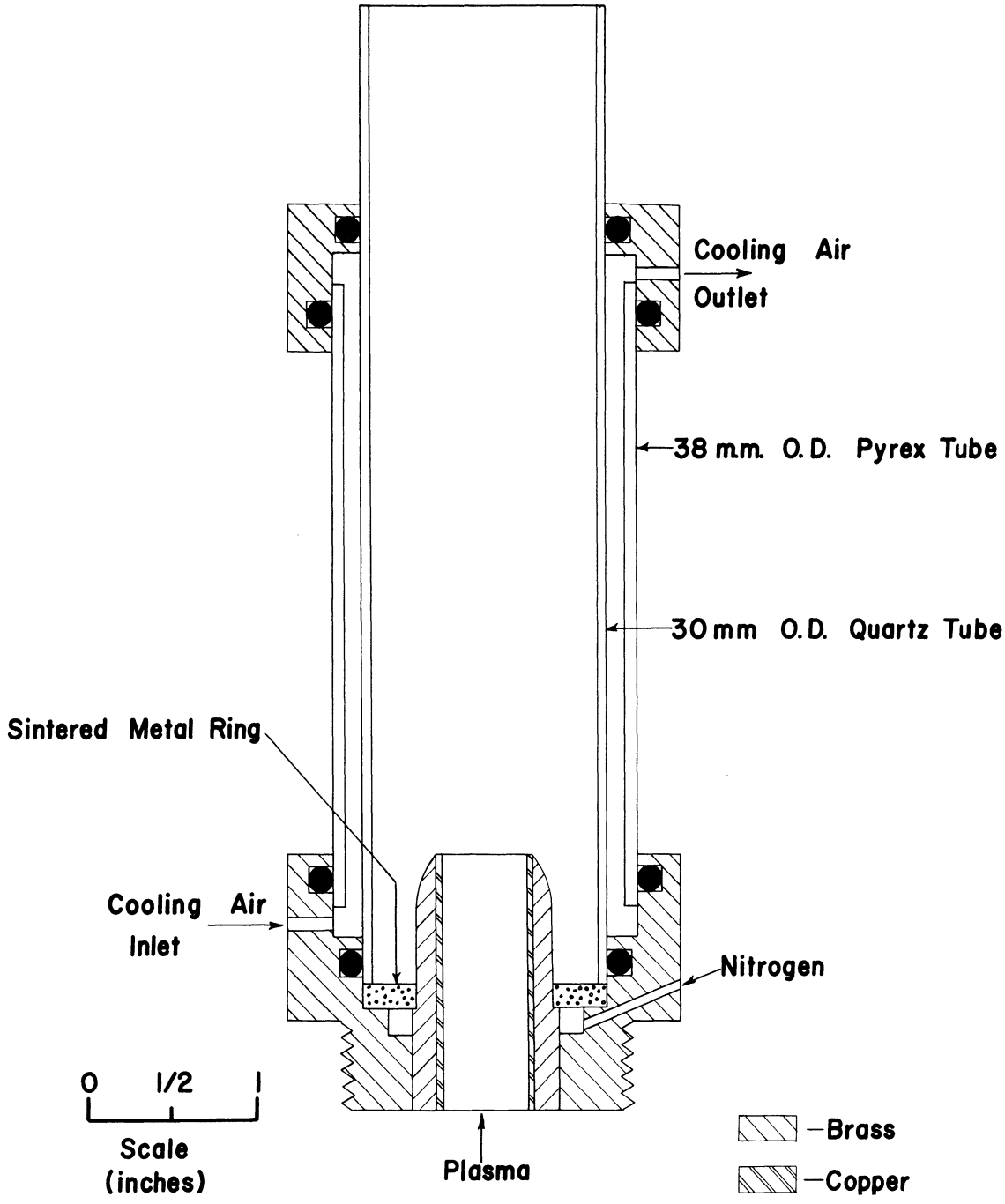

Figure 8. Plasma-coolant gas mixing chamber.

posit greatly attenuated the light output from the plasma. When air cooling was tried, it was found that the deposit formed only very slowly and that its lower edge began about 2 centimeters downstream from the plasma nozzle. The quartz tube, of course, operated at a much higher temperature when air cooled. Its upper end was incandescent when low nitrogen coolant rates were employed. This prevented the use of "o"-rings in the upper brass collar, and the cooling air escaped around the tubes as well as through the regular outlet. Air cooling was used while all of the data reported in this thesis were being taken.

6.2.3 Light Transmittance

The quartz and Pyrex mixing chamber walls transmitted the observed visible and near-ultraviolet light from the plasma without attenuation (20). The walls did act slightly like a lens and the deviations of light rays passing through the walls is illustrated in Figure 9. It is seen that the deviation did not introduce any significant error in the lateral position of chords passing through the plasma.

6.3 SPECTROGRAPH

6.3.1 General Description

The spectrograph used was a 3.4 meter focal length Ebert Mark IV stigmatic plane grating spectrograph manufactured by the Jarrell-Ash Company (57). The spectrograph was equipped with a grating ruled with 15,000 lines per inch which gave a first order linear dispersion of 5.1 Å per millimeter at the focal plane. The useful range of the grating was

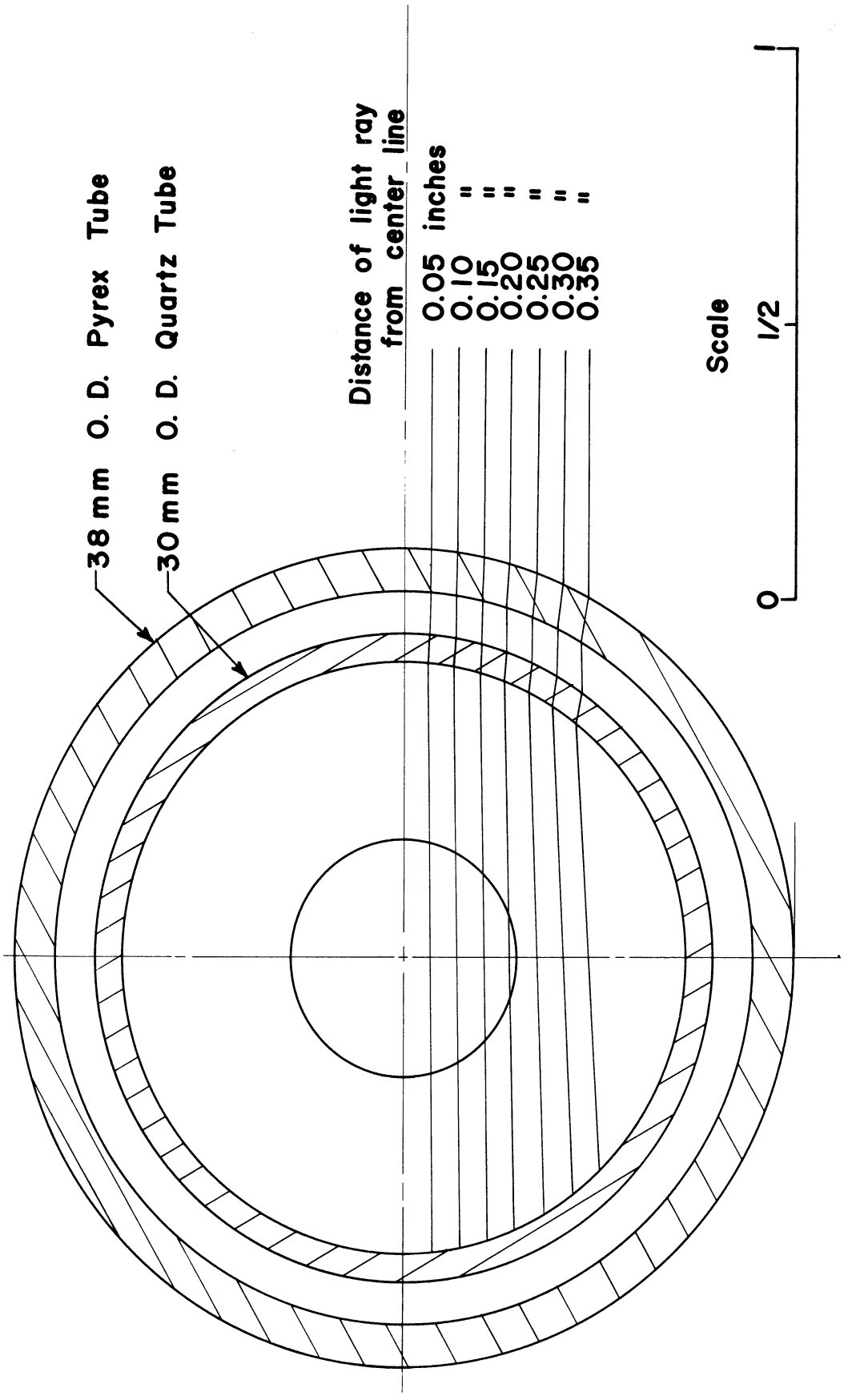

Figure 9. Light path through walls of mixing chamber.

from 2100 to 7500 Å. The effective aperture ratio of the spectrograph was F/35. The entrance slit was adjustable in width from 4 to 400 microns and in height from 1 to 15 millimeters. The spectra was recorded on two glass 4 x 10 inch photograph plates which were placed end to end. Thus the total first order range which could be recorded during one exposure was 2400 Å. The techniques for developing and analyzing the photographic plates are given in Appendix A. The spectrograph was supplied equipped with the accessories described in the following two sections.

6.3.2 Undispersed Radiation Monitor

The undispersed radiation monitor (Jarrell-Ash No. 70-020) used a quartz plate to reflect about 1% of the radiation entering through the slit of the spectrograph onto the cathode of a 1P28 phototube. The output current of the phototube was then read on a microammeter. The monitor normally served as an exposure meter for the spectrograph, but as mentioned previously, it was also used to study fluctuations in plasma intensity.

6.3.3 Scanning and Condensing System

The scanning and condensing system (Jarrell-Ash No. 18-022) could scan and bring selected areas of an extended source into focus on the spectrograph slit. The system of 6 front surface mirrors and 2 quartz-lithium fluoride acromatic doublet lenses maintained focus and alignment with the optical axis of the spectrograph automatically. The

lenses caused a 3 to 1 reduction in image size between plasma source and spectrograph slit.

The plasma was scanned horizontally (perpendicular to the plasma axis of symmetry) by turning a screw drive mechanism which moved the mirror assembly and vertically (parallel to the plasma axis) by pivoting a mirror. The horizontal scan permitted accurate positioning along chords passing through the axial-symmetric plasma. The chord spacing could be as little as 0.0125 inch.

6.3.4 Operating Procedures

The spectrograph and plasma generator were located so that the spectrograph slit was parallel with the axis of the plasma jet. Most of the data were recorded while using a slit width of 20 microns and a slit height of 1.5 millimeters. The 1.5 millimeter slit height permitted 42 exposures to be made on a single set of spectrographic plates. The plasma was scanned at 0.025 inch intervals in the lateral direction and at 0.8 centimeter intervals in the vertical direction.

At various times during the work, Eastman Kodak SA-1, IV-N, and 103a-F spectrographic plates (33) were used. These permitted coverage of the spectral region from the near ultraviolet (2500 Å) to the near infrared (9000 Å). All of the spectrographic results reported in this thesis were taken using the 103a-F plates. The 3000 Å region where many nitrogen bands are present, as well as the 4000 and 5000 Å regions where argon has many lines, could be recorded with a single exposure. Exposure

times, controlled by the electromagnetic shutter in the spectrograph, ranged from 3 to 300 seconds. For calibration purposes, several bands of tungsten continuum radiation were recorded on each plate. More information about the photographic procedures is given in Appendix A.

6.4 SAMPLING PROBE

6.4.1 General Description

The sampling probe is shown in Figure 10. It is essentially a pitot tube equipped with a cooling water jacket. Small stainless steel tubing was used in constructing the probe. At the tip, the annulus between the outer and inner tubes was sealed by silver soldering and a copper ring. The other ends were joined to enlarged sections which served as manifolds for cooling water. Copper-constantan thermocouples were used to measure the temperature of each stream at the entry to, or exit from, the probe. Similar probes have been used by Chludzinski (18) and Grey (46).

6.4.2 Associated Equipment

The probe was mounted on a 3-dimensional traversing mechanism which permitted positioning of the probe tip anywhere in the plasma with an accuracy of $\pm$ 0.01 centimeters. Filtered cooling water was supplied to the probe through a calibrated rotameter from a 90 psig constant pressure water supply. The water supply consisted of a 40 gallon tank pressurized with compressed air. For making impact pressure measurements, an in-

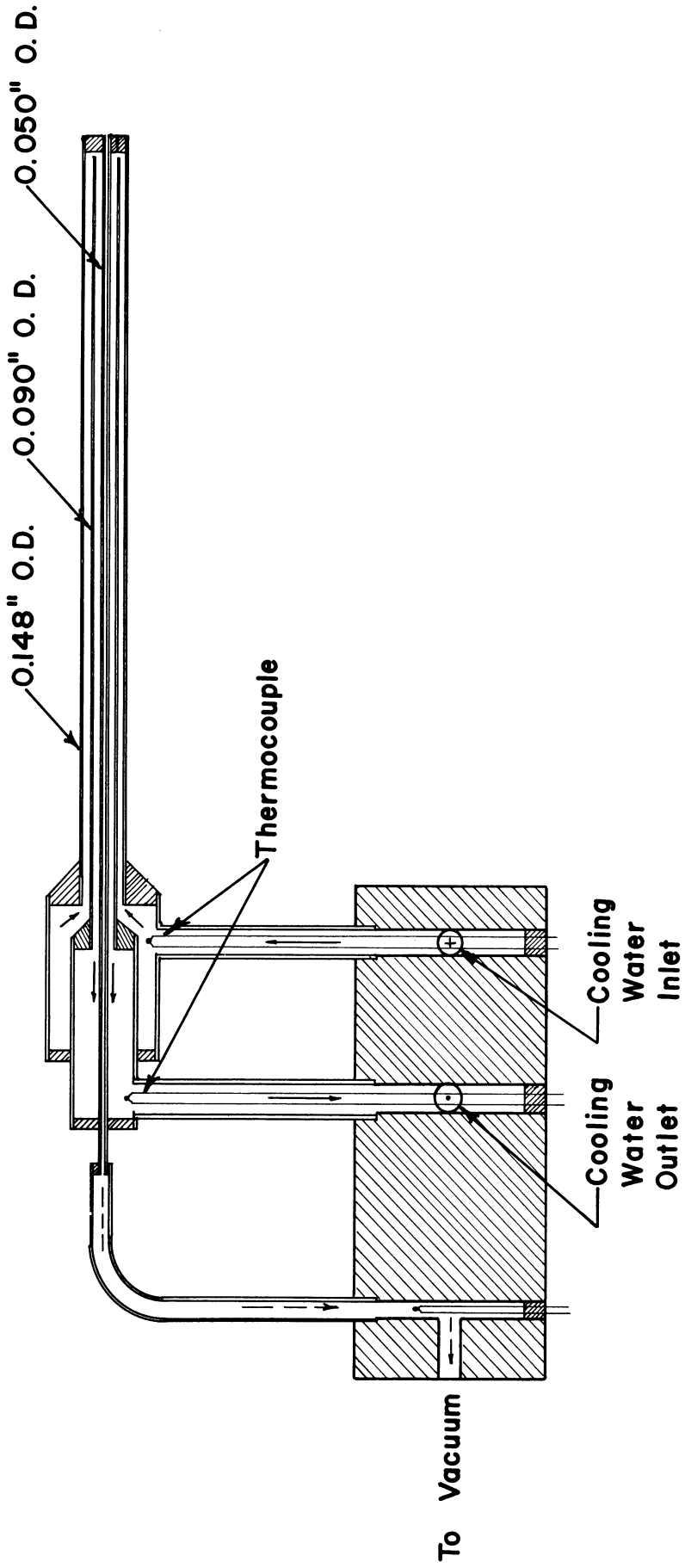

Figure 10. Water-cooled sampling probe.

clined water manometer was used for plasma flow conditions and a 2-fluid methanol-n-heptane manometer was used for cold flow conditions. Calibration of the 2-fluid manometer gave its sensitivity as approximately 10 cm of fluid/cm of water. When making enthalpy and composition measurements, the gas samples were drawn through the probe with a vacuum pump, needle valve, and rotameter system. Additionally, when making composition measurements, the gas sample was passed through a heated thermal conductivity cell (Gow-Mac Instrument Co. Model TR2B). The thermal conductivity cell was directly calibrated with argon-nitrogen mixtures.

6.4.3 Operating Procedures

For impact pressure measurements, the end of the sampling tube was closed off with one of the manometers, and the pressure directly read. During composition measurements, the output from the thermal conductivity cell was recorded with the Leeds & Northrup recording potentiometer. The composition reading reached its equilibrium value in about one minute. Enthalpy measurements were made by recording the rises in probe cooling water temperature (differential thermocouple output) for sampling and non-sampling conditions. The response was almost instantaneous.

6.5 RADIATION LOSS MONITOR

An estimate of the radiation losses from the plasma jet was obtained by using a Leeds & Northrup mirror type rayotube (No. 8843). This device uses a spherical mirror to focus incident radiation upon a thermopile. Because of the mirror, and a protective lens, the rayotube responds ef-

fectively to only visible, near ultraviolet, and infrared radiation. The temperature calibration of the rayotube was converted into intercepted energy per unit area units.

6.6 EXIT GAS CALORIMETER

The exit gas calorimeter, shown in Figure 11, provided a check on the energy content of the plasma. The calorimeter, constructed from various sizes of copper tubing, fitted over the end of the quartz mixing chamber tube. The gases were drawn through the calorimeter with a vacuum cleaner blower.

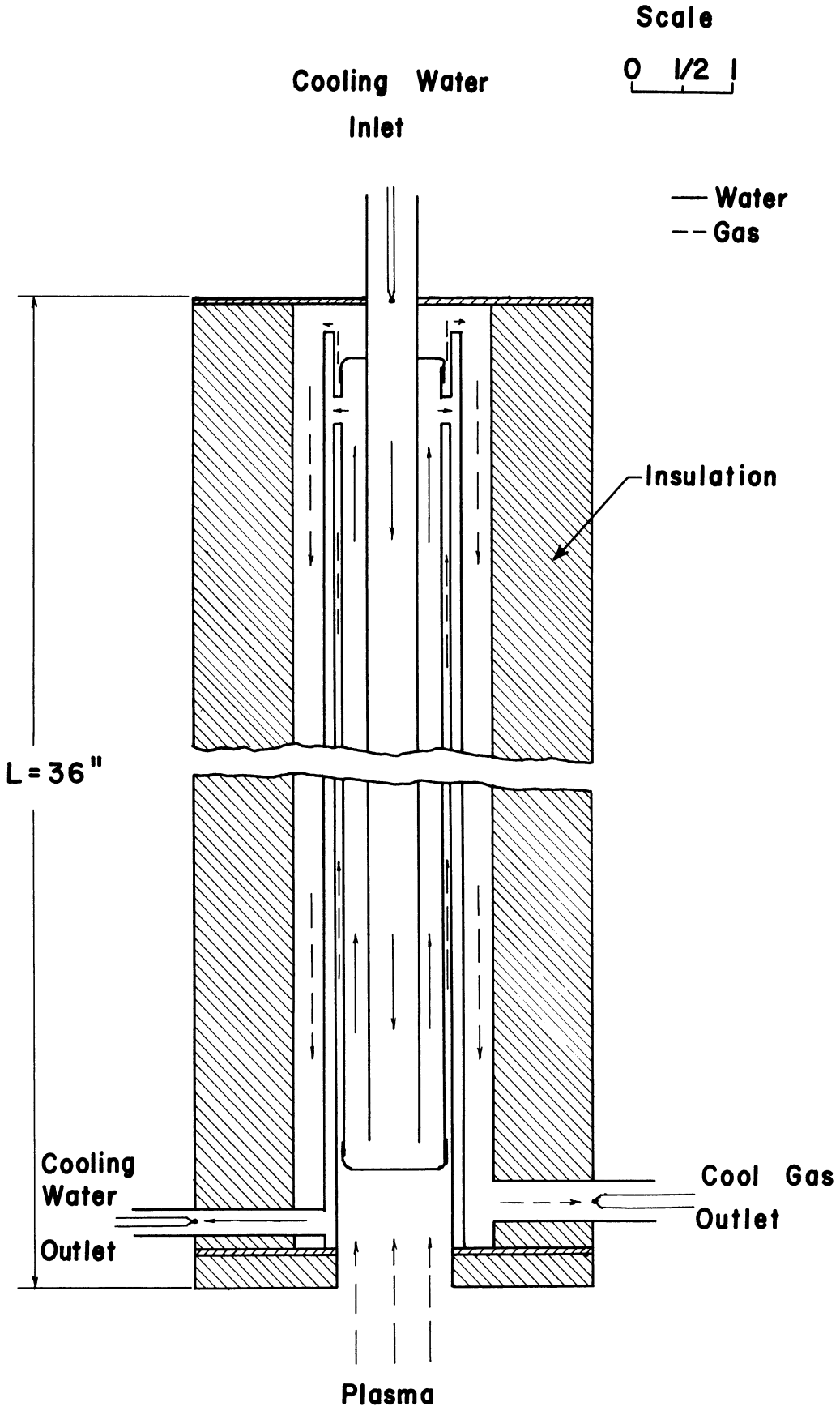

Figure 11. Exit gas calorimeter.

7. EXPERIMENTAL RESULTS AND THEIR ANALYSIS

7.1 INTRODUCTION

7.1.1 Preliminary Work in Selecting System

The factors considered in the selection of the system for study have already been mentioned in Chapter 1. The three systems tried experimentally were an argon plasma with helium coolant, a helium plasma with argon coolant, and an argon plasma with nitrogen coolant. In the argon plasma-helium coolant system, no helium spectral lines could be detected in the luminous mixing region even with long spectrographic exposures. Even for an equilibrium system at 10,000°K this result is expected since Equation (4.5) indicates that the strong helium line intensities would be only 10^{-3} times that of the strong argon lines. In the helium plasma-argon coolant system, the argon lines were not detectable with reasonable spectrographic exposures. This result was unexpected, but still plausible. A monoatomic gas like argon has only a relatively small number of widely spaced electronic energy levels. Excitation requires that the full amount of energy be supplied in one collision. The required energetic collisions are rare. Similar results have been noted by Gaydon (40). In the argon plasma-nitrogen coolant system, good spectra from both argon and nitrogen were obtained. This system was used for all of the mass and energy transfer studies.

7.1.2 Scope and Nature of Data Obtained

The various plasma and flow conditions considered are listed in Table I. As can be seen, the majority of the work was performed with a plasma

TABLE I

KEY TO FLOW CONDITIONS

Flow Condition Designation	Flow Rate (gm/min)		Energy Input Rate (kw)
	Plasma	Coolant	
1	58.7 argon	1.90 nitrogen	3.06
2	58.7 argon	8.22 nitrogen	3.06
3	58.7 argon	18.4 nitrogen	3.15
4	42.3 argon	8.22 nitrogen	2.5
5	78.0 argon	8.22 nitrogen	3.4
6	58.7 argon	9.70 argon	2.87
7	58.7 argon + 0.04 to 0.38 nitrogen	9.70 same composition as plasma	2.9
8	58.7 argon	8.22 nitrogen	2.79
9	58.7 argon	8.22 nitrogen	0.20

flow rate of 58.7 grams per minute of argon. With this flow rate, operation was very stable, and the phenomena occurring could be duplicated from day to day. The plasma flow was considered turbulent at this flow rate. Flow conditions 1, 2, and 3 used different nitrogen coolant rates to determine the effect of this variable. Flow condition 4 employed a low plasma flow rate which resulted in operation just into the "laminar" region. Operation was somewhat unstable and some flow characteristics were difficult to duplicate exactly. Flow condition 6 used argon for the

coolant to determine the purity of the argon supply and to compare the quenching efficiencies of argon and nitrogen. In flow condition 7, nitrogen was mixed with the argon plasma gas before it was passed through the electric arc. The jet Reynolds number for all plasma flows was of order 10^3. There was no electric power input in flow condition 9. The energy input rates listed include the room temperature enthalpy referred to absolute zero of the gases involved.

Spectrographic argon temperature measurements were made for all of the plasma flow conditions. Because of the large amount of data reduction required, spectrographic nitrogen temperatures were determined only for flow conditions 1, 2, and 3. Sampling probe measurements were made for flow conditions 1 through 5 and for 9.

Photographs of the plasma during typical operation are presented in Figure 12. The "A" photograph shows the appearance of the plasma flow when no nitrogen was present, the "B" photograph illustrates the typical appearance of the plasma when mixing with the nitrogen coolant, and the "C" photograph shows the sampling probe in the plasma. The luminous streaks outside of the plasma region are due to reflections from imperfections in the quartz confining tube.

A reproduction of a representative spectrographic plate in shown in Figure 13. The plate shown covers the spectrum from approximately 3200 to 4500 Å. Another plate, placed end-to-end with this one in the spectrograph, could simultaneously cover the 4500 to 5700 Å region. On the plate some of the strong argon lines and nitrogen bands are identified.

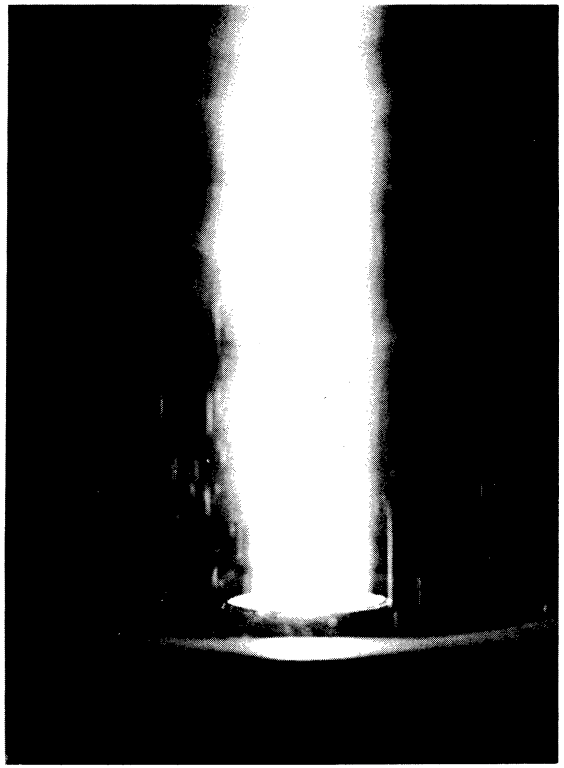

A

Flow condition 6 (no nitrogen)

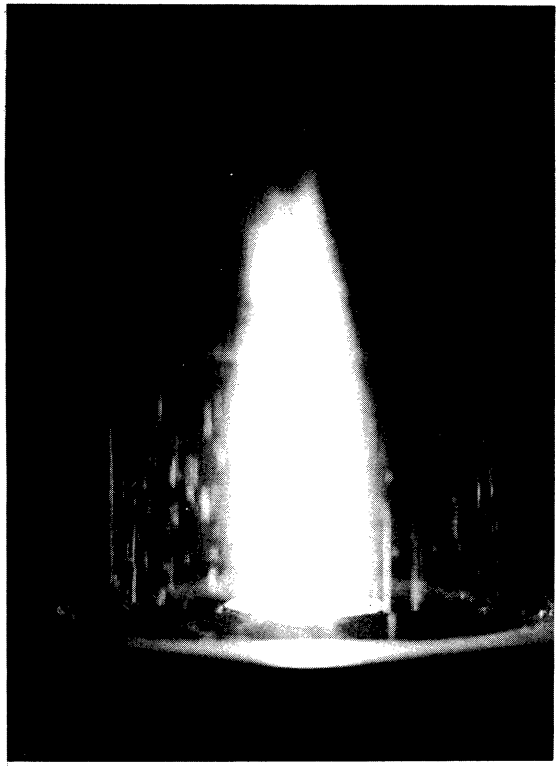

B

Flow condition 2

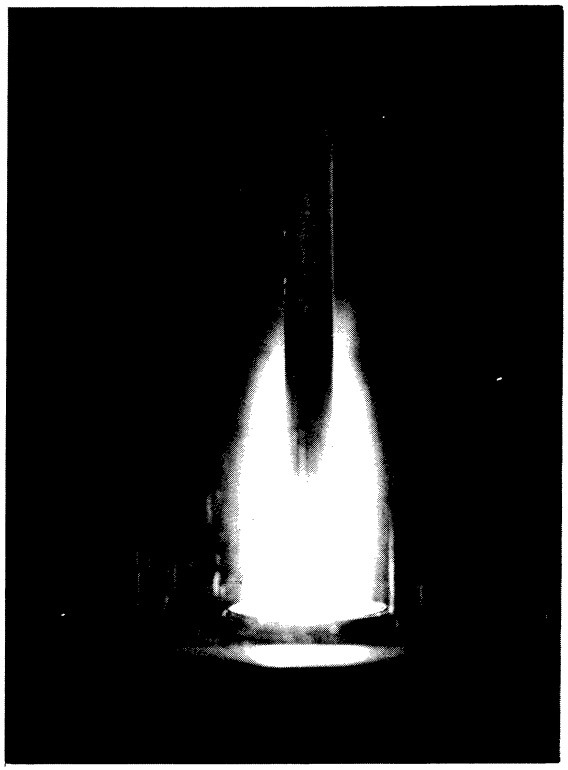

C

Flow condition with sampling probe located at z = 0.4 cm

Figure 12. Photographs of plasma during typical operation.

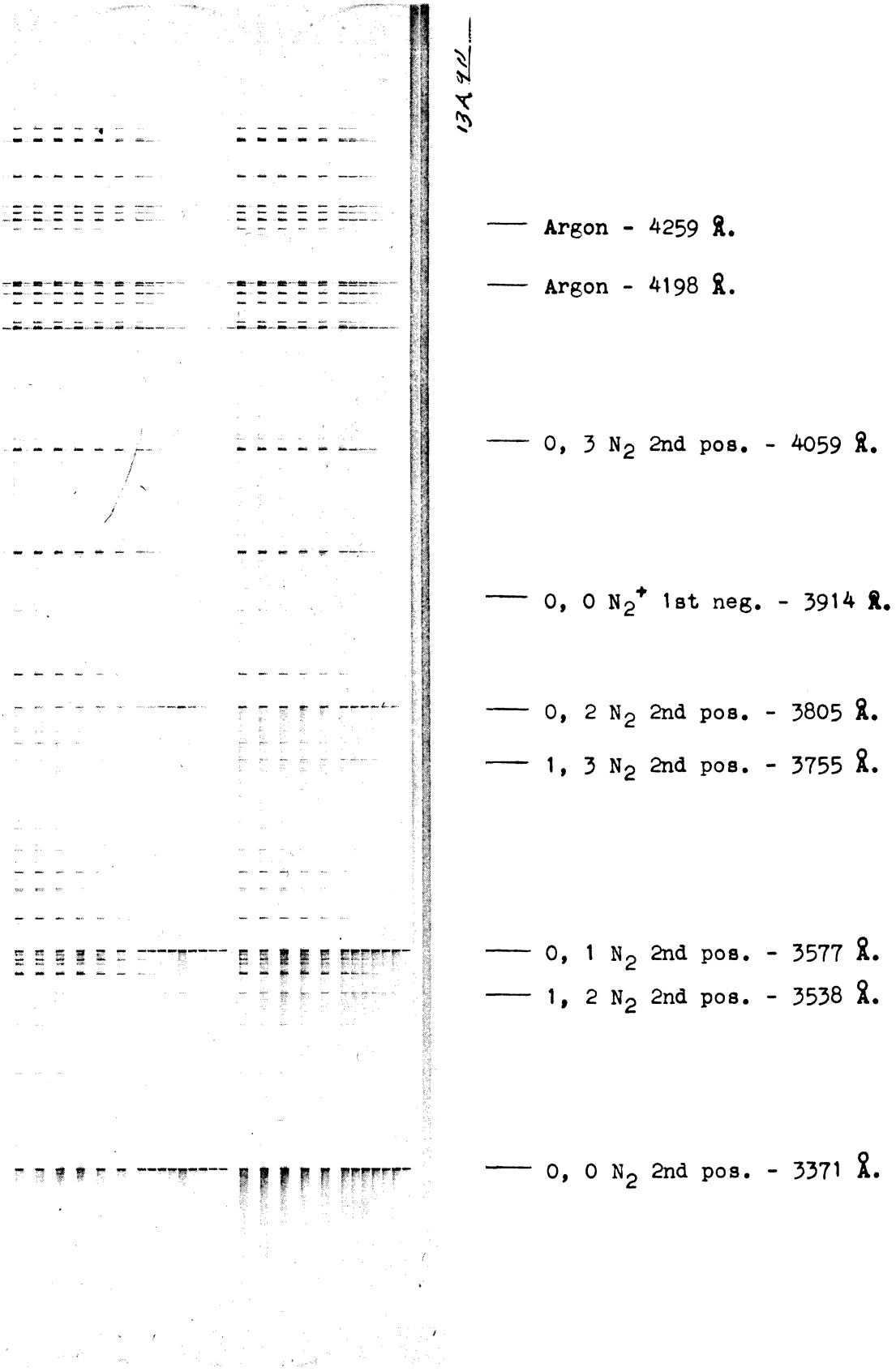

Figure 13. Reproduction of typical spectrographic plate (flow condition 5 at z = 0.4 and 1.2 cm).

The nitrogen band identification was based upon information from Pearse (70). The two strips along the edge of the plate are bands of tungsten continuum radiation which were exposed on all plates for calibration purposes.

The coordinate system used in this work measures the axial distance z from the downstream edge of the plasma nozzle and the radial distance r from the centerline of the plasma. The lateral distance x was also measured from the centerline.

7.2 SPECTROGRAPHIC RESULTS

7.2.1 Argon Temperature Measurements

Argon temperatures were determined by using both the multi-line and the absolute intensity single-line methods. During preliminary phases of the work, every line for which a reliable transition probability was known (2) was used for multi-line temperature determinations. On the basis of these studies, four representative argon lines were selected for further use. Two of the lines, 4198 and 4259 Å, were transitions from 5p to 4s energy levels. The 4s levels contain the first excited states of argon. The other two lines, 5558 and 5600 Å, were transitions from 5d to 4p levels. None of the transitions were between metastable levels although there are metastable levels among the 4s states. As expected, the lines from the p (principal) levels were sharp and the lines from the d (diffuse) levels were diffuse.

The nature of the line intensity data recorded is illustrated in

Figures 14 and 15. The two flow conditions shown resulted in the least intense and the most intense radiation. From center to plasma edge, the measurable intensity varied by over two orders of magnitude. The radiation recorded beyond 0.5 centimeter is due to reflections from the quartz tube rather than from the flow system at that point. The details about how the line intensities were determined from the spectrographic plates are given in Appendix A. The measured lateral intensities were converted to the corresponding radial distribution by using the inversion method described in Section 4.5.

Temperatures determined by the single- and multi-line methods are compared in Figures 16 and 17. The temperatures beyond a radius of 0.5 centimeter have no meaning since they were calculated from the intensity of the radiation reflected from the quartz tube. The absolute intensity of the 4259 Å line would have given a result equivalent to that of the 4198 Å line and the 5558 Å would have given a result equilvalent to that of the 5606 Å line. The energy levels spacings are such that the results of the multi-line method are dependent upon the intensities of the 4198 - 4259 Å pair relative to the 5558 - 5606 Å pair. The figures, which compare temperatures based upon exactly the same data, illustrate the extreme sensitivity of the multi-line as compared to the absolute intensity method as was already mentioned in Section 4.2.4. The consistent trend in the disagreement in temperatures determined by the absolute intensities of the 4198 and 5606 Å lines is due to the problems in the measurement of the intensity of the diffuse 5606 Å line. Winter and Cremers

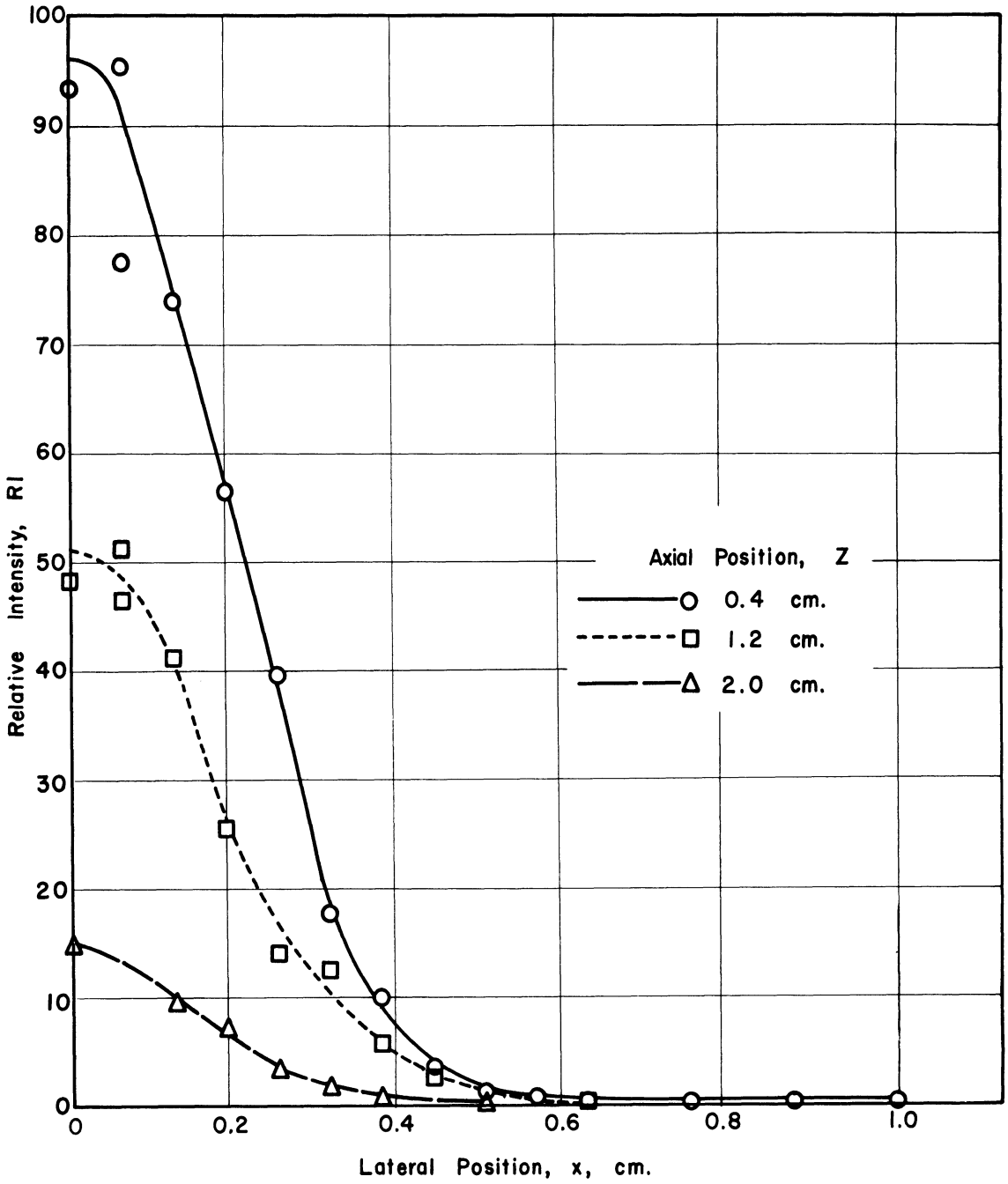

Figure 14. Argon line (4198 Å) lateral intensity profile for flow condition 8.

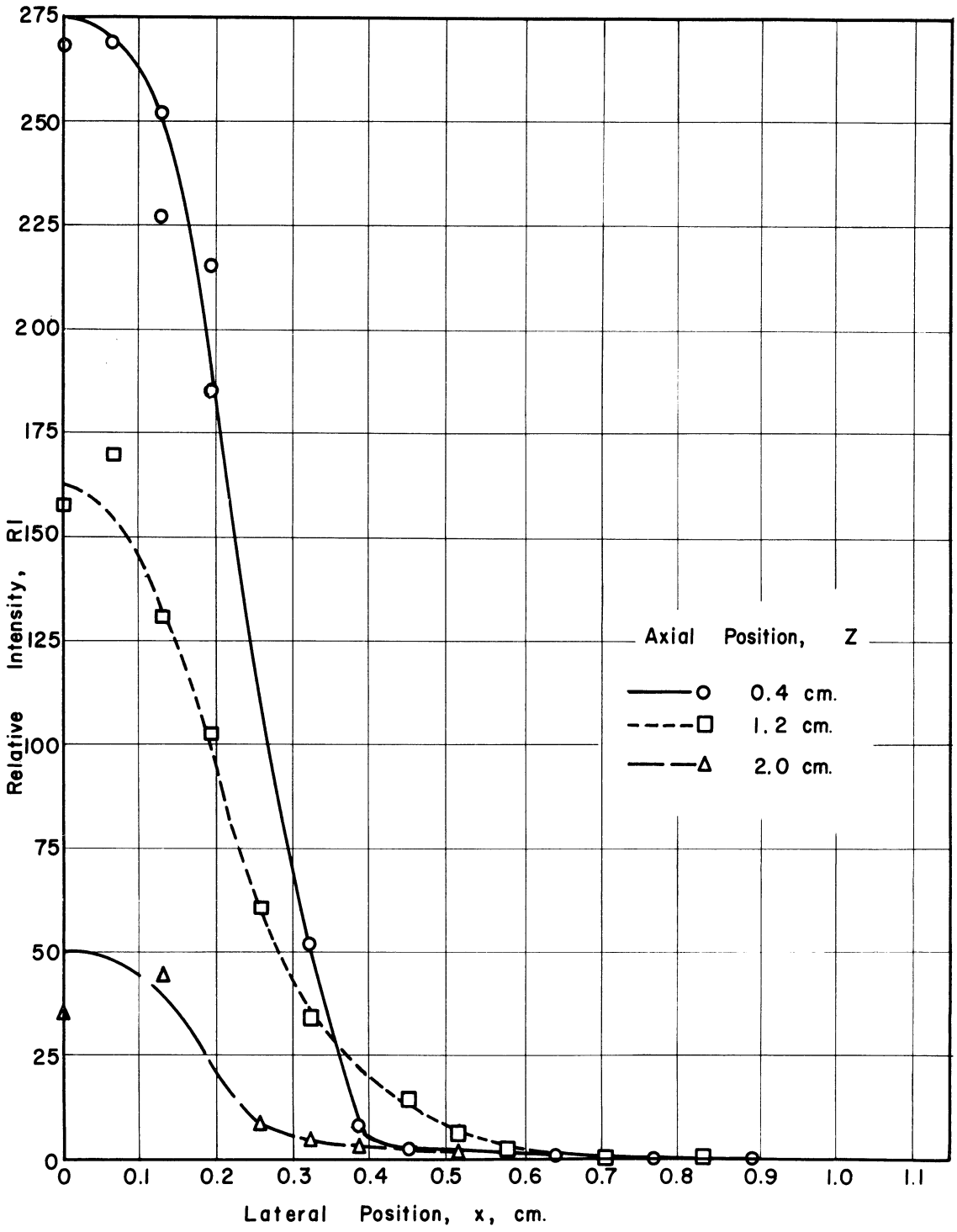

Figure 15. Argon line (4198 Å) lateral intensity profile for flow condition 4.

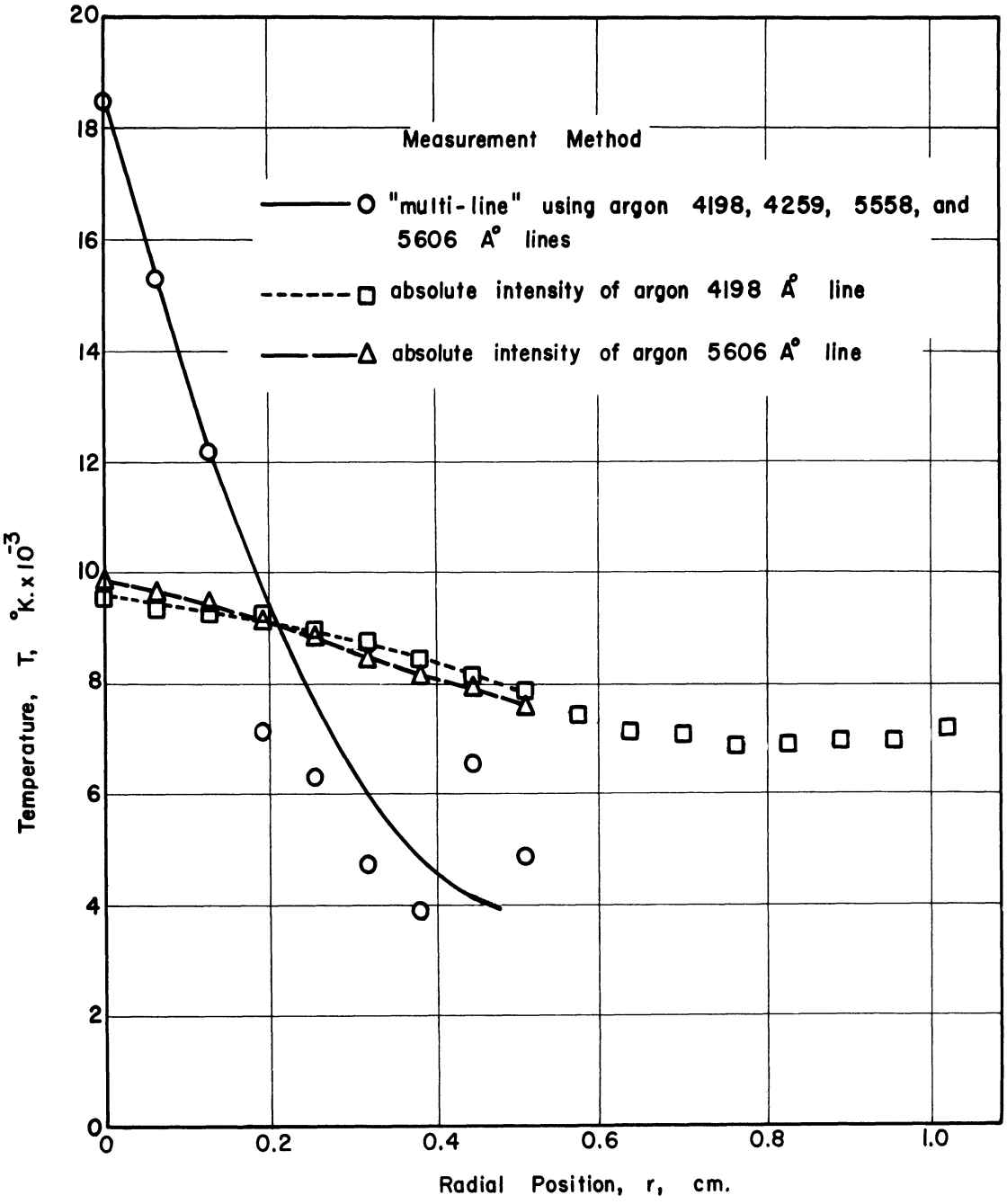

Figure 16. Comparison of argon temperatures determined by absolute intensity and "multi-line" methods at z = 0.4 cm for flow condition 1.

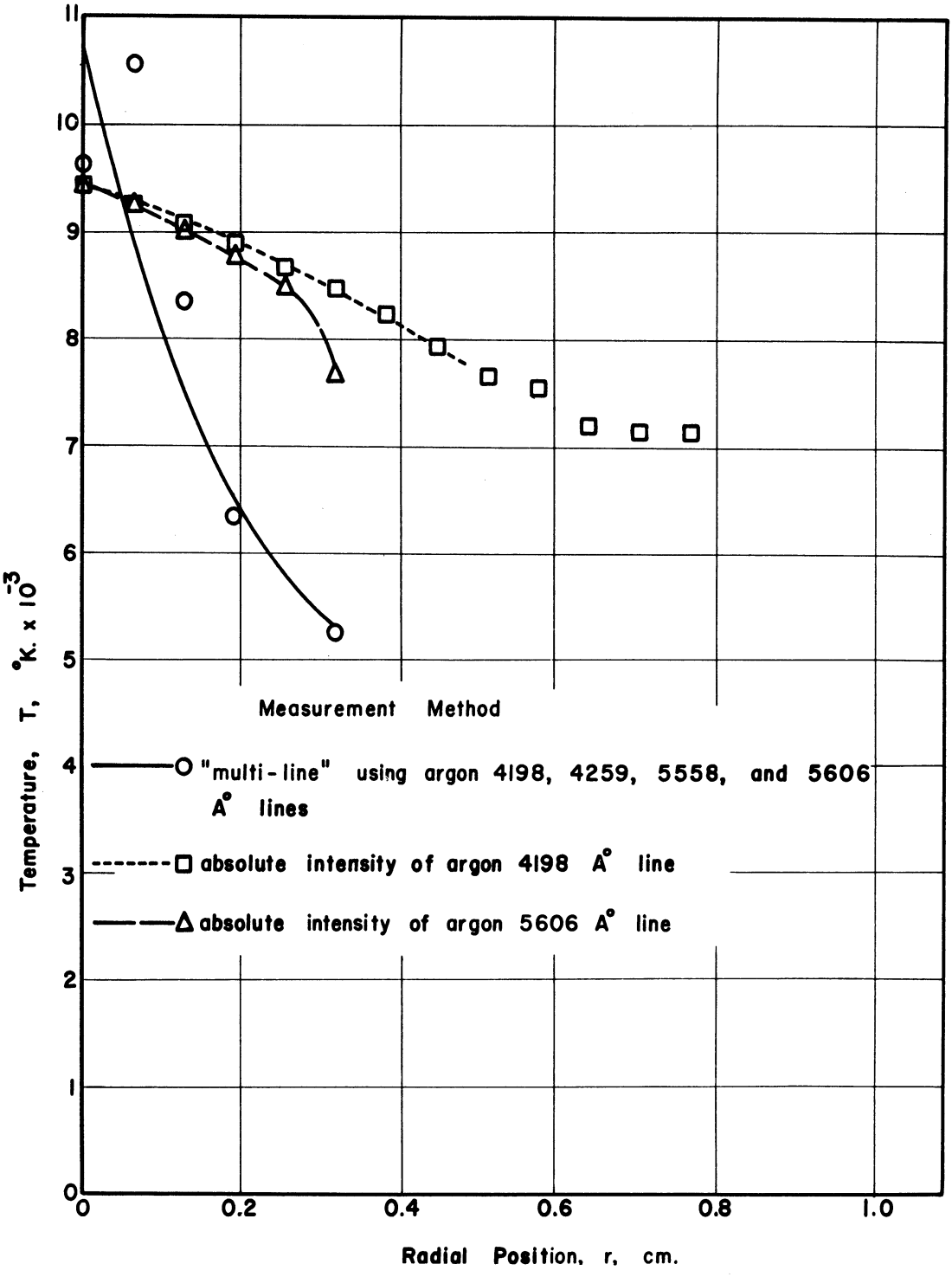

Figure 17. Comparison of argon temperatures determined by absolute intensity and "multi-line" methods at z = 1.2 cm for flow condition 1.

(84) apparently encountered a similar problem with the multi-line method but did not realize it. Their temperatures, which were entirely determined by the 2-line method, are inconsistent with an intensity profile which they present.

Argon temperatures were determined by the absolute intensity of the 4198 Å line in the remainder of the work. An additional check of the validity of the intensity measurements was made since the region where the plasma flow was studied was in the path of intense radiation coming axially from the arc region. It is possible for such radiation to induce emission from the plasma (16). Calculations based upon conservative assumptions indicated that the intensity of such induced radiation would be less than 10^{-2} times the true emission from the plasma. Thus it could be neglected.

The argon temperatures determined for the various flow conditions are shown in Figures 18 through 24. The temperatures determined beyond a radius of 0.5 centimeter again have no meaning. When calculations using the temperature data were made, the observed temperatures were extrapolated down to a temperature of 1000°K at the surface of the plasma nozzle. Although the conversion from lateral to radial intensities introduced some scatter into the temperature results, the various fluctuations in the profiles shown are believed to be true. They are consistent and reproducible. Based upon the uncertainty in the transition probability of the 4198 Å argon line ($\pm$ 15%) possible errors in the calibration of the tungsten filament lamp used for absolute intensity reference ($\pm$ 9%) and vari-

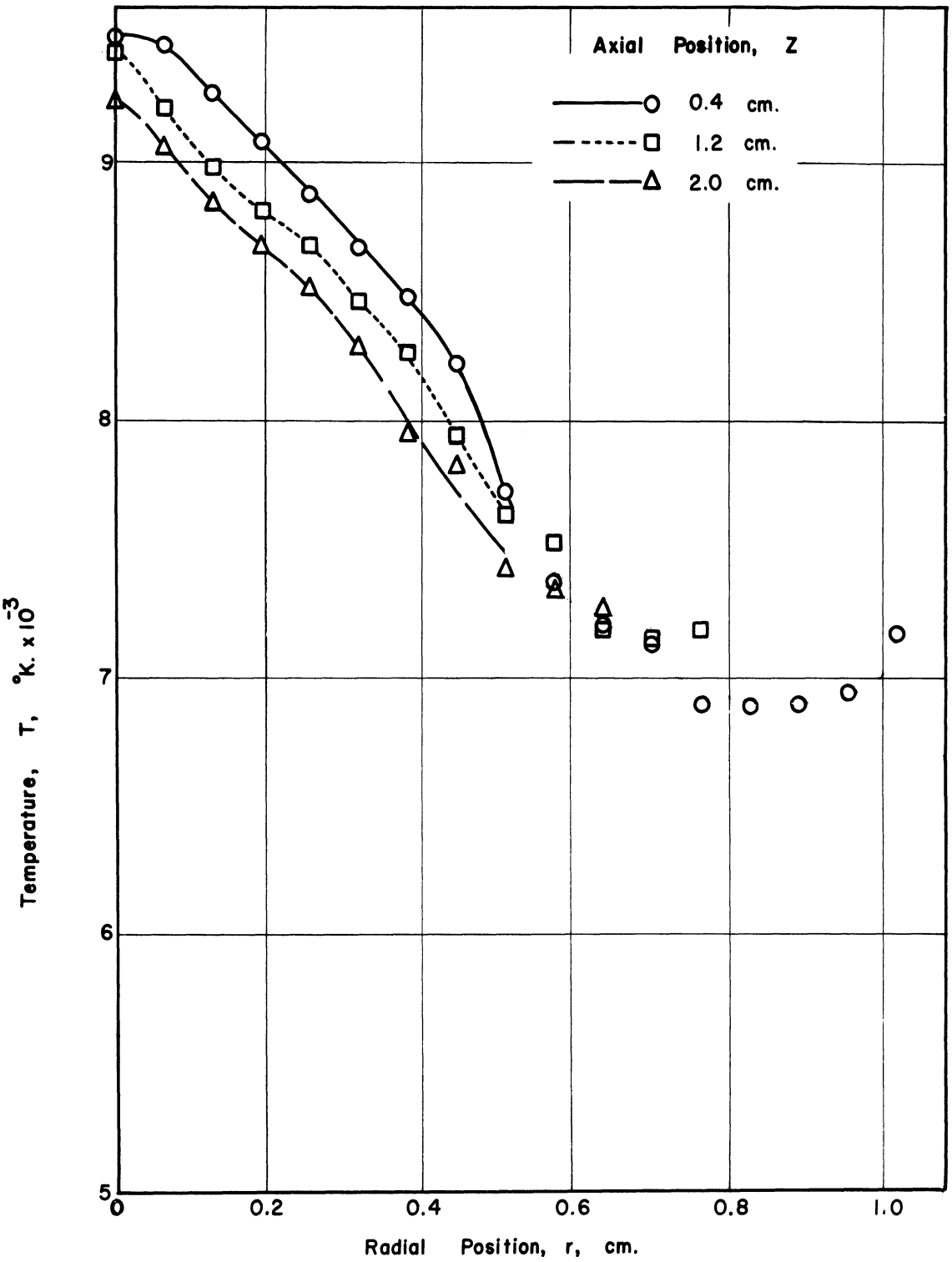

Figure 18. Argon temperature versus position for flow condition 1.

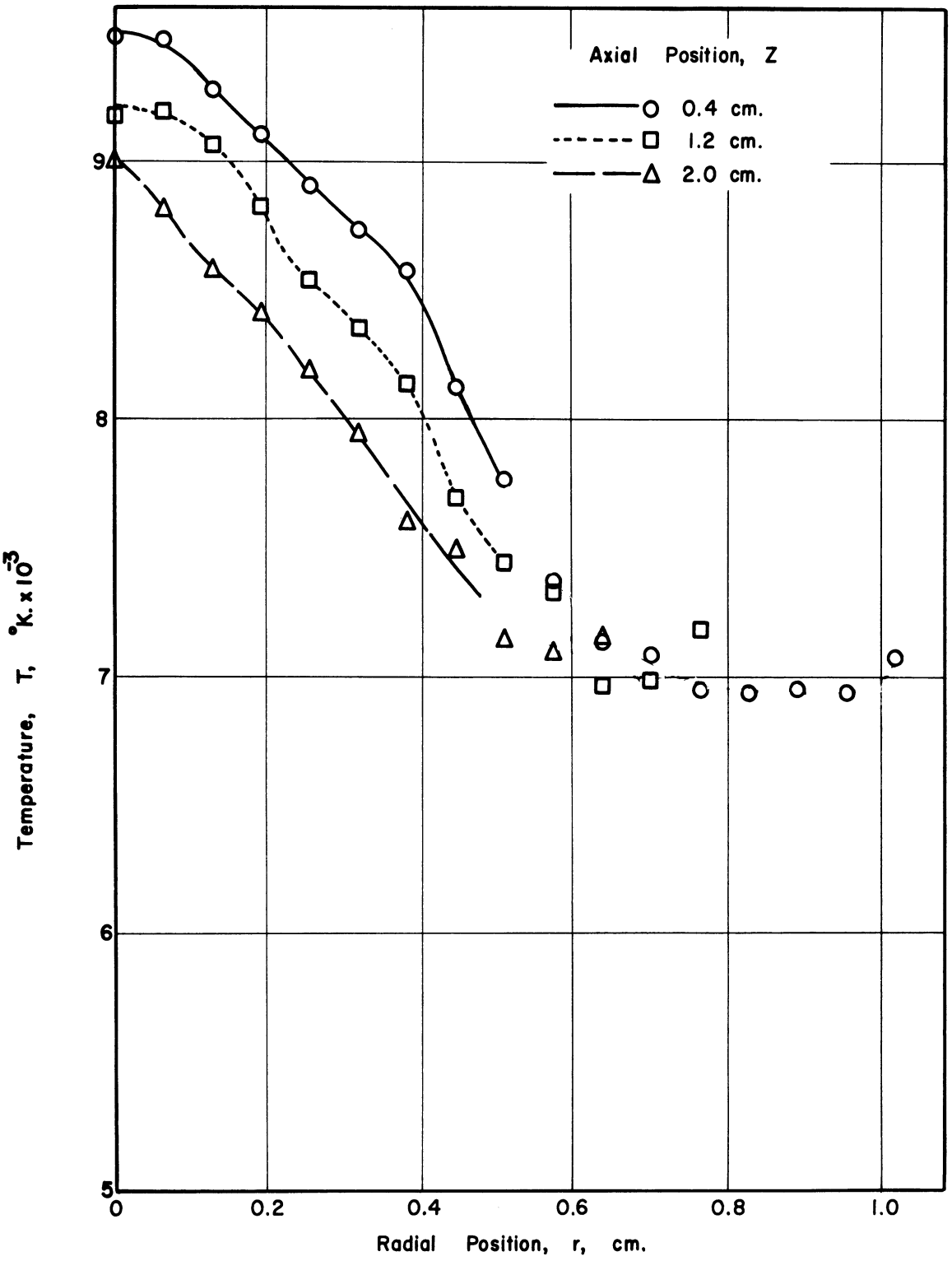

Figure 19. Argon temperature versus position for flow condition 2.

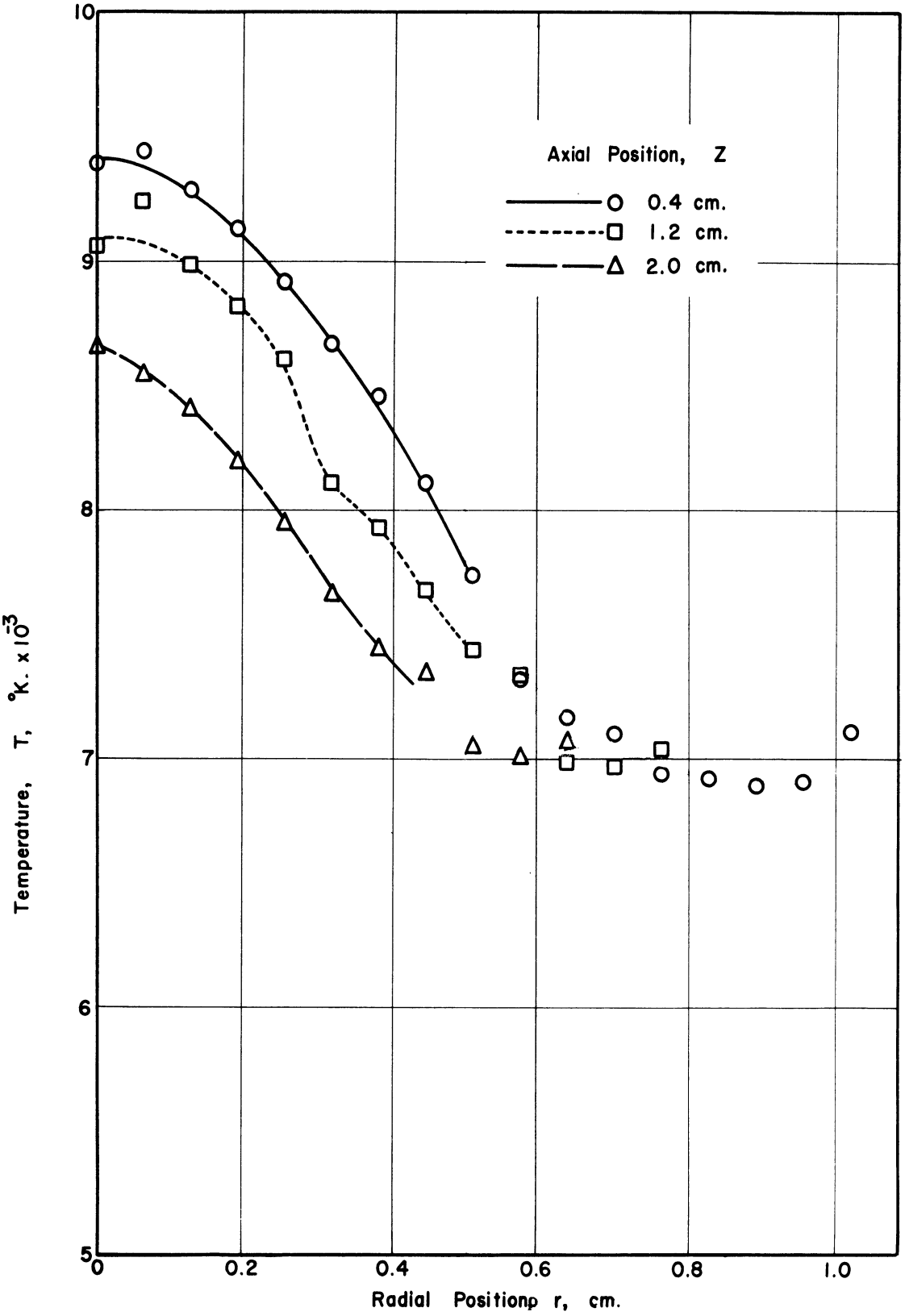

Figure 20. Argon temperature versus position for flow condition 3.

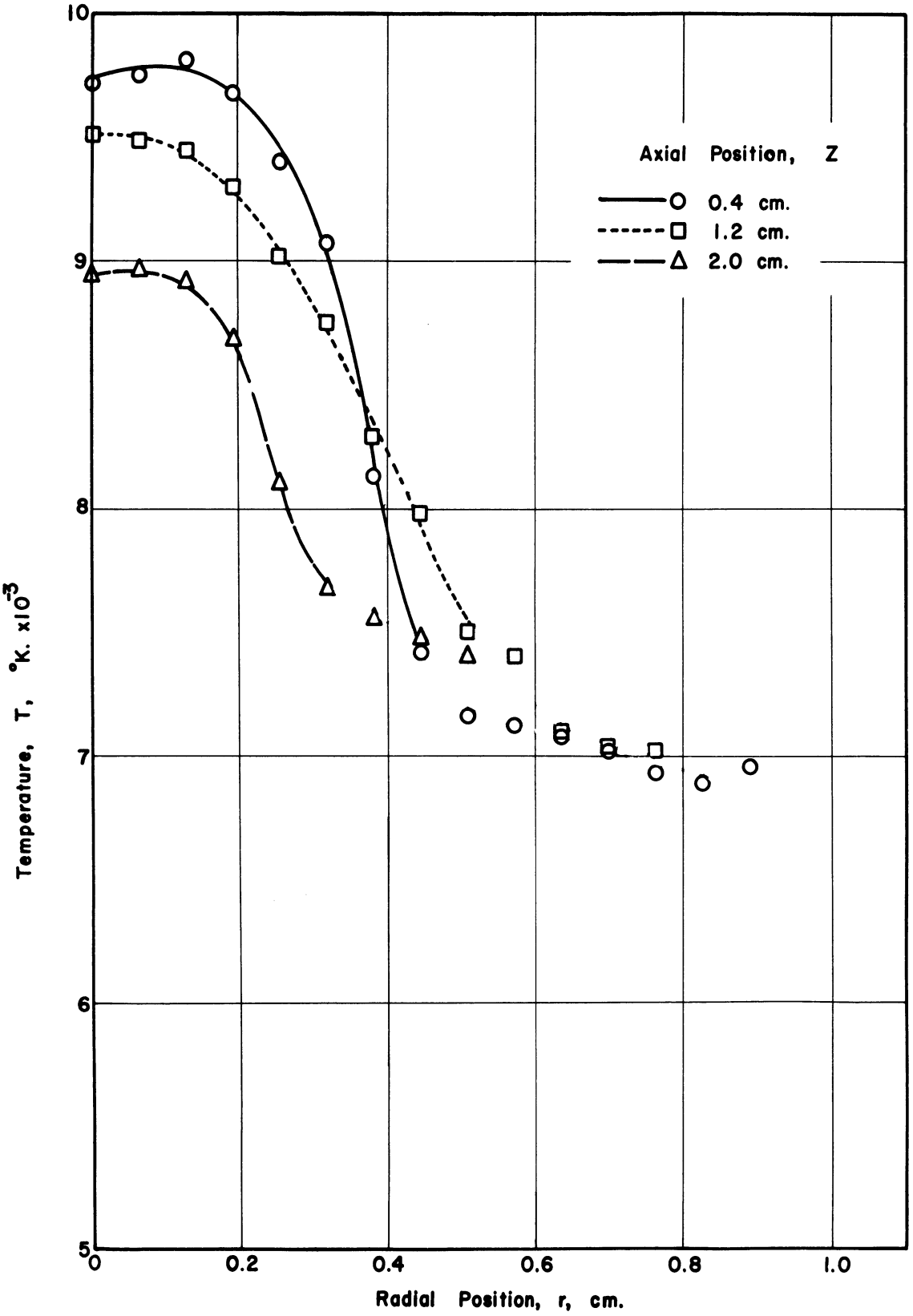

Figure 21. Argon temperature versus position for flow condition 4.

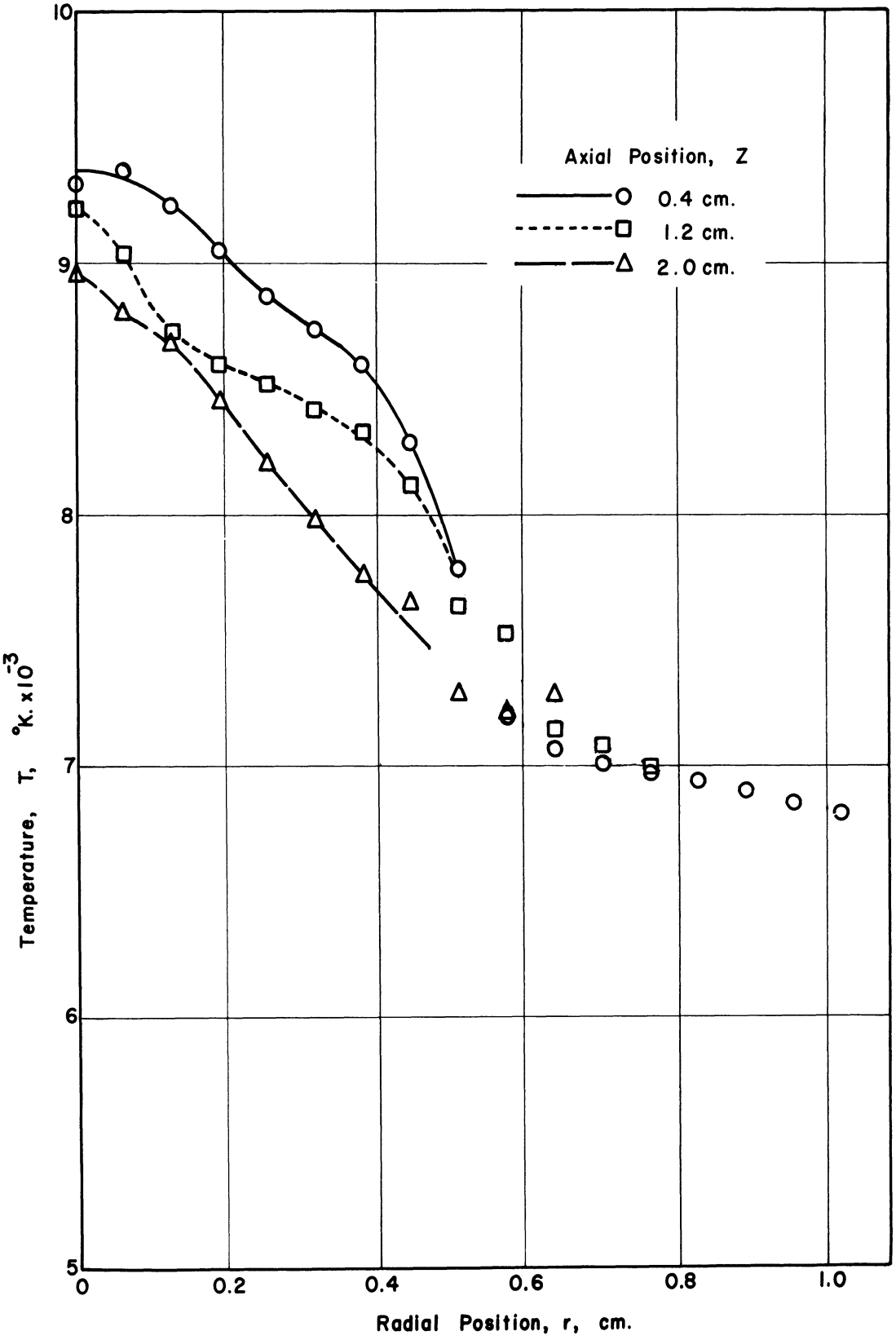

Figure 22. Argon temperature versis position for flow condition 5.

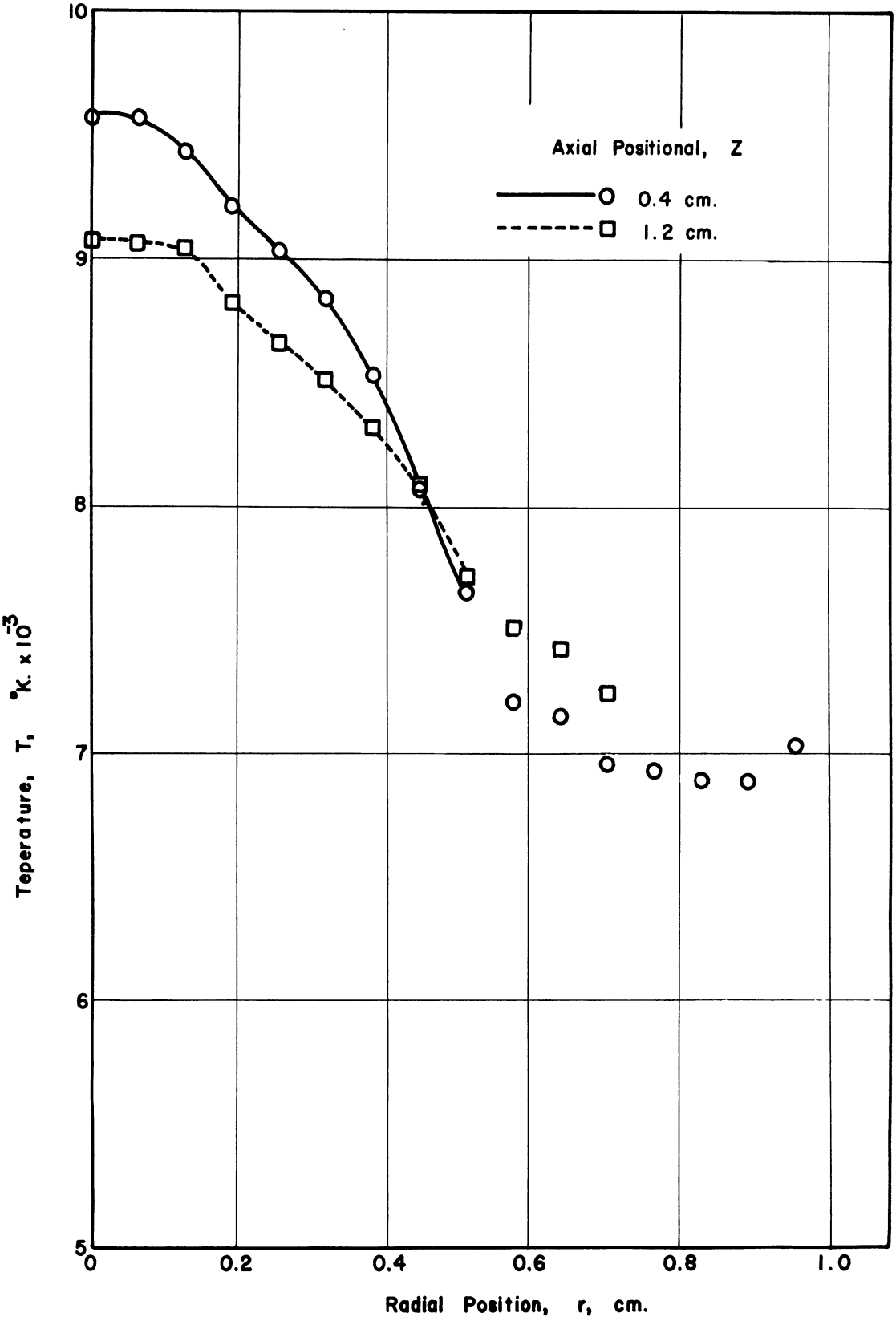

Figure 23. Argon temperature versus position for flow condition 6.

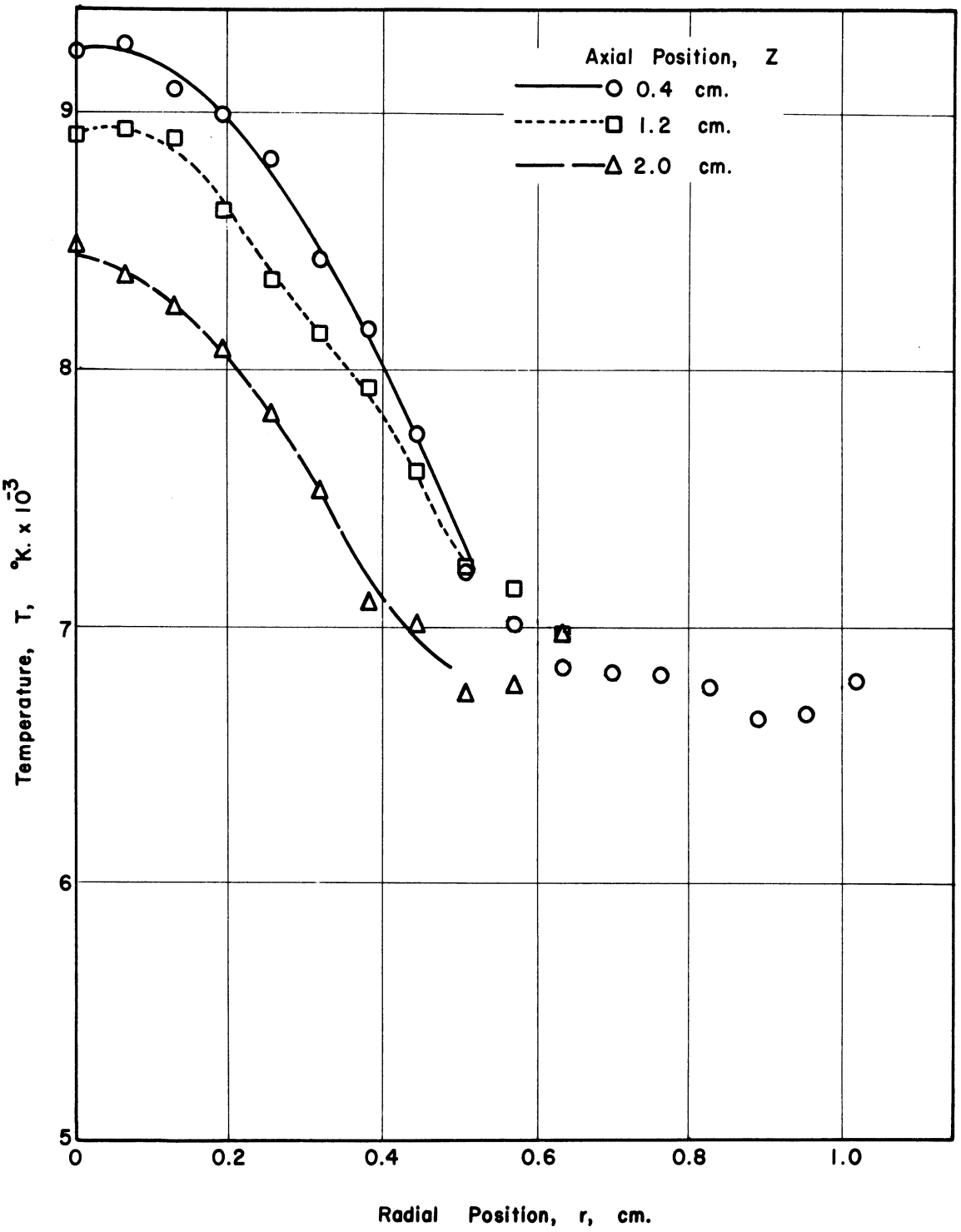

Figure 24. Argon temperature versus position for flow condition 8.

ations in the photographic and photometering processes ($\pm$ 7%), the calculated temperatures have a possible error of $\pm$ 2%. At 9000°K this amounts to a range of $\pm$ 180°K. Since the transition probability and absolute intensity reference errors are constant, the temperature measurements have a scatter of less than 0.5%.

Figures 18 through 20 show the progressive change in the cooling of the argon plasma as the nitrogen coolant rate was increased. The dips in the temperature profiles for axial positions of 1.2 and 2.0 centimeters are discussed in Section 7.5 in connection with coolant induction and recirculation. Figure 21 shows the temperature profiles for the low-argon flow rate condition. The slight drop in the indicated temperature near the centerline is thought to be due to lateral to radial intensity conversion problems rather than being a true drop. The temperature determinations for flow condition 5 which are shown in Figure 22 are similar to those for flow condition 1. The plasma to coolant ratio was similar for the two cases. Figure 23 shows the results when argon replaced the nitrogen coolant. There appears to be no great difference in the plasma cooling produced. However the photographs presented in Figure 12 show that nitrogen is much more effective in quenching what probably is the phosphorescence radiation caused by the metastable states of argon. Brewer (13) observed similar quenching behavior. The results for the lower power input case, flow condition 8, are shown in Figure 24. No change in the basic phenomena is evident.

7.2.2 Nitrogen Temperature Measurements

Rotational temperatures were determined from the band spectra of both neutral and singly ionized nitrogen molecules.

The measured lateral intensity profile of a typical line in the 0, 0 band of the second positive system of N_2 is shown in Figure 25. The profile was obtained at an axial position 0.4 centimeter from the plasma nozzle. Figure 26 shows the corresponding radial distribution. For such an intensity profile which has a peak at a large radius, the calculated values near the centerline show a large scatter. At larger axial distances, the off-axis peak was not as prominant, and better results were obtained near the centerline. By using a number of lines, the method described in Section 4.3.3 could be used to determine the temperature. A typical determination is shown in Figure 27. The solid lines in the figure correspond to the calculated values of Figure 4. The particular distribution shown was assigned a temperature of 1150°K. The deviation of the points from the shape of the lines is probably due to both experimental measurement problems and a slight departure from a Maxwell-Boltamann distribution of energy states. A plot like that shown in Figure 27 was required for each point at which a temperature was determined.

The 0, 0 band of the first negative system of N_2^+ was also used for temperature determination. As discussed in Section 4.3.3, the molecular Boltzmann plot method was used. The determination at the centerline for z = 2.0 centimeters is shown in Figure 28. Because of coupling with nu-

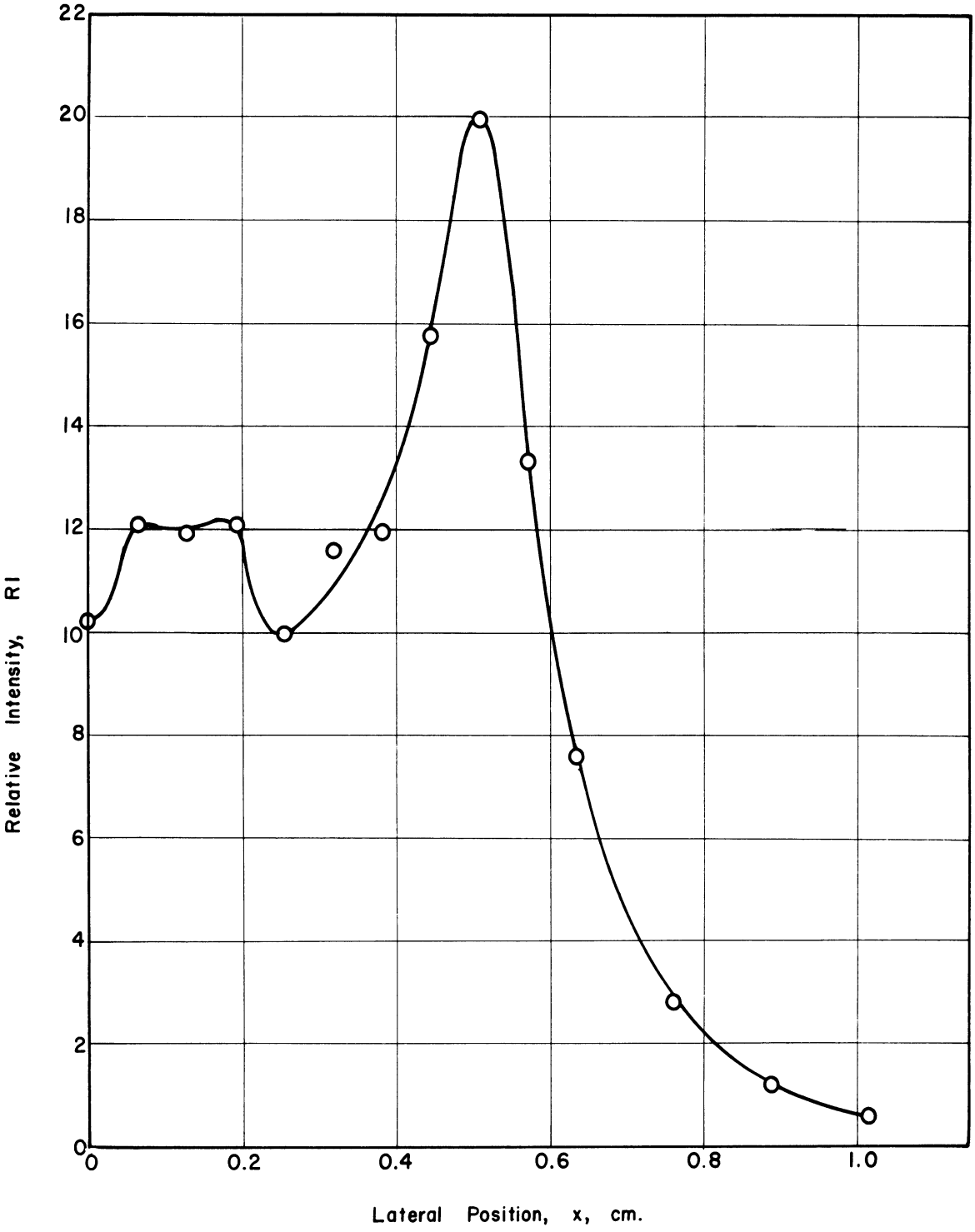

Figure 25. Typical nitrogen band line lateral intensity profile (K_R = 16, z = 0.4 cm).

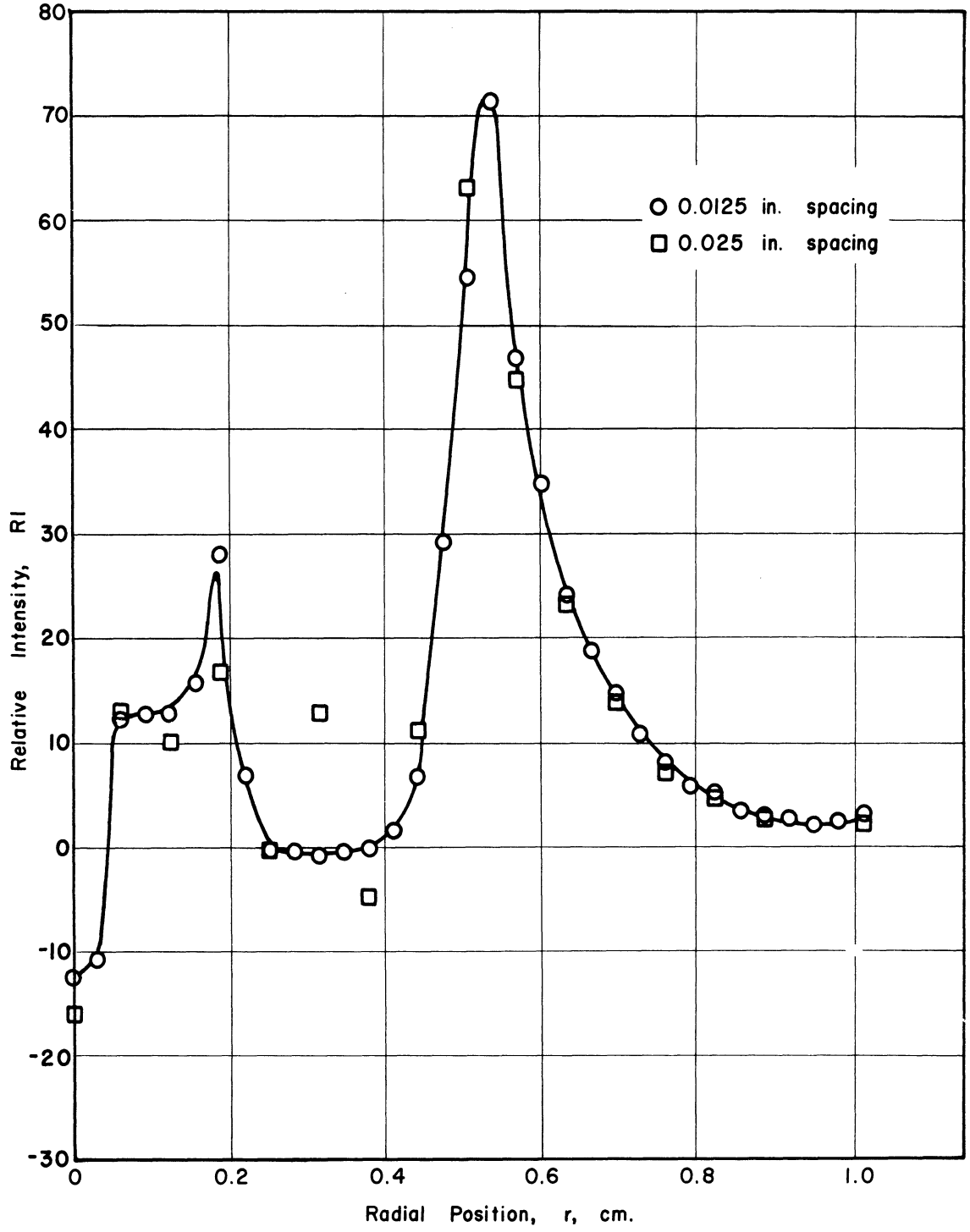

Figure 26. Typical nitrogen band line radial intensity profile (K_R = 16, z = 0.4 cm).

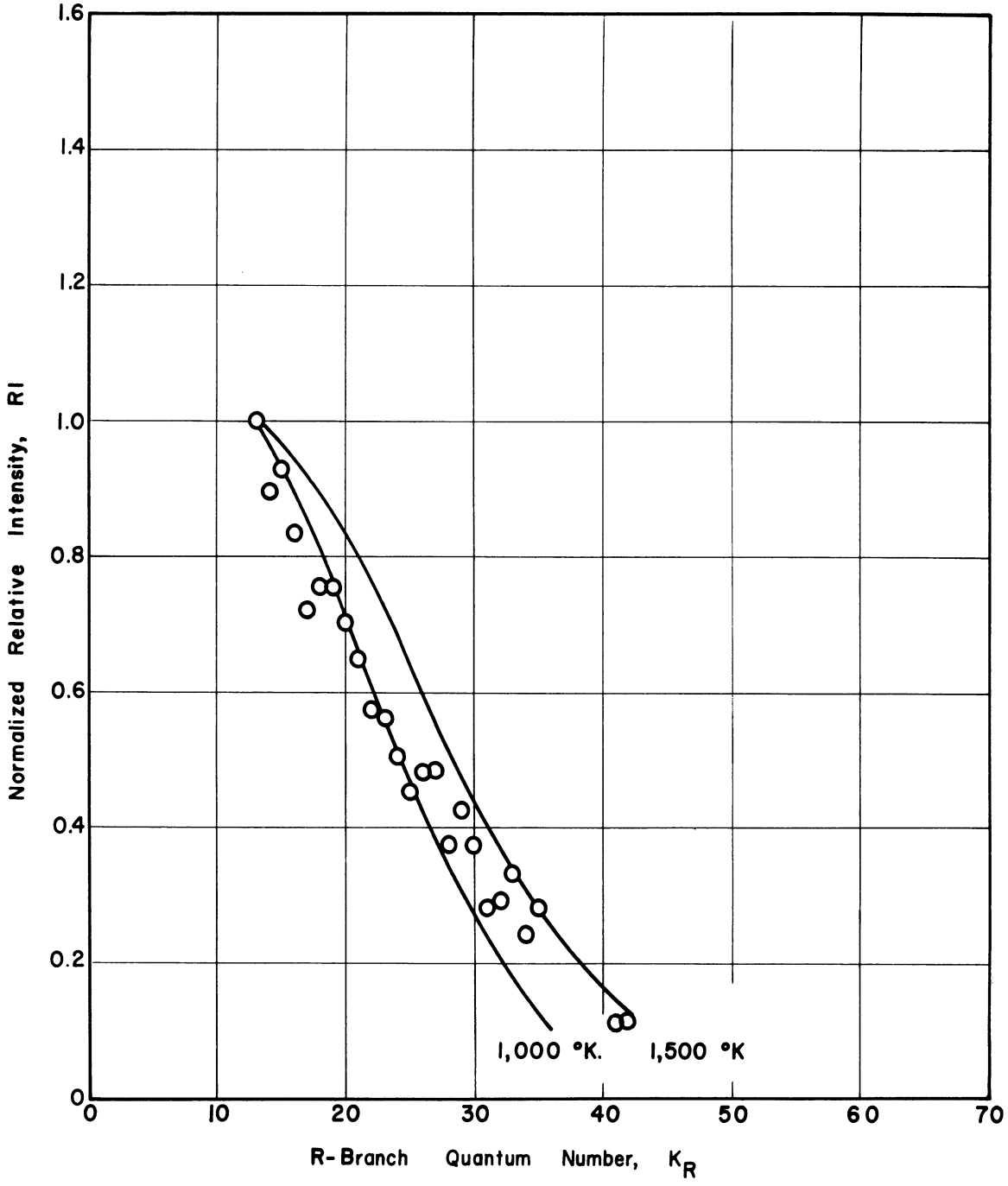

Figure 27. Typical temperature determination using the 0, 0 band of the nitrogen second positive system (z = 0.4 cm, r = 0.7 cm).

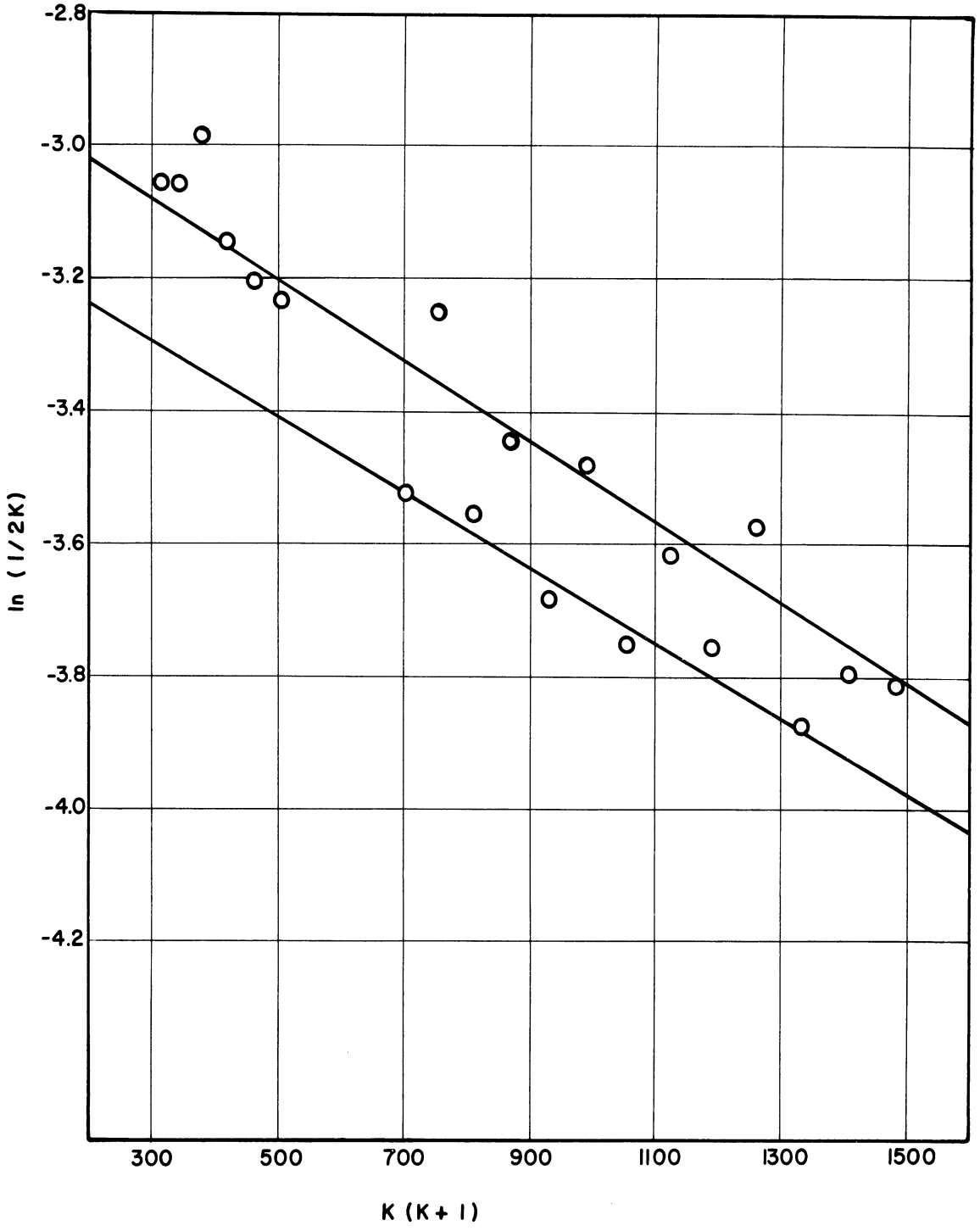

Figure 28. Temperature determination using the 0, 0 band of the N_2^+ first negative system.

clear spin, the two distinct lines shown on the plot are expected. However, they should be spaced 0.693 units apart on the ordinate. The closer spacing shown here probably is due to intensity measurement problems. The R-branch intensities which were used in the plot may also have been affected by the very weak overlapping P-branch.

The results of the nitrogen rotational temperature determinations are shown in Figures 29 and 30. The temperatures determined from the N_2 and N_2^+ molecules agree reasonably well. The temperatures determined by either method are estimated to have an accuracy of $\pm$ 20%.

Tourin et al. (81) measured average temperatures of the same order when they mixed molecular gases with an argon plasma jet.

7.3.2 Comparison of Argon and Nitrogen Temperatures

Comparison of Figures 18 through 20 with Figures 29 and 30 reveals that the determined argon and nitrogen rotational temperatures are different at the same point within the plasma.

Before advancing reasons for the difference, the validity of the determinations needs to be established. The mass and energy balances which are discussed in Section 7.4 were one source of verification. As will be explained, only when the argon temperature was used for the argon fraction of the flow and nitrogen temperature was used for the nitrogen fraction were good balances obtained. Another source of verification were the spectrographic plates obtained for flow condition 7. When the nitrogen was passed through the electric arc along with the ar-

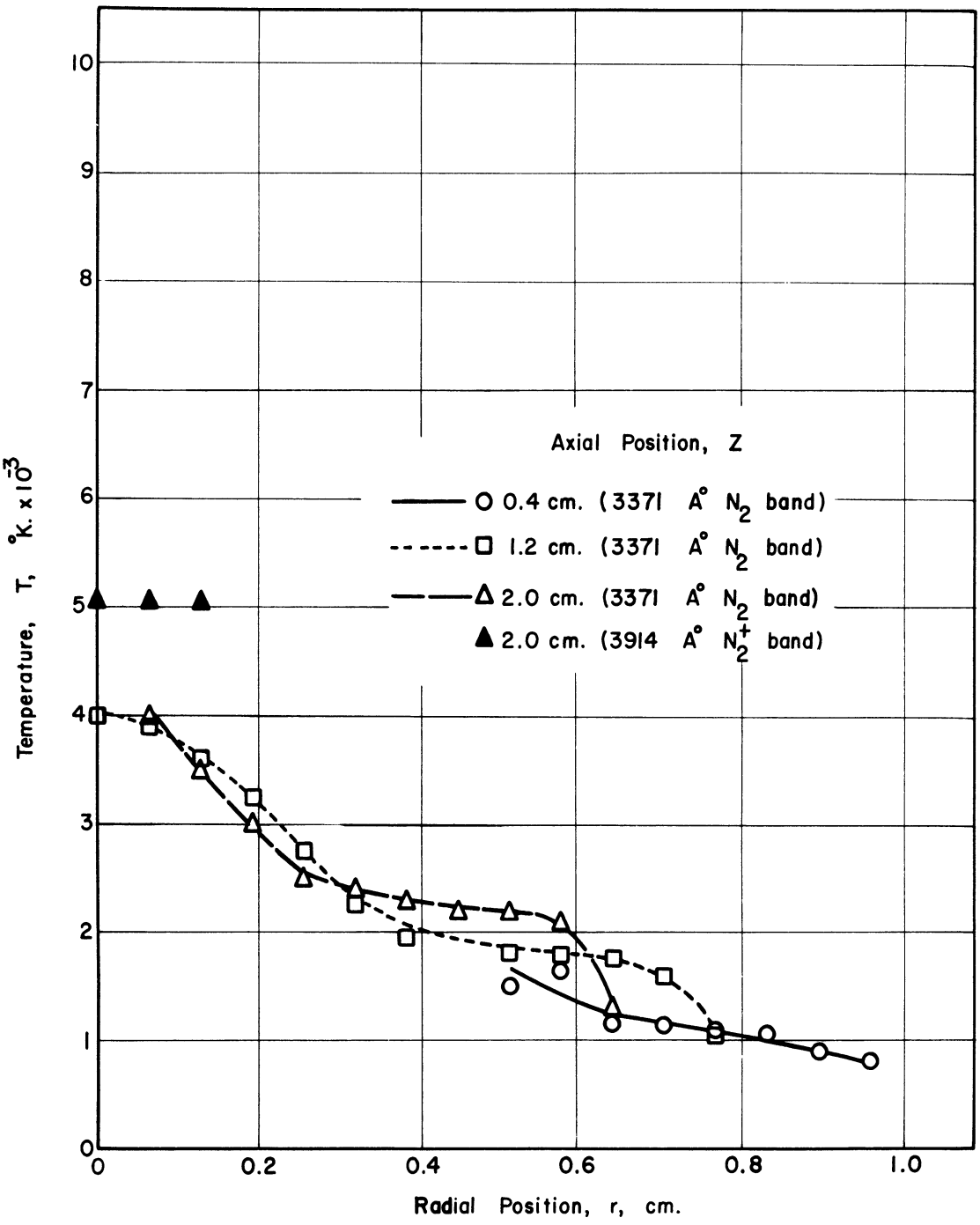

Figure 29. Nitrogen temperature versus position for flow condition 1.

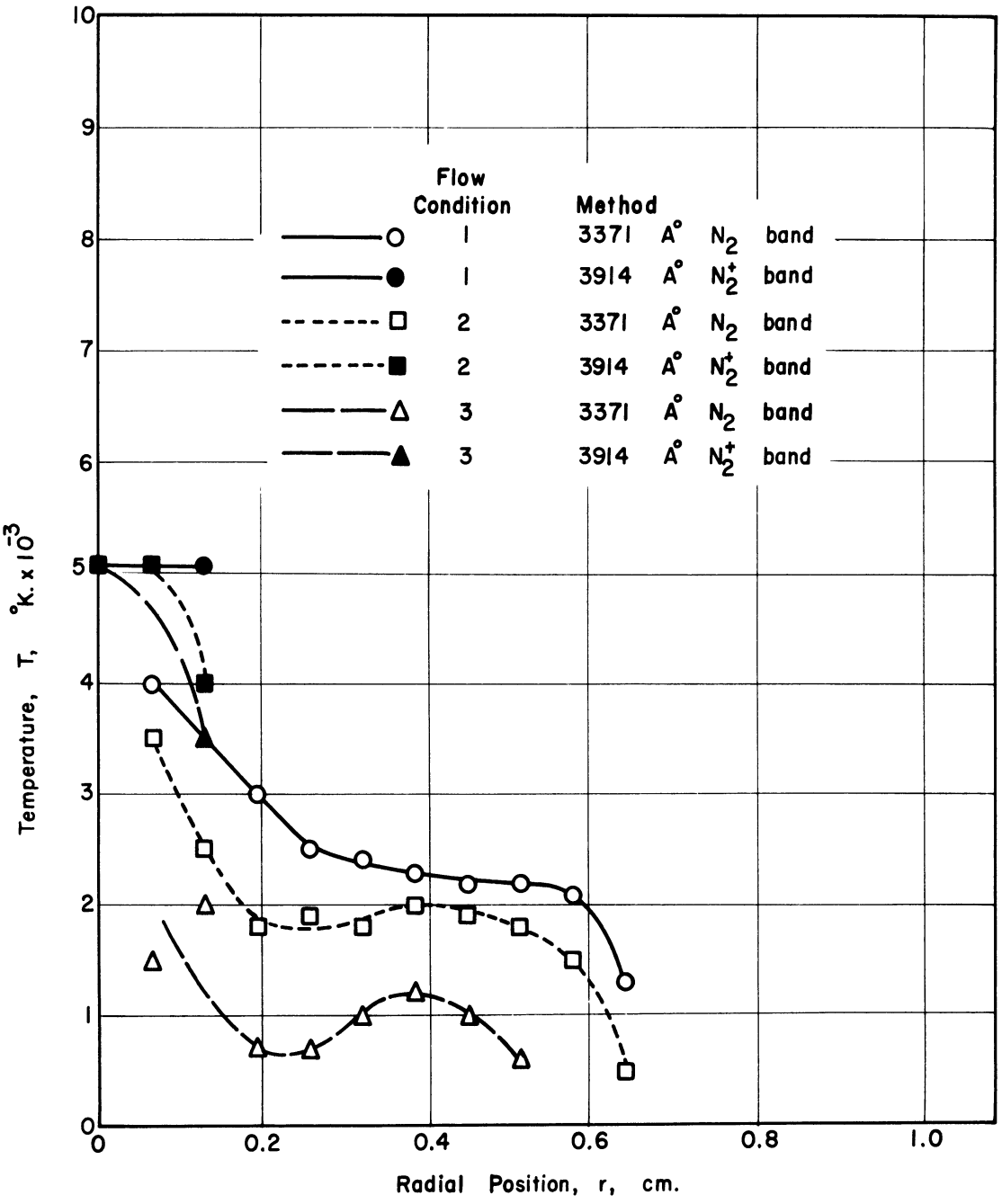

Figure 30. Radial distribution of nitrogen temperatures at z = 2.0 cm for flow conditions 1, 2, and 3.

gon, atomic nitrogen lines were visible in the spectra indicating a high temperature. When the nitrogen mixed only with the argon plasma, no atomic nitrogen lines were visible even though the overall nitrogen concentration at the points observed was greater. The band spectra produced by the nitrogen passed through the arc was too weak for quantitative measurements.

To gain insight into the energy transfer mechanism between the argon atoms and nitrogen molecules, their collision frequency was calculated on the basis of the hard sphere approximation. Benson (8) gives equations for calculating the collision frequency between molecules having Maxwellian velocity distributions. Actually in a high velocity plasma jet, only the horizontal velocity components are Maxwellian while in the vertical direction a non-zero flow component is superimposed upon the Maxwellian distribution. Kadlec (58) has considered this situation, and for the ratio of random to bulk velocities found in the plasma jet, the flow component alters the collision rate by under 1%. The calculations indicated that a nitrogen molecule would undergo approximately 8×10^4 collisions between the time it entered the plasma jet and the time that it was observed at an axial distance of 2.0 centimeters. On the basis of the hard sphere model, the nitrogen would have been able to exchange enough energy with the argon for equilibrium to have been reached. This is no doubt true insofar as translational energy is concerned, but for the rotational and vibrational energy modes, the hard sphere model does not apply. For rotational energy transfer a "rough" sphere model is

normally used (17). In collisional energy transfer, the amount of energy transferred is then governed by the conservation of angular momentum. For the argon atom-nitrogen molecule system, the moment of inertia of the molecule is about 10^4 times that of the atom, so little if any rotational energy exchange takes place. Thus only collisions between nitrogen molecules are effective for achieving rotational equilibrium. The following energy transfer scheme can be postulated:

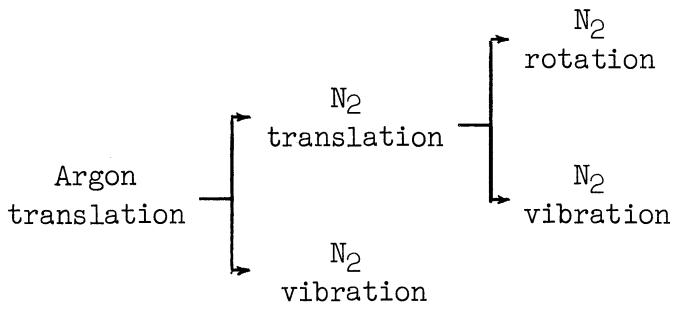

(7.1)

The concentration of N_2 in the plasma system was always under 10%. Thus on the basis of the scheme of Equation (7.1), a molecule would undergo only 4 "effective" (N_2 to N_2) collisions during its residence time in the observed plasma region. Greene et al. (44) found that pure nitrogen required about 20 collisions for rotational relaxation (the reaching of equilibrium). Thus the nitrogen rotational temperature would be expected to be lower than the argon translational temperature.

Vibrational relaxation is slow even in pure nitrogen. Blackman (11) reports that something like 10^4 to 10^5 collisions are required. Argon collisions in this case are about as effective as nitrogen collisions. Although the vibrational temperatures were not measured, the energy balance and spectra findings indicate that they probably were close to the rotational temperatures.

The above discussion tacitly assumed that the plasma energy consisted entirely of argon translation. On the basis of the statistical mechanics results of Drellishak (32), this is close to the true situation. Even at 9000°K, argon translation makes up 94% of the plasma energy. Most of the remainder consists of ionization energy which would largely revert to the argon atoms upon ion-electron recombination. The nitrogen molecules acquire some energy by quenching the metastable states of argon in inelastic collisions. However even at equilibrium at 9000°K, these states only contain about 10^{-3} percent of the plasma energy.

7.3 SAMPLING PROBE RESULTS

7.3.1 Composition Measurements

The results of the composition measurements are shown in Figures 31 through 36. Figure 36 is for the no electric power input case while all of the other figures apply to plasma conditions. The most interesting feature of the plots is the peak in nitrogen concentration which occurs for the plasma flow conditions which employed a low nitrogen to argon ratio. With no electric power input, such peaks did not occur for any composition ratio nor have any such peaks been reported in the literature. These peaks will be explained in Section 7.5 which considers induction and recirculation.

The composition data are considered accurate and they were reproducible.

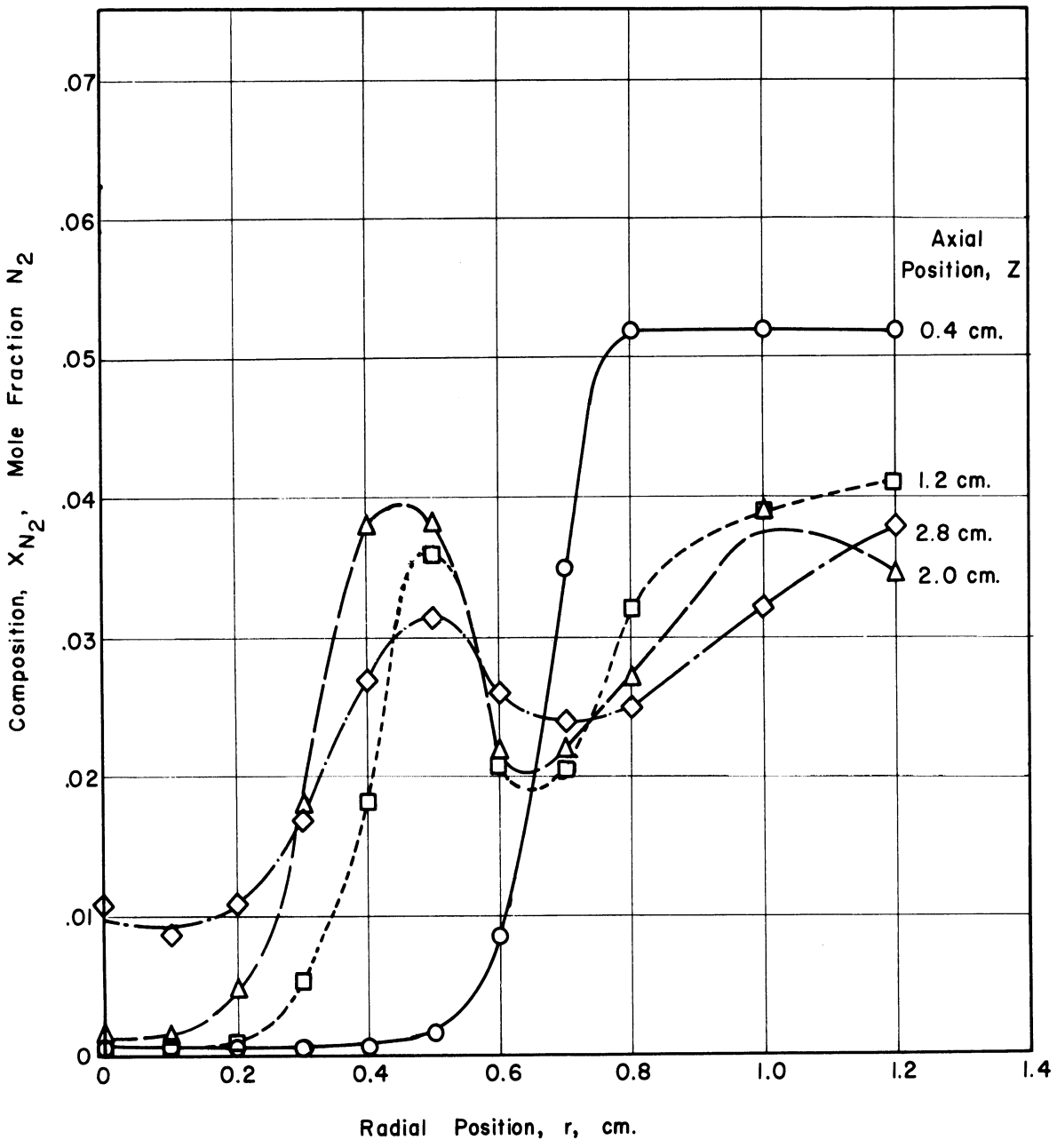

Figure 31. Composition versus position for flow condition 1.

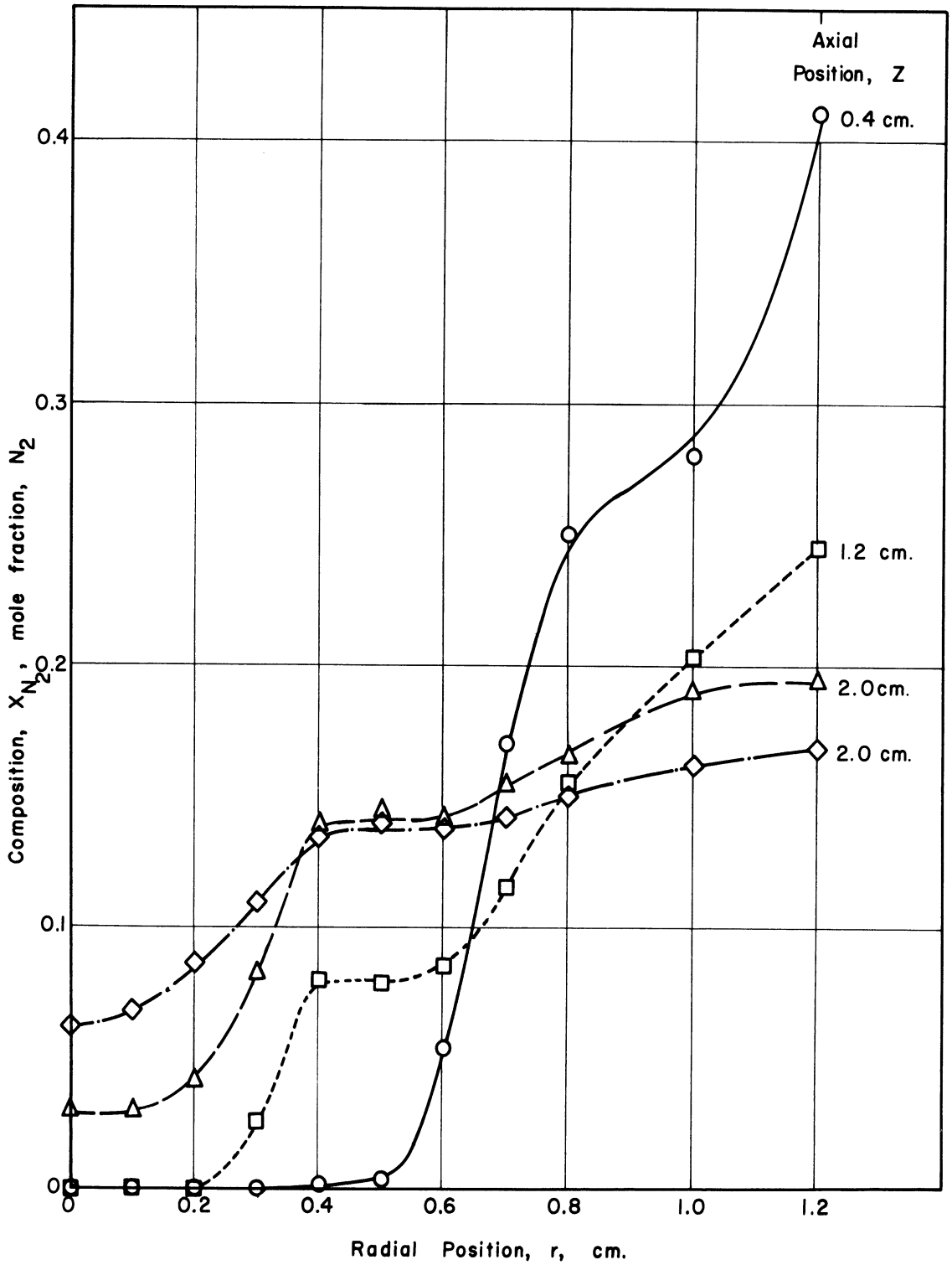

Figure 32. Composition versus position for flow condition 2.

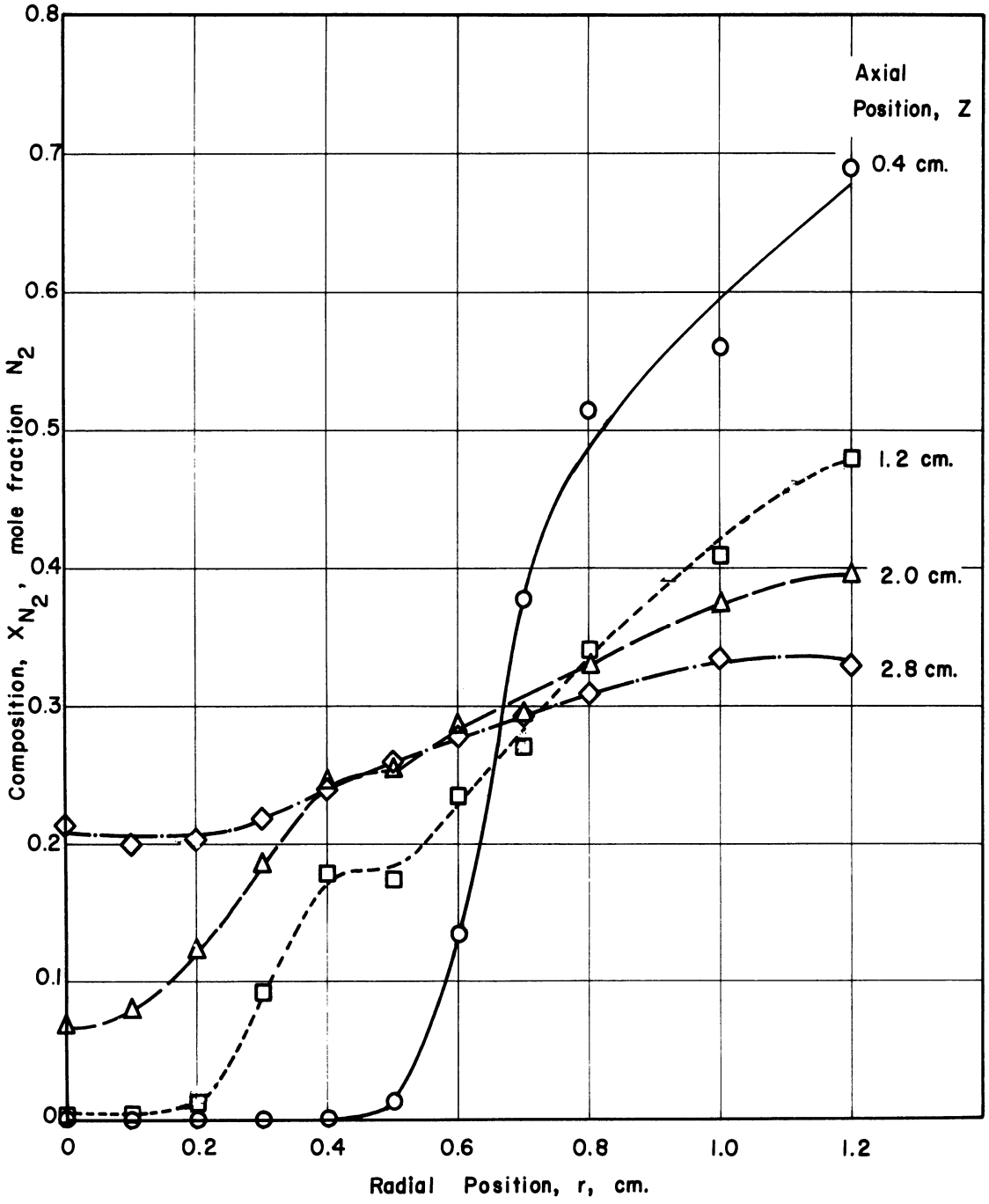

Figure 33. Composition versus position for flow condition 3.

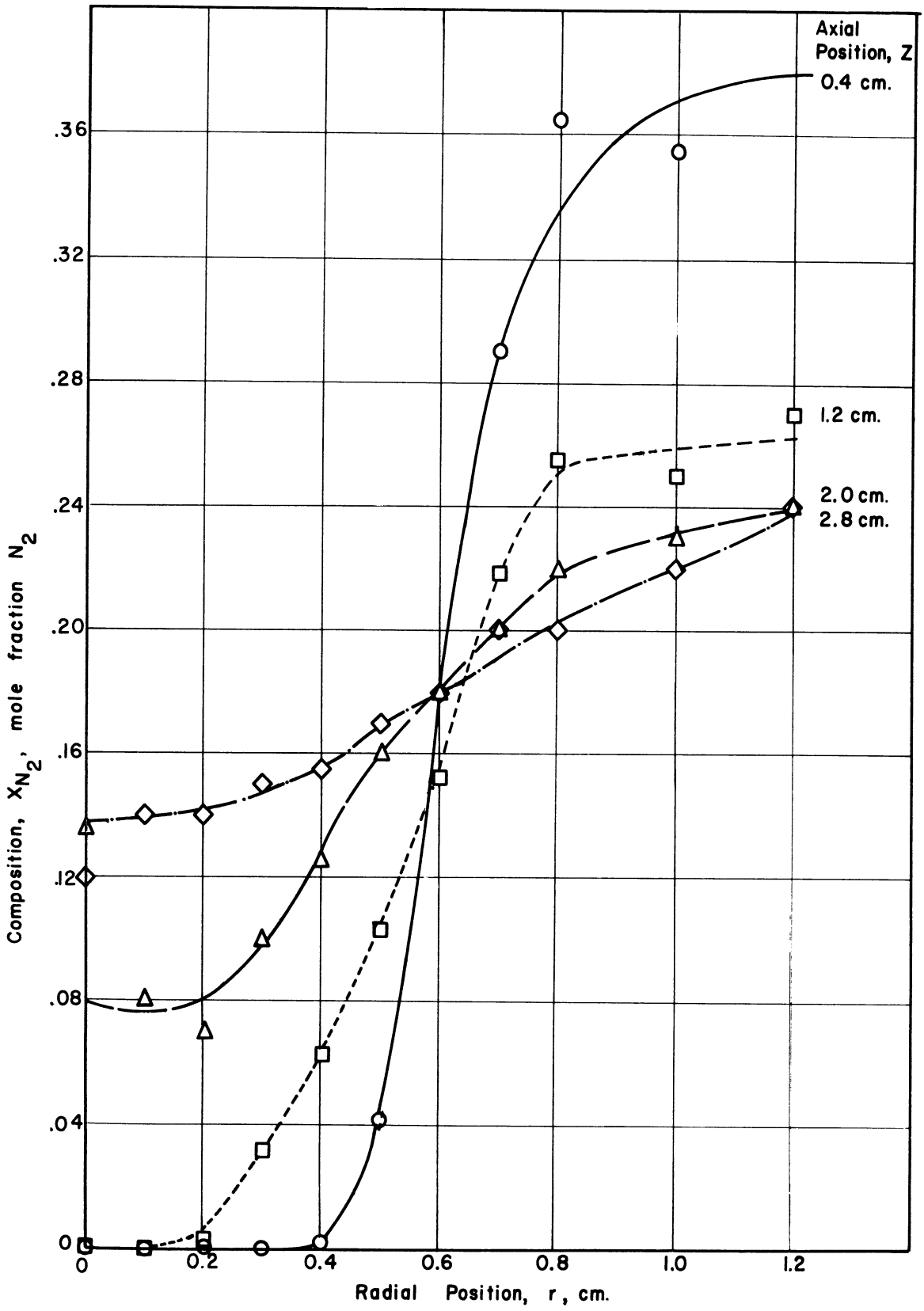

Figure 34. Composition versus position for flow condition 4.

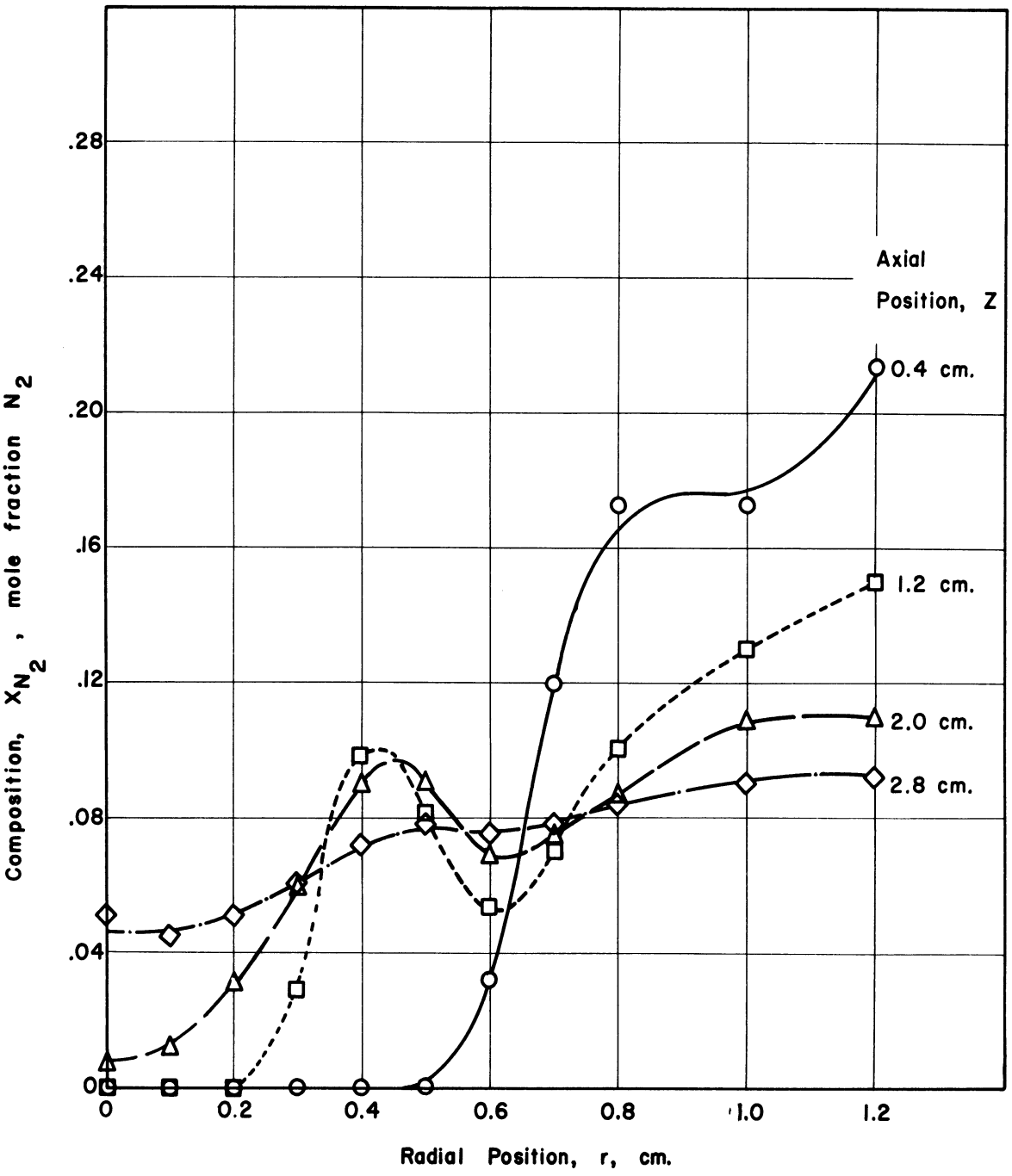

Figure 35. Composition versus position for flow condition 5.

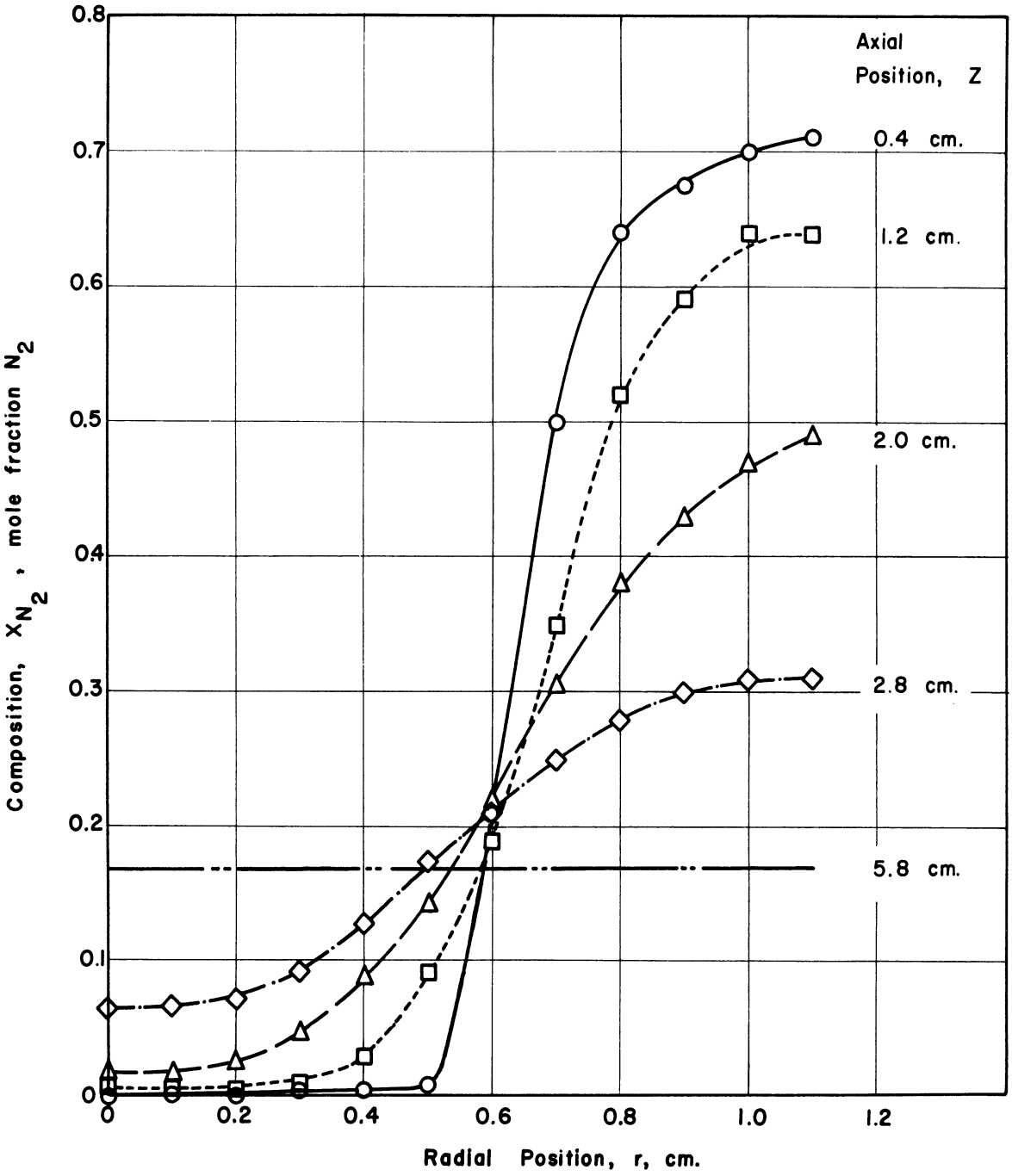

Figure 36. Composition versus position for flow condition 9.

7.3.2 Flow Velocity Measurements

The pitot tube determined velocity profiles are shown in Figures 37 through 40. The cold flow condition shown in Figure 40 has an off-center peak due to a slight lack in flow symmetry. The plasma flow conditions were completely symmetrical. All of the plasma flow velocities were calculated while using the probe temperature correction discussed in Section 5.3. Argon temperatures were used in this correction since they represented the translational energy mode. Both composition and temperature data were used to calculate the required free stream densities.

The plasma velocity profiles are seen to spread very little and to decrease in the axial direction relatively rapidly. In contrast, the velocity profiles for the cold flow spread rapidly and had little drop in velocity at the greater axial distances. The primary reason of course is that the plasma flow is cooling and increasing in density. Cleaves and Boelter (19) noted similar behavior for their heated and unheated jets. Velocity data of this type are sometimes compared at various axial distances by plotting the velocity divided by the velocity at the half-width of the jet. For the data here, this shows little because of the small axial distance range covered. In the case of a jet which is cooling, the product of density and velocity should be used, since the jet momentum is actually of interest.

The determinations of the velocities in the high velocity jet region are considered quite accurate. Outside of this high velocity region reliable velocities could not be determined because of lack of sensitivity

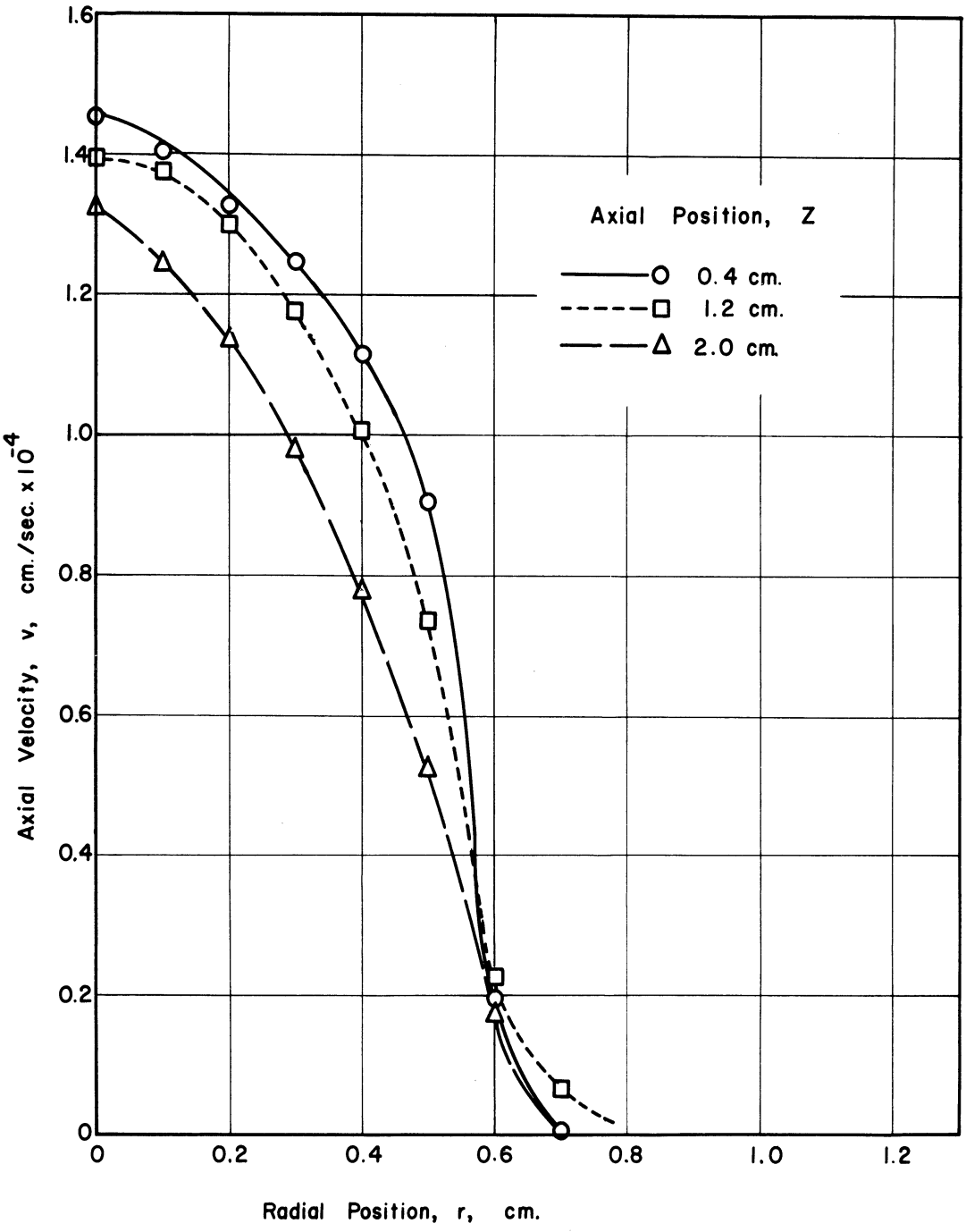

Figure 37. Axial velocity versus position for flow condition 1.

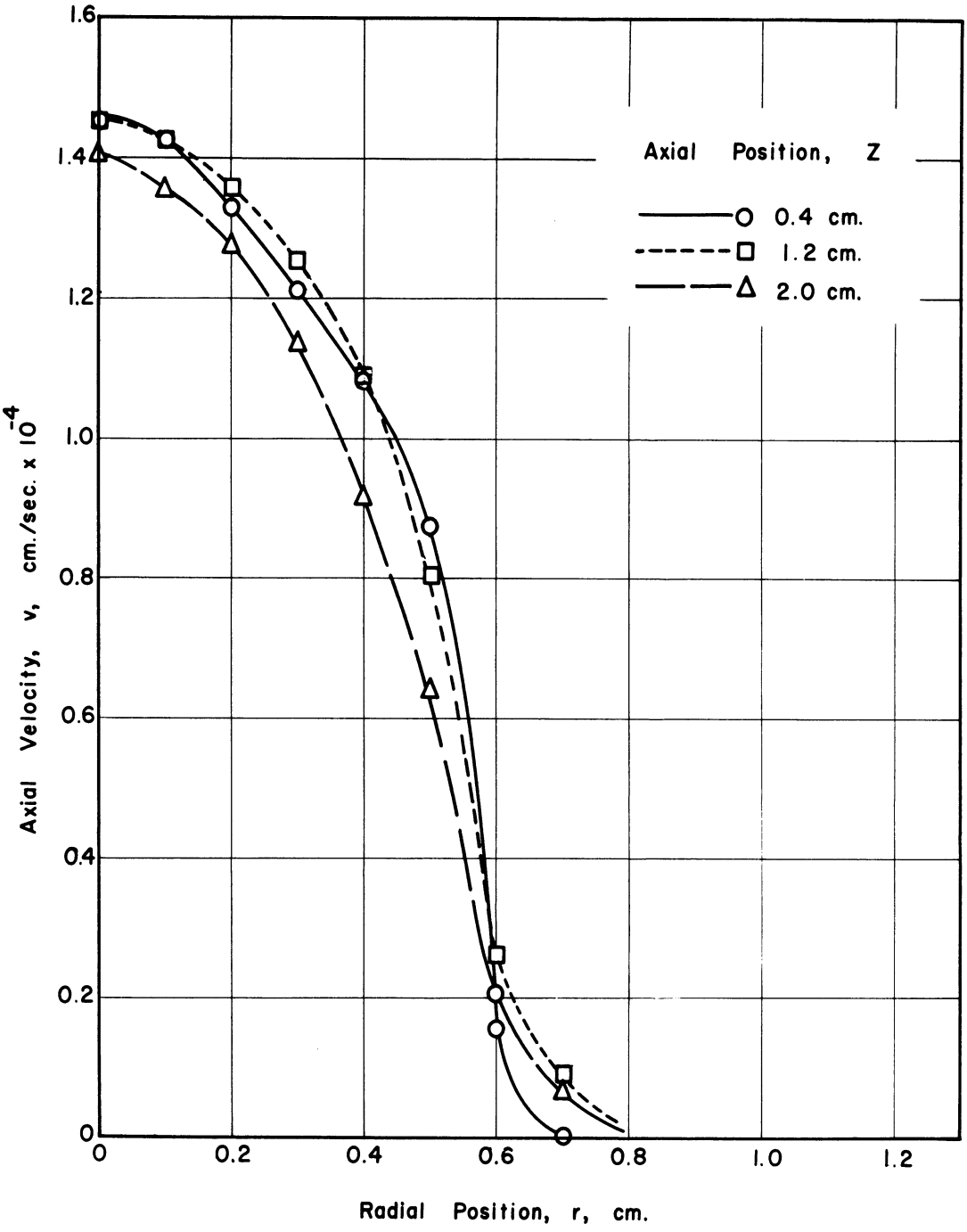

Figure 38. Axial velocity versus position for flow condition 2.

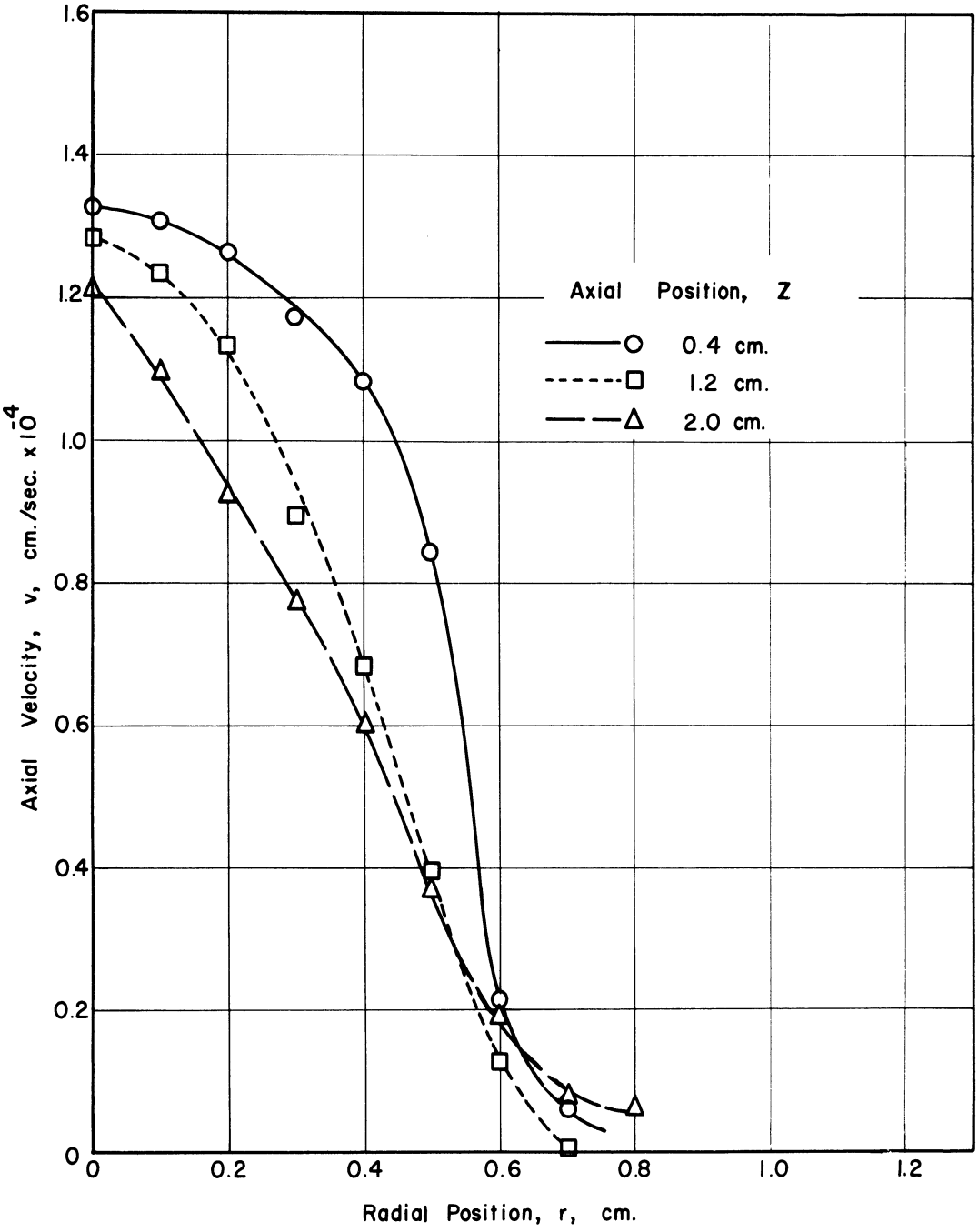

Figure 39. Axial velocity versus position for flow condition 3.

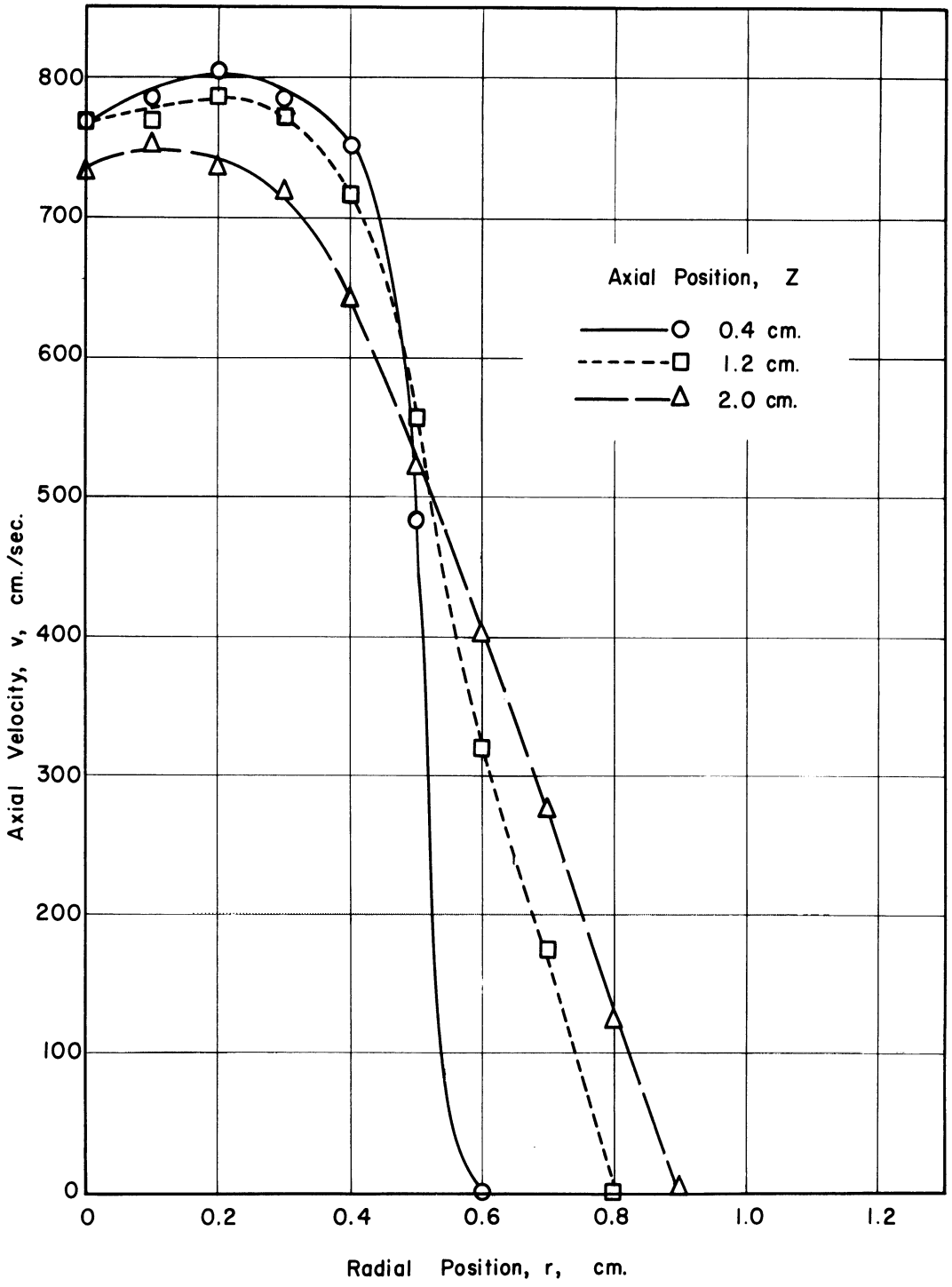

Figure 40. Axial velocity versus position for flow condition 9.

in the water manometer used. The sampling probe measured only the stagnation (impact) pressure. For the free stream pressure which also is required for use in velocity Equation (5.2), the probe reading at the wall was used. The flow velocity was so low at this point that the impact reading was equivalent to the free stream pressure. As is normal in confined jet work (1), the same free stream pressure was used for all radial measurements at a given axial position. For both plasma and cold flow conditions, the free stream pressure was negative (below atmospheric) at all of the axial positions used. There was little variation between positions. Dealy (26) also measured negative wall pressures at small axial distances in his confined jet work.

7.3.3 Enthalpy Measurements

Reliable enthalpy data could not be obtained by using the sampling probe. Figure 41 shows how the measured enthalpy (plotted here as temperature) varied with the sampling rate through the probe. The reason for this behavior can be postulated. At low sampling rates the probe samples to a large extent from the cool boundary layer of gas surrounding the probe. The order of magnitude lower viscosity of cool compared to plasma gas may aid in this effect. At higher sampling rates a greater portion of the gas which normally flows past the outside of the probe and transfers heat to it is drawn through the sampling probe. Since this makes the assumption of constant heat flux to the outside of the probe no longer valid, an erroneously low enthalpy value is obtained. The

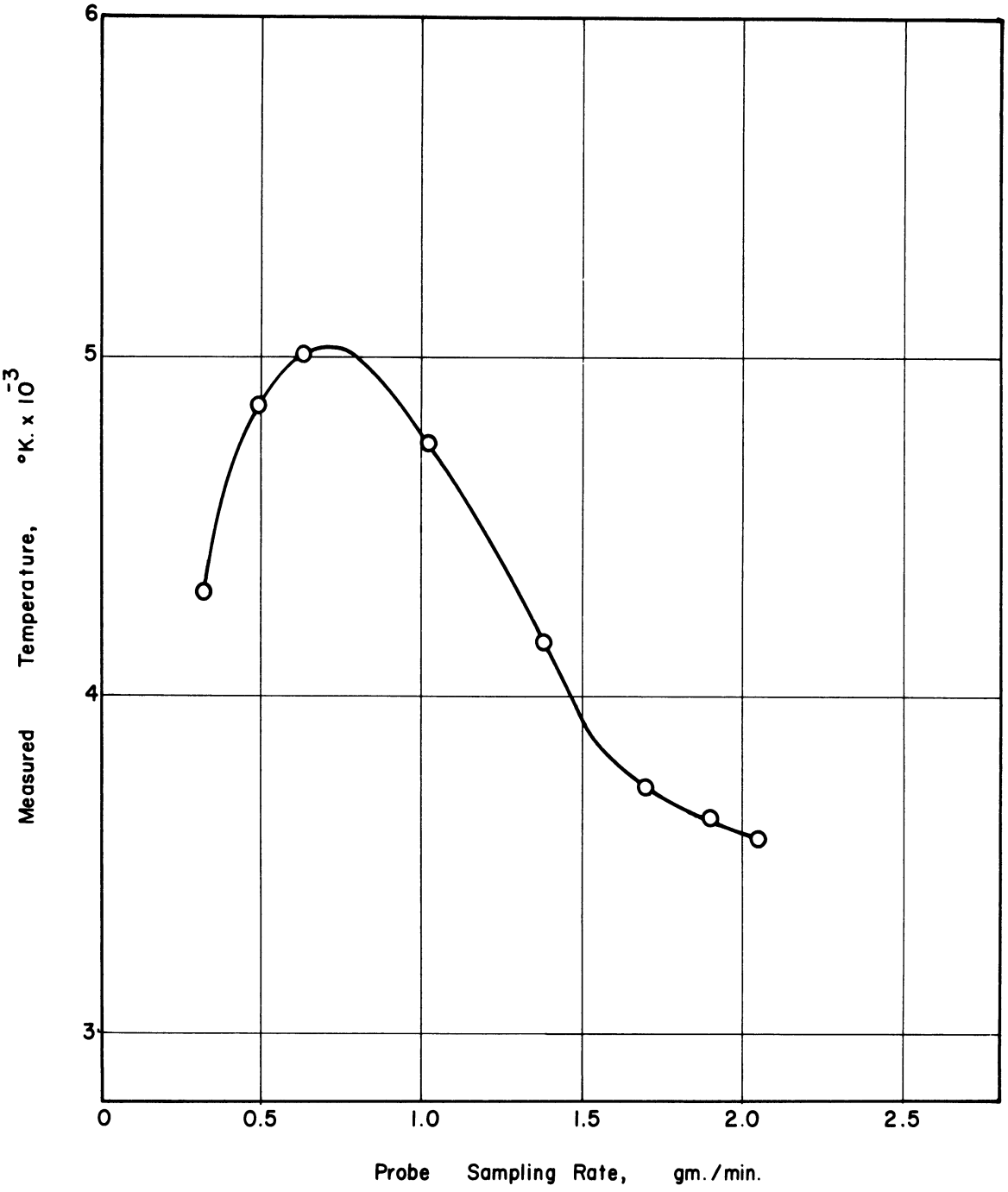

Figure 41. Variation of measured temperature with probe sampling rate (probe located at r = 0, z = 0.4 cm).

peak in the curve corresponds to no variable of interest. It simply represents the sampling rate at which the sampling effect overtakes the boundary layer effect. This discussion indicates that no one sampling rate can be expected to give a meaningful enthalpy value. Some extrapolation of a set of data for various sampling rates back to zero flow appears to offer little promise because of lack of exact knowledge concerning the energy transfer mechanisms to the outside of the probe.

As Figure 41 shows the peak temperature measured by the probe was approximately 5000°K. At the same point in the plasma, spectrographic results gave a temperature of over 9000°K. Pure argon plasmas were used for these measurements. Chludzinski (18) who used a similar probe in induction generated plasmas noted a corresponding difference between probe and spectrographic temperatures. He used only low sampling rates.

Grey and co-workers (46-48, 54, 83) also made measurements of plasma temperatures using sampling probes. They do not discuss the effect of sampling rate, if any, upon their results. They only state that their measured enthalpies agree with a total energy balance. Their plasma jet was larger than the one used for this thesis, so the sampling rate effect may have been less.

7.4 MASS AND ENERGY BALANCES

By using the spectrographically determined temperatures and probe determined compositions and velocities, mass and energy balances could be made for the plasma flows. A digital computer was used to perform

the calculations. Drellishak's (31, 32) data for density and enthalpy were fitted numerically, and the required integrations across the plasma flow were performed by using Simpson's rule. Because of lack of data, the integrations were made only out to r = 0.9 centimeter even though the confining tube wall was located at r = 1.35 centimeters. The results of the mass and energy balances are shown in Table II. Ranges are listed because of the uncertainty in the velocity values in the low velocity region beyond the edge of the jet. The nitrogen results are subject to error since the integration was stopped at r = 0.9 centimeter.

It is interesting to note how the mass and energy balance results are dependent upon temperature. The mass flow rate M and the energy flow rate H are proportional to the following

$$M \sim \int_0^R \sqrt{\frac{\Delta P}{\rho}}\, \rho r \, dr \tag{7.2}$$

$$H \sim \int_0^R \sqrt{\frac{\Delta P}{\rho}}\, \rho h r \, dr \quad . \tag{7.3}$$

Since the density ρ is approximately inversely proportional to temperature and the specific enthalpy h is approximately directly proportional to temperature. The resulting temperature dependence of the rates are

$$M \sim \frac{1}{\sqrt{T}} \tag{7.4}$$

$$H \sim \sqrt{T} \quad . \tag{7.5}$$

TABLE II

MASS AND ENERGY BALANCE SUMMARY

Flow Condition Designation	Axial Position of Measurement (cm)	Overall Mass Flow Rate (gm/min)	Overall Energy Flow Rate (kw)	Nitrogen Mass Flow Rate (gm/min)	Nitrogen Energy Flow Rate (kw)
1	0.4	44.2 - 66.5	2.94 - 3.15	0.063 - 0.78	0.0018 - 0.0135
	1.2	64.5 - 80.9	3.14 - 3.30	0.859 - 1.23	0.0292 - 0.0361
	2.0	53.4 - 70.5	2.68 - 2.85	0.897 - 1.23	0.0331 - 0.0392
	input rate	60.6	3.06	1.90	0.0099
2	0.4	46.8 - 69.6	3.04 - 3.25	0.34 - 4.17	0.0042 - 0.0379
	1.2	59.9 - 77.3	3.02 - 3.18	2.90 - 4.87	0.0616 - 0.0791
	2.0	43.4 - 66.2	2.45 - 2.67	3.45 - 6.19	0.0999 - 0.125
	input rate	66.9	3.06	8.22	0.044
3	0.4	59.2 - 77.0	3.07 - 3.24	4.43 - 11.6	0.039 - 0.102
	1.2	47.6 - 70.9	2.78 - 3.00	4.91 - 10.6	0.059 - 0.109
	2.0	81.9 - 95.8	3.10 - 3.24	15.3 - 18.9	0.171 - 0.202
	input rate	77.1	3.15	18.4	0.096

Thus too high of a temperature results in a low mass rate and a high energy rate. Conversely, too low of a temperature causes a high mass rate and low energy rate. When the argon temperatures were used for both the argon and nitrogen fractions, the calculated mass rate was too low and the energy rate too high. When the nitrogen temperatures were used for both fractions, the mass rate was too high and the energy rate too low. When the argon temperatures were used for the argon fraction and the nitrogen temperatures for the nitrogen fraction, the results shown in Table II were obtained. Both mass and energy are seen to agree with the input rates. The results also show that from 1/2 to 3/4 of the nitrogen coolant ended up in the high temperature part of the flow where the measurements were made. The nitrogen fraction, however, contained less than 10% of the plasma energy at the end of the luminous region.

The energy input rates shown in Table II were calculated from the electric power input rate to the electric arc. The energy rate to the walls of the mixing chamber and to the exit gas calorimeter was measured as being about 7% less. The difference is thought to be due to problems in measuring the energy rate to the walls of the mixing chamber rather than being due to direct radiation losses from the plasma. The crude radiation monitor used could detect no radiation loss from the sides of the plasma but measured radiation equivalent to about 1.5% of the net plasma energy when viewing the plasma end on (looking into the plasma nozzle). Grey et al. (47, 53) used a more refined radiation monitor and found that the total radiation loss amounted to about 4% of their net plasma energy. The plasma used in this thesis contained at

least 94% of its energy in argon translation, so the radiation loss would be expected to be small.

7.5 INDUCTION AND RECIRCULATION

The observed temperature and composition profiles can be explained on the basis of jet induction (or entrainment) and recirculation. For all plasma flow conditions a large amount of nitrogen coolant appears to be inducted into the argon plasma jet near the start of the mixing region. The nitrogen composition peak caused by this induction is visible in the composition profiles for flow conditions 1 and 5 (Figures 31 and 35). The nitrogen to argon composition ratio was very low for these flow conditions. For the other flow conditions, greater diffusion caused by the higher concentrations of nitrogen, smoothed out the peaks. The gradual change with increasing nitrogen is evident in going between flow conditions 1, 2, and 3 (Figures 31, 32, and 33). Flow conditions 4 and 5 which used different plasma flow rates are roughly equivalent to conditions 3 and 1 respectively. The formation of the peaks shown also requires that argon rich gas recirculate back to near the start of the mixing region. Additional insight into the flow pattern can be gained from plots of constant composition. Such plots for flow conditions 1 and 2 are shown in Figures 42 and 43. In regions where flow is controlling the distribution of the gases, the flow lines and lines of constant composition should be parallel. On the basis of the composition contour plot for flow condition 1, a possible recircu-

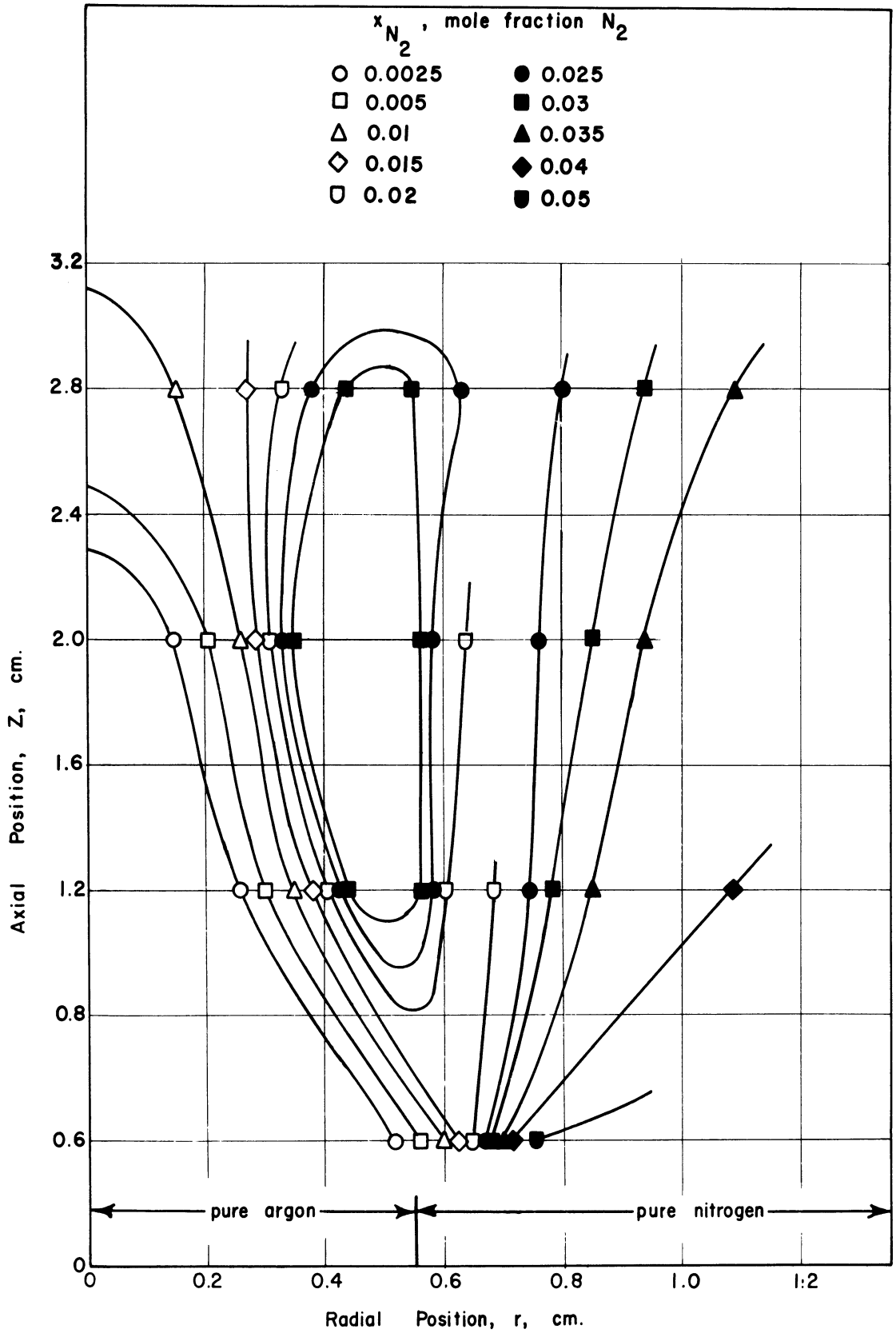

Figure 42. Contours of constant composition for flow condition 1.

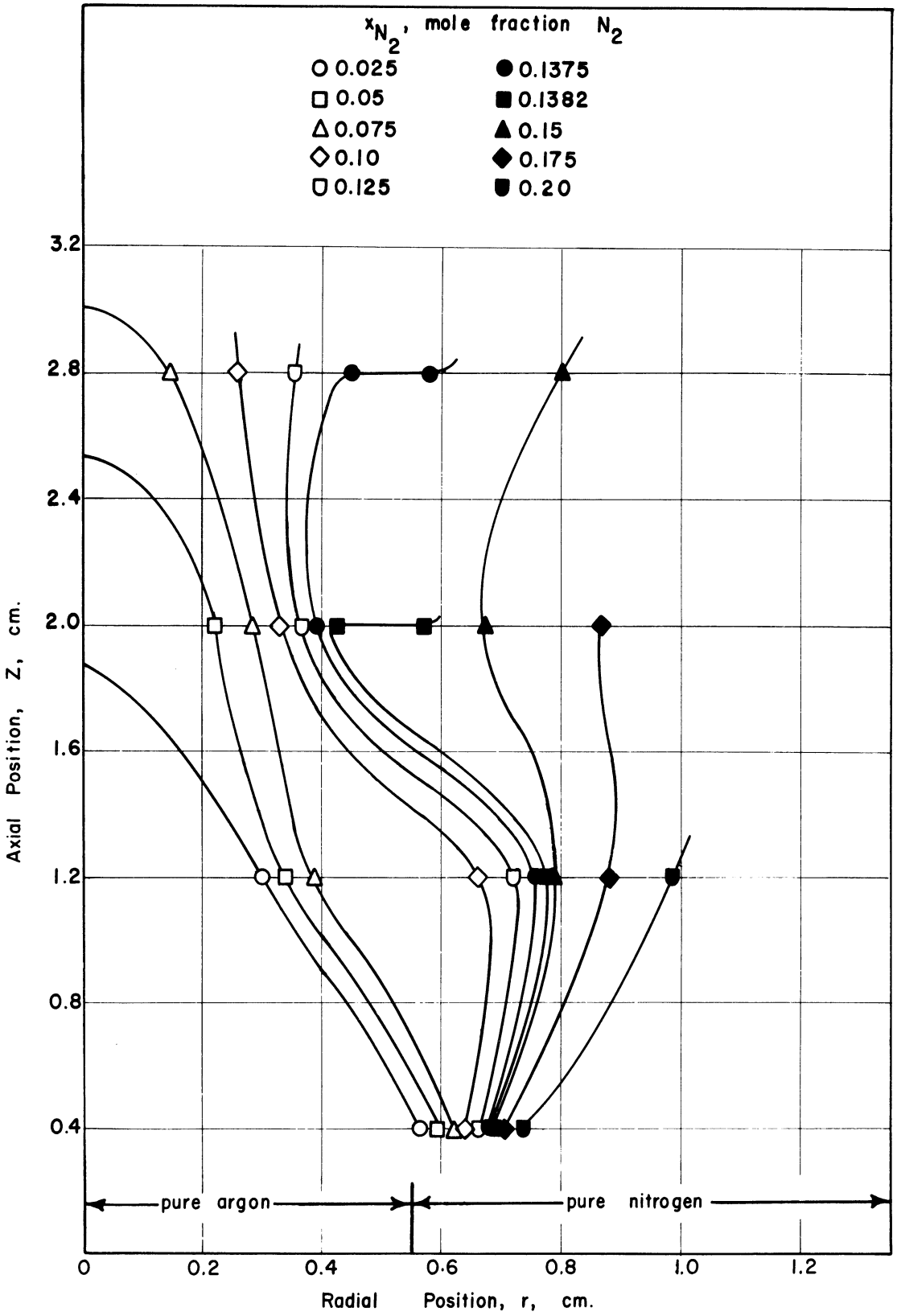

Figure 43. Contours of constant composition for flow condition 2.

lation pattern for this flow condition is shown in Figure 44. Since the manometer used for the pitot tube velocity measurements was low in sensitivity, the recirculation pattern could not be confirmed experimentally.

The dips in the argon temperature profiles at the axial distances of 1.2 and 2.0 centimeters can be explained on the basis of induction of large amounts of cool nitrogen into the jet near its axis. The temperature profiles are thus affected by the flow pattern in addition to the usual diffusion and conduction mechanisms.

Some of the confined jet research discussed in Section 3.2 can be used to support the induction and recirculation conclusions. The Ricou and Spalding correlation can be used to calculate the entrainment capacity of the plasma jet. From Equation (3.5) the amount of nitrogen entrained by the jet up to an axial distance of 2.0 centimeters would be 22.3 grams per minute. Thus for all flow conditions the jet was capable of entraining more than the entire nitrogen coolant flow. A recirculation eddy would then supply the remainder of the entrainment capacity.

The Craya-Curtet number for the jet flows can also be estimated to see if recirculation would be expected. Since the Craya-Curtet number was derived for constant density systems, Equations (3.3) and (3.4) had to be modified to include the effects of different source and secondary flow densities. Since the momentum of the streams is actually of interest, all of the velocity terms were multiplied by their related densities. Average source and secondary velocities were used. The re-

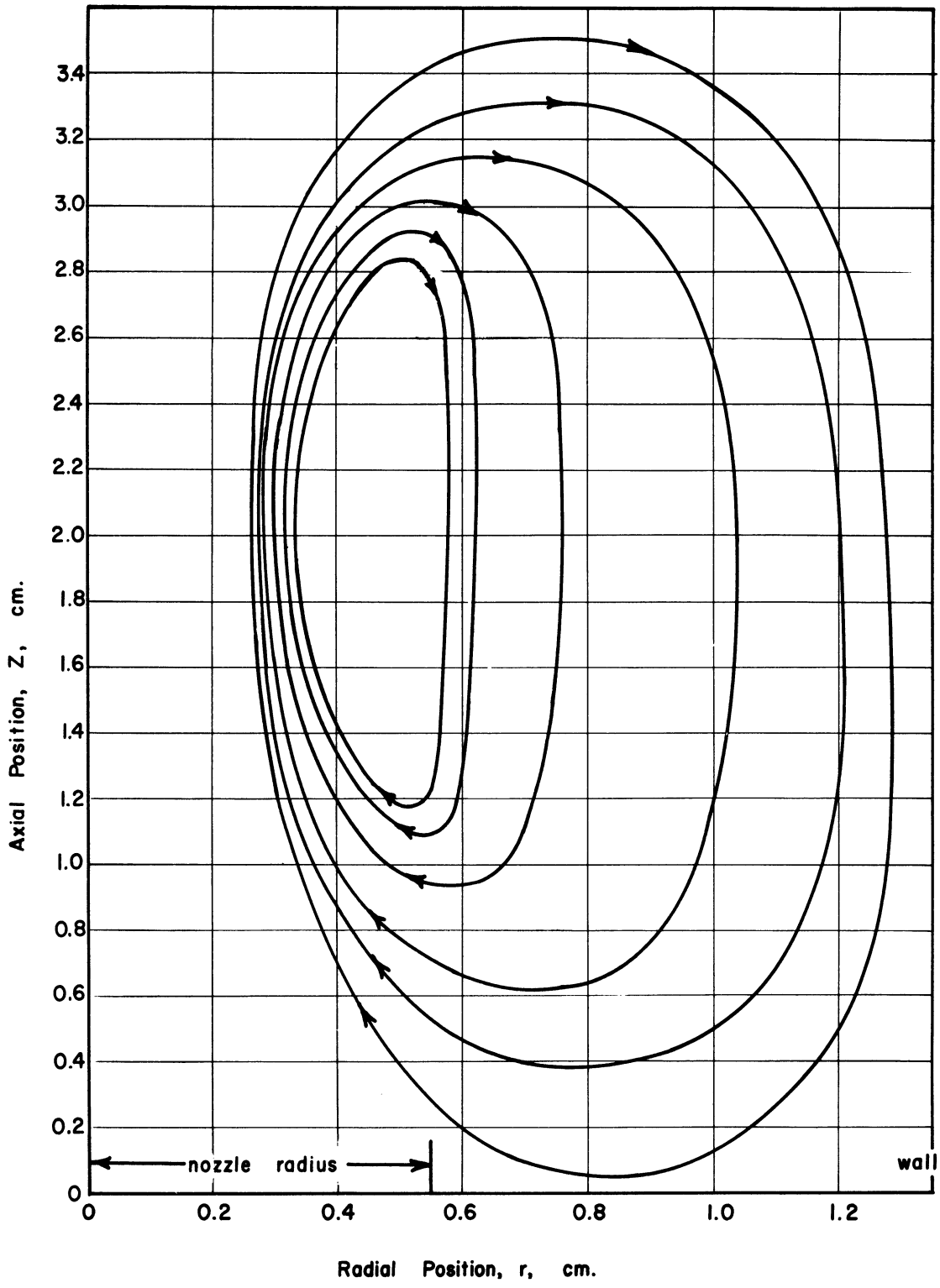

Figure 44. Possible recirculation pattern for flow condition 1.

sults of the Craya-Curtet number calculations are given in Table III. The values indicate that recirculation would be expected for all flow conditions.

TABLE III

SUMMARY OF CRAYA-CURTET NUMBERS

Flow Condition Designation	Craya-Curtet Number
1	0.436
2	0.461
3	0.520
4	0.472
5	0.451
9	0.506
no coolant flow	0.430

From a chemical reaction standpoint, the induction and recirculation phenomena make it unimportant how the reactants are injected into the mixing chamber. Either radial or axial introduction should have about the same effect since induction and recirculation will control the mixing. Such an observation is consistent with the experimental finding of Biggerstaff (9).

7.6 DIFFERENTIAL EQUATION MODEL

A simplified version of the differential equation which describes the mixing of the plasma and coolant by flow and diffusion was solved. The results could be used to estimate the order of magnitude of the effective diffusion coefficient required to give composition profiles

similar to those observed experimentally.

For steady state conditions with no component generation, the mass fraction w_B of component B (nitrogen) is governed by

$$\nabla \cdot \rho_B \vec{v} = \nabla \cdot \rho D_{AB} \nabla w_B \tag{7.6}$$

where D_{AB} is the effective binary diffusion coefficient. Component A is argon. For constant radial velocity v_r, axial velocity v_z, and diffusion coefficient and neglecting axial concentration gradients, Equation (7.6) expands and simplifies to

$$\frac{\partial w_B}{\partial z} = \frac{D_{AB}}{v_z} \frac{\partial^2 w_B}{\partial r^2} + \left\{ \frac{D_{AB}}{v_z} \left[\frac{1}{r} + \frac{1}{\rho} \frac{\partial \rho}{\partial r} \right] - \frac{v_r}{v_z} \right\} \frac{\partial w_B}{\partial r}$$

$$- \frac{v_r}{v_z} \left[\frac{1}{r} + \frac{1}{\rho} \frac{\partial \rho}{\partial r} \right] w_B \ . \tag{7.7}$$

The solution of the equation is subject to the following initial

$$w_B(0,r) = \begin{cases} w_{B1} = 0 & (0 < r < R_1) \\ w_{B2} & (R_1 < r < R_2) \end{cases} \tag{7.8}$$

and boundary conditions

$$\frac{\partial w_B(z,0)}{\partial r} = 0 \ , \qquad \frac{\partial w_B(z,R_2)}{\partial r} = 0 \ . \tag{7.9}$$

Equation (7.7) is a parabolic partial differential equation. It was solved numerically on a digital computer by using an implicit formulation. The solution of an equivalent differential equation with simi-

lar boundary conditions is discussed in detail in Lapidus (63). The same approach was used here. Also used were some computer algorithms given by Carnahan (15) for the solution of the tri-diagonal coefficient matrix which was involved in the numerical solution. Complete velocity data had to be supplied as an input to the computer program. The experimentally determined plasma jet axial velocities were used where applicable.

When radial and axial velocities equivalent to the recirculation pattern shown in Figure 44 were used, peaks were obtained in the composition profiles for flow condition 1. The solution was very dependent upon the exact radial velocities used. Because of lack of knowledge about the true recirculation and induction velocities, no effort was made to duplicate the experimentally determined composition profiles.

For flow condition 3, which had a high nitrogen to argon ratio, and for flow condition 9, which used no electric power input, good duplication of the experimentally determined composition profiles could be obtained by using only axial velocities (no recirculation). This indicates that diffusion was controlling for these cases. The computed composition profiles are shown in Figures 45 and 46. For flow condition 3 an effective diffusion coefficient of 200 cm^2/sec was used. For flow condition 9 the coefficient was 10 cm^2/sec.

Levenspiel (65) presents correlations for effective diffusion (dispersion) coefficients. The correlations actually are for uniform flow through a pipe, but if the plasma and coolant velocities are averaged

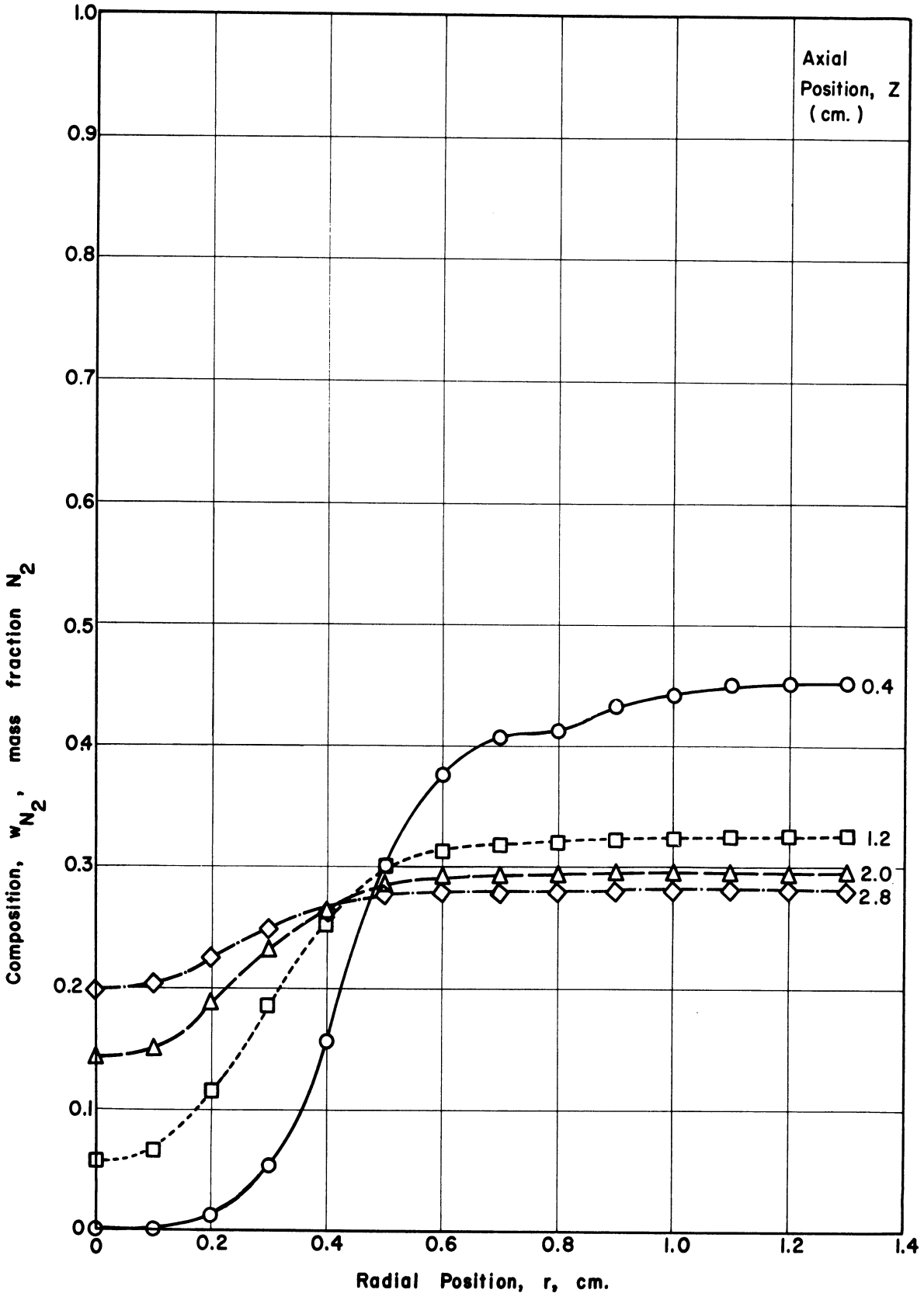

Figure 45. Solution of diffusion equation for flow condition 3.

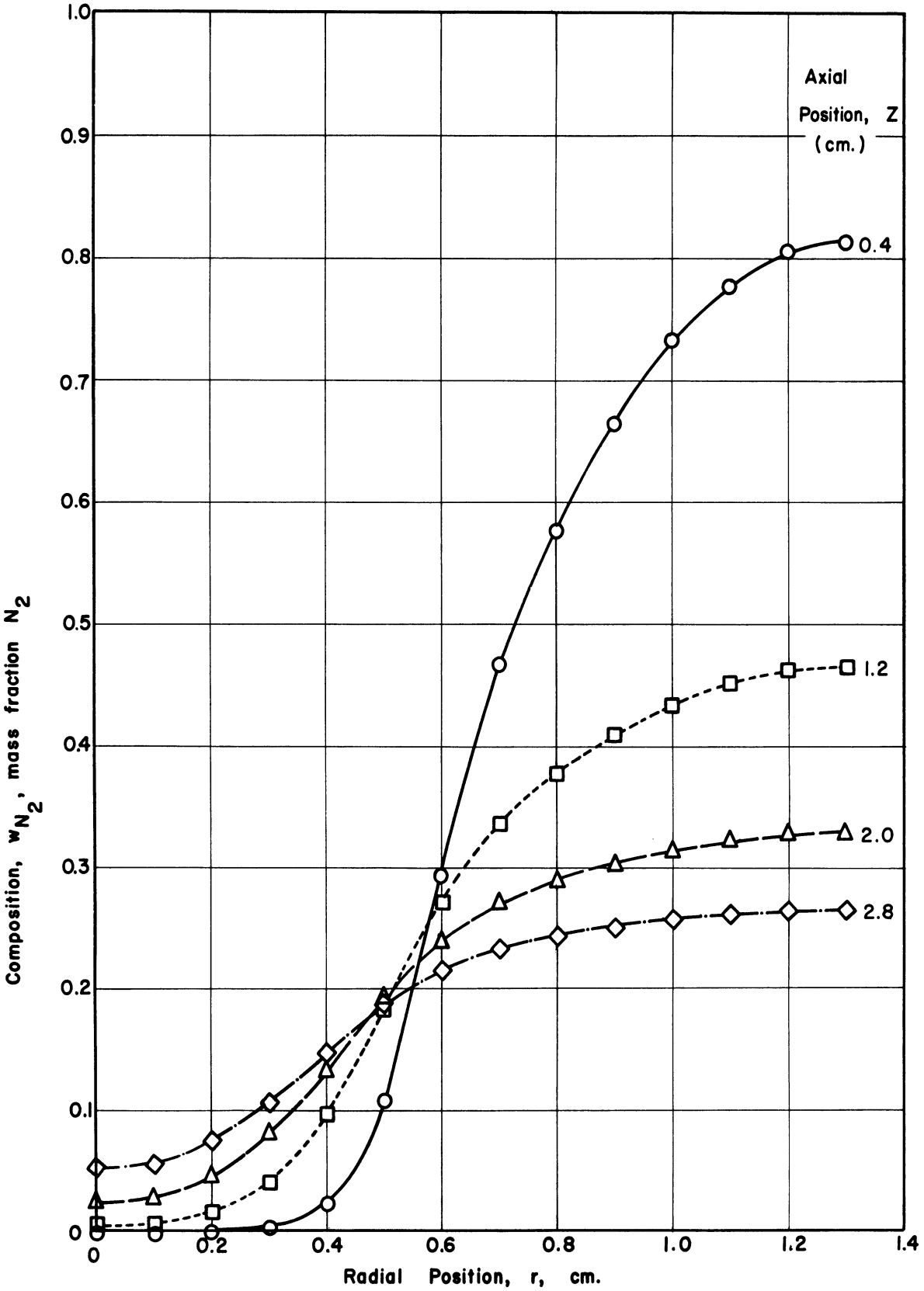

Figure 46. Solution of diffusion equation for flow condition 9.

across the mixing tube, order of magnitude agreements with the correlations are obtained for both plasma and cold flow conditions. The viscosity used was that of the jet.

Laminar diffusion coefficients and thermal diffusion ratios for argon and nitrogen at high temperatures are given by Amdur (4). The coefficients listed are much smaller than the 200 cm^2/sec found above. Thus the primary transport of matter is by turbulent diffusion.

8. CONCLUSIONS

The mass and energy transfer between confined plasma jet and coolant streams was studied experimentally. Argon was used for the plasma gas and nitrogen for the coolant gas. The plasma was generated without employing tangential velocity components.

The electronic excitation temperature of the argon atoms and the rotational temperature of the nitrogen molecules were determined by spectrographic methods. The measured argon temperatures were from 7000 to 9500°K and had an estimated accuracy of $\pm$ 2%. The nitrogen temperatures were from 500 to 5000°K and had an estimated accuracy of $\pm$ 20%. The compositions and the axial velocities present in the plasma-coolant mixing region were determined by sampling probe methods. Sampling probe measurements of enthalpy were found to be unreliable.

The measured nitrogen temperatures were found to be much lower than the argon temperatures present at the same point in the flow. The difference could be explained on the basis of the inability of argon atoms to give their translational energy directly to the rotational modes of nitrogen molecules. The composition profiles indicated that direct induction of coolant into the high velocity plasma jet and the formation of a recirculation eddy greatly increased the mixing of plasma and coolant. The induction and recirculation phenomena were found to be consistent with correlations developed for ordinary temperature confined jets. Mass and energy balances computed at various

axial distances in the mixing region indicated that from 1/2 to 3/4 of the nitrogen coolant was present in the high temperature region of the flow but that this coolant fraction contained less than 10% of the total energy present. Total mass and energy balances based upon the different argon and nitrogen temperatures agreed with the input rates and thus confirmed the accuracy of the temperature measurements. The solution of the differential equation describing argon-nitrogen diffusion indicated that flow and turbulent diffusion controlled the mixing of the plasma and coolant. The diffusion coefficients could be approximated by standard correlations.

From a plasma jet chemical reaction standpoint, the results of this study indicate that the mixing with the plasma of a reactant injected into a plasma jet reaction chamber would be very rapid but that the internal energy modes of the reactant molecule would not be fully excited during the short residence time in the high velocity flow.

9. SUGGESTIONS FOR FURTHER STUDIES

Additional insight into the mass and energy transfer phenomena found in the present work could be gained from further work.

A better experimental documentation of the jet induction and recirculation would be of value. By using a very sensitive pressure measuring instrument and a pitot tube which could respond to radial as well as axial velocities, the extent and velocity of the recirculation eddy might be measurable. Temperature measurements in the non-luminous region would be required to complete the velocity calculation.

Measurement of the vibrational temperatures of the nitrogen molecules would add to the energy transfer knowledge. To make measurement of the necessary total band intensities experimentally feasible, some type of direct spectrographic readout and integration equipment would be needed. The nitrogen coolant could, of course, be replaced by other gases.

APPENDIX A

PHOTOGRAPHIC MEASUREMENT OF SPECTRAL LINE INTENSITIES

A.1 BACKGROUND

The intensity of a spectral line can be determined from the density of the silver image which it causes to be deposited on a photographic plate. Unfortunately, the amount of silver deposited is a non-linear function of both the intensity and wavelength of the line. Thus to determine the intensities of lines of differing intensities and wavelengths,a plate, or emulsion, calibration is required. The various optical components of the scanning system used, and especially the diffraction grating in the spectrograph itself, also vary in their transmittance or reflectance of light of different wavelengths. It is convenient to include these variations in the emulsion calibration.

A.2 CALIBRATION PROCEDURE

The calibration of the photographic emulsion and the optical system was made by using a ribbon filament tungsten lamp which served as a source whose spectral intensity was known as a function of wavelength. The lamp was positioned so that its rays followed the same optical path as those from the plasma and so that the spectrograph slit subtended the same solid angle of radiation from either source.

The lamp used was a 6 volt, 108 watt unit manufactured by the General Electric Company (normally used as a microscope illuminator).

The power supply for the lamp consisted of a 120 volt constant voltage transformer, a Variac, and a 117 to 6 volt step down transformer. The apparent temperature of the tungsten ribbon was measured with a calibrated Leeds & Northrup disappearing filament optical pyrometer (Cat. No. 8622). The apparent temperature was corrected to the true temperature by using De Vos's (28) values for the emissivity of tungsten, the transmittance of the pyrex glass lamp envelope as given in Ref. 20, an estimate of reflection, and the National Bureau of Standards pyrometer correction tables (72). Under normal operation conditions, the Variac was adjusted so that the ribbon filament operated at a true temperature of 2800°K. The temperature was uniform over the central portion of the filament and this portion was much larger than the area focused upon the slit of the spectrograph. With the temperature now known, Planck's radiation law and De Vos's values for the emissivity of tunsten were used to calculate the intensity of the radiation emitted as a function of wavelength.

The calibration procedures required only the use of relative intensities (symbol RI). As described later, absolute intensities of spectral lines (symbol I) were obtained from the relative intensities by reference again to the tungsten filament. Throughout this thesis, intensity refers to the source. In the case of lines, it is the integrated spectral intensity in units of energy per unit time per unit area per steradian. In the case of continuum radiation, a wavelength interval had to be chosen to obtain corresponding integrated intensities.

The actual plate calibration was made by exposing the photographic plates in the spectrograph for various time intervals with the tungsten filament lamp and with plasma line radiation. To obtain an emulsion calibration in this manner it was necessary to assume that intensity-time reciprocity held; i.e., all exposures having the same intensity-time product would produce equal silver densities. For the Eastman Kodak type 103a-F plates which were used for all of the reported quantitative measurements, this is an excellent assumption for the exposure times of 3 to 300 seconds which were employed (33, 67). As far as calibration is concerned, this means that a change in exposure time is equivalent to a change in light intensity. Second order radiation dispersed by the diffraction grating presented no problem in the studied 3000 to 6000 Å region since the tungsten filament had negligible emission below 3000 Å. In spectrographic work, the intensity-time product is called the exposure (symbol E). After exposure the photographic plates were developed in a thermostated rocker type developing machine. Process conditions and reagents used were those recommended by Kodak (33). In addition to the 103a-F plates, IV-N and SA-1 plates were used during preliminary stages of the work.

Silver densities on the plates were measured with a Leeds & Northrup recording microphotometer (Knorr-Albers type). The density of the silver deposit (symbol D) is defined to be negative of the common logarithm of the fractional light transmittance through the deposit. The densities of the calibration exposures were recorded at wavelengths

corresponding to spectral lines of interest. From these records and the calculated relative intensity of the tungsten filament, emulsion calibration curves were drawn. A representative set of curves is shown in Figure 47. Curves of this type are known as Hurter-Driffield characteristic curves. The calibration results indicated that the curves for radiation of different wavelengths were all of the same shape but were displaced along the exposure abscissa in accordance with plate sensitivity. Curves based upon narrow (1.5 mm) bands of tungsten filament continuum radiation were found to have exactly the same shape as those based upon line radiation.

A.3 MEASUREMENT OF RELATIVE LINE INTENSITIES

The photographic plates used to record the intensities of the spectral lines which were used for plasma temperature measurement were developed in the same manner as the calibration plates. The densities of the lines were again measured with the Leeds & Northrup microphotometer. In using the photometer, it was found that only the slow plate scanning speeds (0.1 to 0.5 mm/min) could be used. Otherwise the recording potentiometer associated with the photometer could not follow the change in density as a sharp line was traversed. The scanning beam in the photometer was narrower than the width of the recorded spectral lines and was about 1 mm in height.

For a given spectral line it was found that either peak height or peak area could be used in calculating the intensity. The semi-auto-

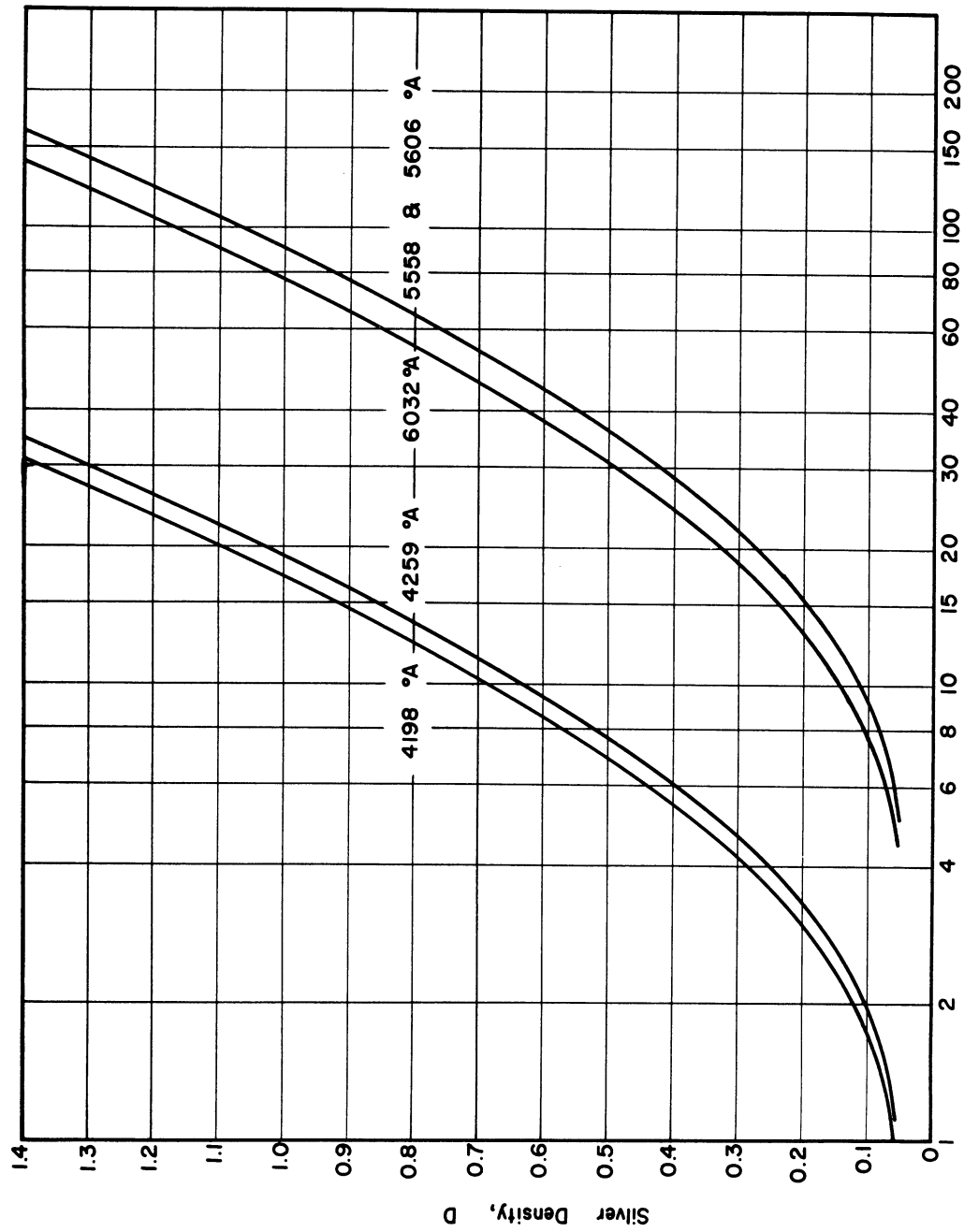

Figure 47. Emulsion characteristic calibration curves for 103a-F plates.

mated method used to compute peak areas is described in Appendix B. To compare the intensities of spectral lines originating from different energy levels, however, the use of peak areas was necessary. When peak heights were used, the relative intensity of a line could be obtained from the calibration plot (Figure 47). The measured density could be entered on the ordinate, and the corresponding exposure then read from the abscissa. The relative intensity then was found by dividing the exposure by the exposure time. The peak area integration method directly gave the exposure.

A.4 CALCULATION OF ABSOLUTE LINE INTENSITIES

Absolute intensities were found by a comparison of integrated line peak areas with integrated tungsten filament continuum radiation. Such an integrated exposure is directly proportional to the quantity of energy which is absorbed by the spectrographic plate. Since the spectrograph slit subtended the same solid angle of radiation from both the plasma and tungsten lamp, equal integrated exposures corresponded to equal amounts of energy leaving the source. By noting what wavelength interval of tungsten continuum was required to equal the line peak area, Planck's law could be used to calculate the absolute intensity of the spectral line. Once the absolute intensity of one line was calculated, the absolute intensity of any line was known from its relative intensity.

APPENDIX B

ANALOG COMPUTER EVALUATION OF SPECTRAL LINE INTENSITIES

B.1 BACKGROUND

In some cases peak area, instead of the more simply determined peak height, must be used in the determination of spectral line intensities. In the present work integration was required when comparing argon lines originating from different energy levels. The lines from d- (diffuse) energy levels were found to be much broader than lines from p- (principal) energy levels. Also with lines in the nitrogen band spectra, integration was required because peaks of varying shapes were produced by differing extents of line overlap. During the course of this work, the peak areas of 170 argon lines, and of 405 nitrogen lines were integrated.

B.2 INTEGRATION PROCEDURE

The Leeds & Northrup recording photometer gave a strip chart recording of the density of the spectra line versus wavelength; i.e., a tracing of the line peak. By using the emulsion calibration curves as described in Appendix A, this tracing could be converted, point by point, to a plot of exposure versus wavelength. The integration of this plot across the width of the line gave the total exposure which then could be converted to intensity by dividing by the exposure time.

An analog computer (Applied Dynamics Corporation Model AD 2-24-PB) was used to electronically perform the density-exposure conversion and

the subsequent integration. The circuit diagram is shown in Figure 48. The density recording was read into the computer by using a Pace Model 1100D X-Y plotter which was equipped with a curve follower. To be used with the curve follower, the strip chart recordings from the photometer had to be retraced with silver conducting ink. In the circuit diagram, amplifiers 4 and 10 and their related circuits provide voltages to the ends of the slide wire of the curve follower corresponding to 0 (0 volts) and ∞ (100 volts) density (density is the y-coordinate). Amplifiers 1 and 3 provide a ramp voltage for driving the follower in the x- or wavelength-direction. The density- or y-signal enters the analog computer and is amplified and inverted by amplifiers 6, 7, and 8. The diode function generator then converts the density signal into the corresponding exposure signal. The diode function generator works by approximating the desired function by using 10 straight line segments. The segments used are shown in Figure 49. The resulting curve agrees with the density-exposure calibration curve within the latter's experimental uncertainty. As mentioned in Appendix A, except for a shift along the exposure axis, the calibration curves for all wavelengths were identical. Amplifier 5 and potentiometer 2 provide a signal which can be subtracted from the exposure signal in summing amplifier 9 to correct for line background. The output from amplifier 2 is the integrated total exposure.

A check of the analog computer procedure by integrating a given line which had been exposed for various time intervals, showed that no error was introduced by the method.

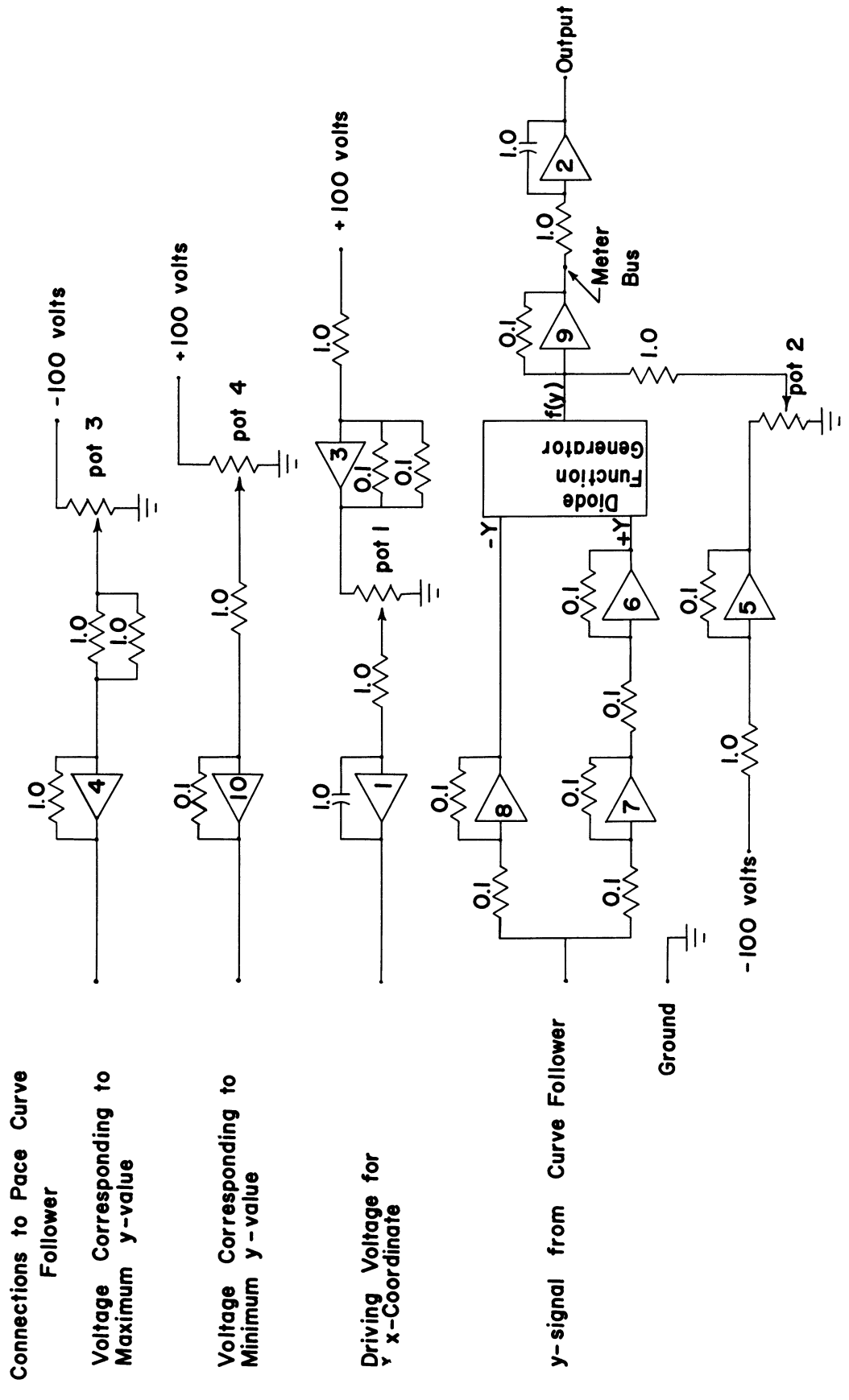

Figure 48. Analog computer circuit for peak area integration.

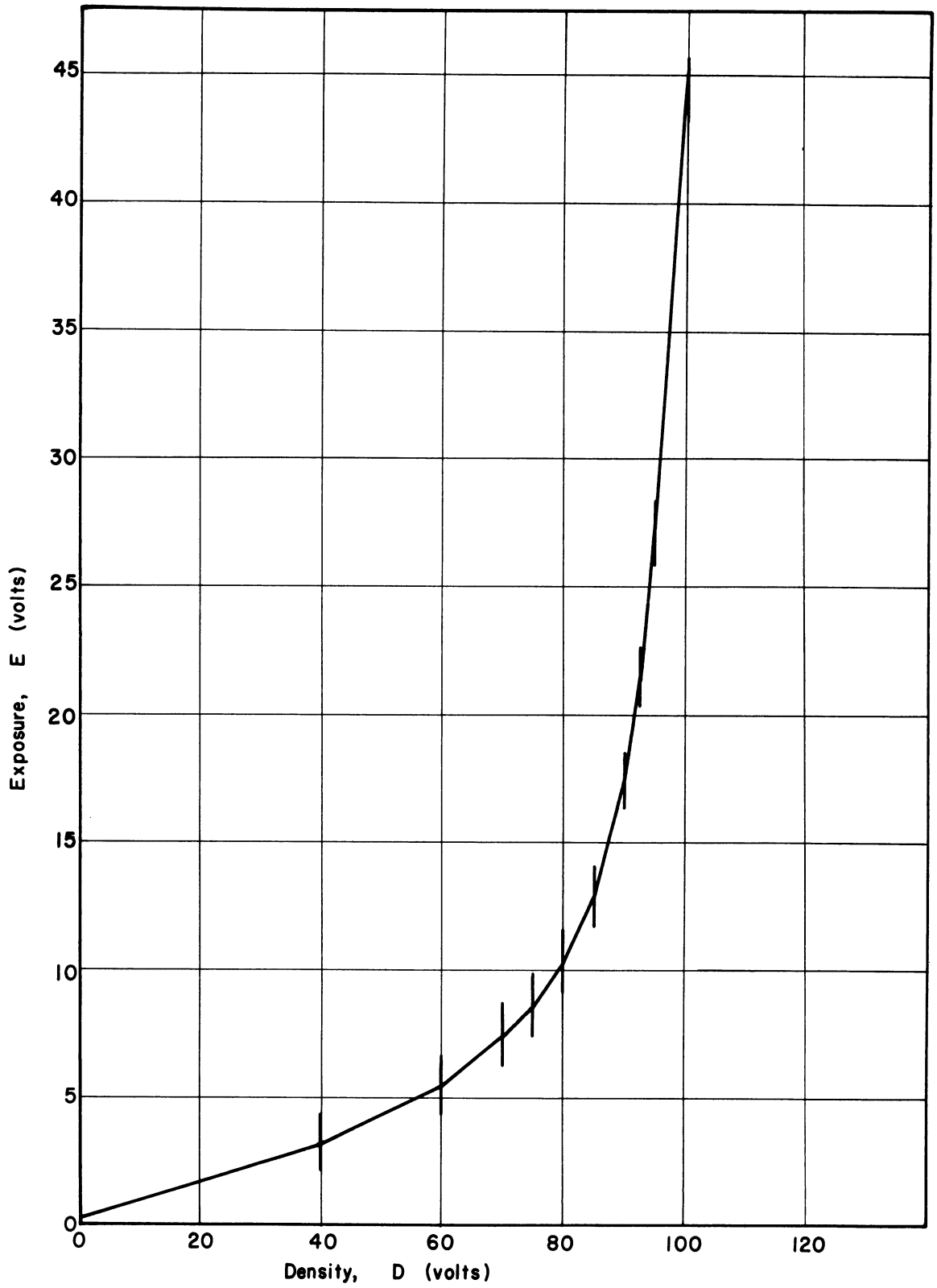

Figure 49. Diode function generator approximation of the emulsion characteristic curve.

REFERENCES

1. Abramovich, G., The Theory of Turbulent Jets, M.I.T. Press, Cambridge, Mass., 1963.

2. Adcock, B. D. and W. E. Plumtree, "On Excitation Temperature Measurements in a Plasma Jet, and Transition Probabilities for Argon Lines," J. Quant. Spectrosc. Radiat. Transfer, 4, 29-39 (1964).

3. Alpinieri, L. J., "Turbulent Mixing of Coaxial Jets," AIAA Journal, 2, 1560-1567 (1964).

4. Amdur, I., "High Temperature Transport Properties of Gases; Limitations of Current Calculating Methods in the Light of Recent Experimental Data," AIChE Journal, 8, 521-526 (1962).

5. Anderson, J. E. and L. K. Case, "An Analytical Approach to Plasma Torch Chemistry," I&EC Process Design Develp., 1, 161-165 (July 1962).

6. Baron, T., and L. G. Alexander, "Momentum, Mass and Heat Transfer in Free Jets," Chem. Eng. Prog., 47, 181-185 (1951).

7. Becker, H. A., H. C. Hottel, and G. C. Williams, "Mixing and Flow in Ducted Turbulent Jets," Ninth Symposium on Combustion—1962, p. 7, Academic Press, 1963.

8. Benson, S. W., The Foundations of Chemical Kinetics, pp. 135-167, McGraw-Hill, New York, 1960.

9. Biggerstaff, G. E., W. R. Golliher, R. L. Harris, and W. R. Rossmassler, "Plasma Torch Production of Elemental Boron," AEC Research and Development Report KY-453, Feb. 1964.

10. Bird, R. B., W. E. Stewart, and E. N. Lightfoot, Transport Phenomena, p. 369, John Wiley & Sons, Inc., New York, 1960.

11. Blackman, V., "Vibrational Relaxation in Oxygen and Nitrogen," J. Fl. Mech., 1, 61-85 (1956).

12. Bowen, S. W., University of Michigan, private communication.

13. Brewer, L. E. and W. K. McGregor, "The Radiative Decay of Metastable Argon Atoms in a Low-Density Argon Plasma Stream," Arnold Engineering Development Center Report No. AEDC-TDR-63-5 (Jan. 1963).

REFERENCES (Continued)

14. Budó, A., "Intensitätsformeln für die Triplettbanden," Zeitschrift für Physik, 105, 579-587 (1937).

15. Carnahan, B., H. A. Luther, and J. O. Wilkes, Applied Numerical Methods, Vol. II, pp. 509-586, John Wiley & Sons, Inc., 1964.

16. Chandrasekhar, S., Radiative Transfer, pp. 354-356, Dover Publications, Inc., New York, 1960.

17. Chapman, S., and T. G. Cowling, The Mathematical Theory of Non-uniform Gases, p. 199, Cambridge University Press, London, 1939.

18. Chludzinski, G. R., "Energy Transfer to Solids in R. F. Generated Plasmas," Ph.D. Thesis, University of Michigan, Ann Arbor, 1964.

19. Cleves, V., and L. M. K. Boelter, "Isothermal and Non-isothermal Air-Jet Investigations," Chem. Eng. Prog., 43, 123-134 (1947).

20. Corning Glass Works, "Glass Color Filters," Bulletin CF-1, Corning, New York, 1960.

21. Corrsin, S., "Investigation of Flow in an Axially Symmetrical Heated Jet of Air," NACA Wartime Report, W-94, 1943.

22. Corrsin, S., and M. S. Uberoi, "Further Experiments on the Flow and Heat Transfer in a Heated Turbulent Air Jet," NACA TN 1865, 1949.

23. Coster, D., F. Brons, and A. van der Ziel, "Die sogenannte zweite positive Gruppe des Stickstoffspektrums," Zeitschrift für Physik, 84, 304-334 (1933).

24. Curtet, R., "Confined Jets and Recirculation Phenomena with Cold Air," Combustion and Flame, 2, 383 (1958).

25. Curtet, R., "Sur L'Ecoulement D'un Jet Entre Parois," Publications Scientifiques et Techniques Du Ministere De L'Air, No. 359, 1960.

26. Dealy, J. M., "Momentum Exchange in a Confined Circular Jet with Turbulent Source," Ph.D. Thesis, University of Michigan, Ann Arbor, 1964.

REFERENCES (Continued)

27. Dealy, J. M., "The Confined Circular Jet with Turbulent Source," pp. 84-91 in Symposium on Fully Separated Flows, ed. by A. G. Hansen, ASME, New York, 1964.

28. De Vos, J. C., "A New Determination of the Emissivity of Tungsten Ribbon," Physica, 20, 714 (1954).

29. Dickerman, P. J., editor, Optical Spectrometric Measurements of High Temperatures, University of Chicago Press, Chicago, 1961.

30. Donald, M. B. and H. Singer, "Entrainment in Turbulent Fluid Jets," Trans. of the Institution of Chemical Engineers, 37, 255-267 (1959).

31. Drellishak, K. S., D. P. Aeschleman, and A. B. Cambel, "Tables of Thermodynamic Properties of Argon, Nitrogen, and Oxygen Plasmas," Arnold Engineering Development Center Technical Documentary Report No. AEDC-TDR-64-12 (Jan. 1964).

32. Drellishak, K. S., C. F. Knoop, and A. B. Cambel, "Partition Functions and Thermodynamic Properties of Argon Plasmas," Arnold Engineering Development Center Technical Documentary Report No. AEDC-TDR-63-146 (Aug. 1963). (Also given in Physics of Fluids, 6, 1280-1288 (1963).)

33. Eastman Kodak Company, "Kodak Plates and Films for Science and Industry," p. 19d, Rochester, New York, 1962.

34. Edels, H., "The Determination of the Temperatures of an Electrical Discharge in a Gas," British Electrical and Allied Industries Research Association Technical Report Reference L/T 230, Leatherhead, Surrey, U. K., 1950.

35. Fassbender, M., "Untersuchungen über das negative Stickstoffbandenspektrum," Zeitschrift für Physik, 30, 73-92 (1924).

36. Forstall, W. F. and A. H. Shapiro, "Momentum and Mass Transfer in Coaxial Gas Jets," J. Appl. Mech., 74, 399-408 (1950).

37. Freeman, M. P., and S. Katz, "Determination of a Radiance-Coefficient Profile from the Observed Asymmetric Radiance Distribution of an Optically Thin Radiating Medium," J. Opt. Soc. Am., 53, 1172-1179 (1963).

REFERENCES (Continued)

38. Freeman, M. P., S. U. Li, and W. Von Jaskowsky, "Velocity of Propagation and Nature of Luminosity Fluctuations in a Plasma Jet," J. Appl. Phys., 33, 2845-2848 (1962).

39. Freeman, M. P. and J. F. Skrivan, "Rate Studies of the Decomposition of Ammonia and Methane in a Plasma Jet," AIChE Journal, 8, 450 (1962).

40. Gaydon, A. G. and I. R. Hurle, The Shock Tube in High-Temperature Chemical Physics, Chapman and Hall, Ltd., London, 1963.

41. Gericke, W. E., "Messung der Übergangswahrscheinlichkeit sowie Halbwertsbreite und Verschiebung von A I—Linien in thermisch leuchtenden Plasmen," Zeitschrift für Astrophysik, 53, 68-79 (1961).

42. Giannini, G. M., A. C. Ducati, W. F. von Jaskowsky, and D. Ragusa, "Experiments with High Intensity Electric Discharges" in Proceeding of an International Symposium on High Temperature Technology, Asilomar, Calif., Oct. 1959, McGraw-Hill, New York, 1960.

43. Gove, P. B., Editor-in-Chief, Webster's Third New International Dictionary of the English Language, Unabridged, G. & C. Merriam Company, Springfield, Mass., 1964.

44. Greene, E. F., G. R. Cowan, and D. F. Hornig, "The Thickness of Shock Fronts in Argon and Nitrogen and Rotational Heat Capacity Lags," J. Chem. Phys., 19, 427-434 (1951).

45. Greenshields, D. H., "Spectrographic Temperature Measurements in a Carbon-Arc-Powered Air Jet," National Aeronautics and Space Administration Technical Note NASA TN D-169, December 1959.

46. Grey, J. and P. F. Jacobs, "A Calorimetric Probe for the Measurement of High Temperatures," Princeton University Aeronautical Engineering Laboratory Report No. 602, April 1962.

47. Grey, J. and P. F. Jacobs, "Experiments on Turbulent Mixing in a Partially Ionized Gas," AIAA Journal, 2, 433-438 (1964).

48. Grey, J., P. M. Williams, M. P. Sherman, and P. F. Jacobs, "Laminar Mixing and Heat Transfer Phenomena between a Partially Ionized Gas and a Gaseous Coolant," Aerospace Research Laboratories, Wright-Patterson Air Force Base Report No. ARL 63-237, Dec. 1963.

REFERENCES (Continued)

49. Griem, H. R., "Validity of Local Thermal Equilibrium in Plasma Spectroscopy," Phys. Rev., 131, 1170-1176 (1963).

50. Grosse, A. V., H. W. Leutner, and C. S. Stokes, "Plasma Jet Chemistry," Research Institute of Temple University, Philadelphia, Dec. 1961.

51. Herzberg, G., Molecular Spectra and Molecular Structure, I. Spectra of Diatomic Molecules, D. Van Nostrand Co., Princeton, N. J., 1950.

52. Hinze, J. O. and B. G. Van der Hegge Zijhen, "Transfer of Heat and Matter in the Turbulent Mixing Zone of an Axially Symmetrical Jet," Appl. Sci. Res., Hague A1, 435-461 (1949).

53. Jacobs, P. F., "Measurements of Total Energy Radiated from an Argon Arcjet," Princeton University Aeronautical Engineering Report No. 621, Aug. 1962.

54. Jacobs, P. F., "Turbulent Mixing in a Partially Ionized Gas," Princeton University Aeronautical Engineering Report No. 625, Oct. 1962.

55. Jahn, R. E., "Temperature Distribution and Thermal Efficiency of Low Power Arc-Heated Plasma Jets," British Journal of Applied Physics, 15, 585-588 (1963).

56. John, R. R. and W. L. Bade, "Recent Advances in Electric Arc Plasma Generation Technology," ARS Journal, 29, 4-17 (1961).

57. Jarrell-Ash Company, "Ebert Convertible Plane Grating Spectrograph," Newtonville, Massachusetts, 1962.

58. Kadlec, R. H., "The Behaviour of Slugging Gas-Fluidized Solids," Ph.D. Thesis, University of Michigan, Ann Arbor, 1961.

59. Kamura, I. and A. Kanzawa, "Measurement of Stream Velocity in an Arc," AIAA Journal, 1, No. 2 (1963).

60. Keck, J. C., J. C. Camm, B. Kivel, and T. Wentink, "Radiation from Hot Air, Part II. Shock Tube Study of Absolute Intensities," Annals of Physics, 7, 1-38 (1959).

REFERENCES (Continued)

61. Knauss, H. D. and M. S. McCay, "Temperature Determinations from Band Spectral Data," Phys. Rev., 52, 1143-1150 (1937).

62. Krzywoblocki, M. Z. von, "Jets—Review of Literature," Jet Propulsion, 26, 760 (1956).

63. Lapidus, L., Digital Computation for Chemical Engineers, pp. 179-183, McGraw-Hill, New York, 1962.

64. Leutner, H. W., "The Production of Cyanogen from the Elements Using a Plasma Jet," I & EC Process Design Develp., 1, 166 (July 1962).

65. Levenspiel, O., Chemical Reaction Engineering, p. 276, John Wiley & Sons, Inc., New York, 1962.

66. Marynowski, C. W., R. C. Phillips, J. R. Phillips, and N. K. Hiester, "Thermodynamics of Selected Chemical Systems Potentially Applicable to Plasma Jet Synthesis," I & EC Fundamentals, 1, 52-61 (Feb. 1962).

67. Nachtrieb, N. H., Principles and Practice of Spectrochemical Analysis, p. 107, McGraw-Hill Book Company, Inc., New York, 1950.

68. Nestor, O. H. and H. N. Olsen, "Numerical Methods for Reducing Line and Surface Probe Data," SIAM Review, 2, 200-207 (1960).

69. Olsen, H. N., "Determination of the Properties of an Optically Thin Argon Plasma" in Temperature: Its Measurement and Control in Science and Industry, Vol. 3, C. M. Herzfeld, Editor-in-Chief, pp. 587-592, Reinhold Publishing Corp., New York, 1962.

70. Pearse, R. W. B. and A. G. Gaydon, The Identification of Molecular Spectra, pp. 166-176, John Wiley & Sons, Inc., New York, 1950.

71. Petschek, H. E., P. H. Rose, H. S. Glick, A. Kane, and A. Kantrowitz, "Spectrographic Studies of Highly Ionized Argon Produced By Shock Waves," J. Appl. Phys., 26, 83 (1955).

72. Poland, D. E., J. W. Green, and J. L. Margrave, "Corrected Optical Pyrometer Readings," NBS Monograph 30, U. S. Govt. Printing Office, April 21, 1961.

REFERENCES (Continued)

73. Reed, T. B., "Growth of Refractory Crystals Using the Induction Plasma Torch," J. Appl. Phys., 32, 12 (1961).

74. Ricou, F. P. and D. B. Spalding, "Measurements of Entrainment by Axisymmetrical Turbulent Jets," J. Fliud Mech., 11, 21-32 (1961).

75. Rieppel, P. J., "Plasma-Jet Cutting, Machining, and Welding," Metals Engineering Quarterly, 3, (Nov. 1963).

76. Rittenhouse, L. E., E. E. Anspach, and M. H. Nesbitt, "Experimental Aerodynamic Data Concerning Vortex Flow and the Gas Velocity in a Small D-C Arc Heater Operated with Argon," Arnold Engineering Development Center Report No. AEDC-TDR-63-124 (July 1963).

77. Rutowski, R. W. and D. Bershader, "Shock Tube Studies of Radiative Transport in an Argon Plasma," Physics of Fluids, 7, 568-577 (1964).

78. Ryan, L. R., H. J. Babrov, and R. H. Tourin, "Infrared Spectra and Temperatures of Plasmajets," Aeronautical Research Laboratories, Wright-Patterson Air Force Base, Report No. ARL 63-35, Feb. 1963.

79. Selover, T. B., "Properties of Nickel Fume Generated in a Plasma Jet," Symposium on Flames and Plasmas in Chemical Processing, American Institute of Chemical Engineers, Dec. 1961.

80. Thring, M. W. and M. P. Newby, "Combustion Length of Enclosed Turbulent Jet Flames," Fourth International Symposium on Combustion--1952, p. 789, The Williams and Wilkins Co., 1953.

81. Tourin, R. H., et al., "Measurement of Temperatures in Ionized Gases by Means of Infrared Radiation," Aeronautical Research Laboratory, Wright-Patterson Air Force Base, Report No. ARL 62-314, March 1962. (Also reported in ASME Trans. Ser. C, 84, 164-168 (1962).

82. Wheaton, J. R. and R. C. Dean, "On Anode Gas-Sheath Electrical Breakdown in a High-Pressure Plasma Generator," Research Report, School of Engineering, Dartmouth College, Hanover, New Hampshire, Oct. 1961.

REFERENCES (Concluded)

83. Williams, P. M., M. P. Sherman, and P. F. Jacobs, "Heat Transfer from a Partially Ionized Gas to a Gaseous Coolant," Princeton University Aeronautical Engineering Report No. 651, June 1963.

84. Winter, E. R. F. and C. J. Cremers, "Temperature Distribution in a Low Mass Flux Argon Plasma Jet," Wright-Patterson Air Force Base Report ARL 62-388 (July 1962).

NOMENCLATURE

Symbol	
A_{nm}	Einstein transition probability for spontaneous transition from level n to level m
B_v	rotational constant for vibration level v
c	velocity of light
c_p	heat capacity
Ct	Craya-Curtet number (defined in Equation (3.4))
D	photographic density
D_{AB}	binary diffusion coefficient
E	photographic exposure
E	energy
g	statistical weight
h	specific enthalpy
h	Planck's constant
H	total enthalpy flow rate
i	intensity of radiation from point source (energy time^{-1} unit volume^{-1} steradian^{-1})
I	absolute intensity of radiation (energy time^{-1} unit area^{-1} steradian^{-1})
J	rotational quantum number (including electron spin)
k	thermal conductivity
k	Boltzmann constant
K	rotational quantum number (not including electron spin)

Symbol	
L	path length or source thickness
m	Curtet momentum parameter (defined in Equation (3.2))
M	mass flow rate
N	number density
P	pressure
Q	volumetric flow rate
Q	partition function
r	radial coordinate
RI	relative intensity
R_1	jet source radius
R_2	radius of mixing tube
S_J	line strength
T	absolute temperature
v	vibrational quantum number
v	velocity in axial direction
$\vec{v}$	velocity vector
V_1	jet source average velocity
V_2	secondary flow average velocity at z = 0
w	mass fraction
x	mole fraction
x	lateral coordinate (normal to direction of main flow)
z	axial coordinate measured from source
μ	viscosity

Symbol

ν	frequency
ρ	fluid density

Subscripts

e	electronic
m	lower energy state
n	upper energy state
P	P-branch of band spectra
R	R-branch of band spectra
r	rotational
r	radial direction
r	arbitrary energy state
s	arbitrary energy state
t	total flow
v	vibrational
z	axial direction
0	initial value or ground level
1	primary flow (jet source)
2	secondary flow (coolant)

Superscripts

'	upper (initial) energy level
"	lower (final) energy level
P	P-branch
R	R-branch